The Dissertation Committee for Bongsu Kim
certifies that this is the approved version of the following dissertation:

Development of An Upper-Body Robotic Rehabilitation Platform that Furthers Motor Recovery After Neuromuscular Injuries

Committee:

Ashish D. Deshpande, Supervisor

Raul G. Longoria

Jonathan B. Dingwell

Dongmei Chen

James S. Sulzer

Development of An Upper-Body Robotic Rehabilitation Platform that Furthers Motor Recovery After Neuromuscular Injuries

by

Bongsu Kim, B.S.M.E.; M.S.

DISSERTATION

Presented to the Faculty of the Graduate School of

The University of Texas at Austin

in Partial Fulfillment

of the Requirements

for the Degree of

DOCTOR OF PHILOSOPHY

THE UNIVERSITY OF TEXAS AT AUSTIN

May 2016

Dedicated to my wife and daughter.

Acknowledgments

I would like to first express my sincere gratitude to my advisor, Dr. Ashish D. Deshpande, for continuous support of my Ph.D study and research. His support helped me immensely to bring my research alive. I also appreciate that I have been learning a lot from his advice and feedback toward becoming an independent investigator with a good set of skills.

Besides my advisor, I would like to thank the rest of my dissertation committee members: Dr. Raul G. Longoria, Dr. Jonathan B. Dingwell, Dr. Dongmei Chen, and Dr. James S. Sulzer, for their insightful feedback and suggestions that have significantly enhanced the quality of my dissertation with better comprehensiveness.

Thanks must also go to Dr. Rebecca Clearman, Cynthia Card, Dr. David Chu, Curtis Merring, and Dr. Pathasarathy for their clinical advice that has greatly enhanced the clinical viability of my research.

I thank my fellows: Kaci Madden, Evan Ogden, Jonas Fox, and other ReNeu lab members, for greatly helping the research project, specifically in designing and manufacturing parts and conducting experiments.

Last but not the least, I deeply thank my wife, Seonhwa Shin, for her unconditional support and sacrifice throughout the long journey. She has always been with me, even at my death's door in the middle of the study, encouraging me to

keep pursuing my goal with a right vision. Lastly, I sincerely thank my daughter, Robin Kim, for letting me and wife know and feel the best part of our life.

Development of An Upper-Body Robotic Rehabilitation Platform that Furthers Motor Recovery After Neuromuscular Injuries

Publication No. _____

Bongsu Kim, Ph.D.
The University of Texas at Austin, 2016

Supervisor: Ashish D. Deshpande

This dissertation presents the development of an upper-body exoskeleton and its control framework for robotic rehabilitation of the arm and shoulder after a neurological disorder such as a stroke. The first step is designing an exoskeleton hardware that supports natural mobility of the human upper body with a wide range of motion for enabling most rehabilitation exercises. The exoskeleton is equipped with torque-controllable actuation units for implementing various robotic rehabilitation protocols based on force and impedance behaviors. The control framework is designed to exhibit a highly backdrivable behavior with a gravity compensation for the robot's weight and optional gravity support for user's arm weight to promote voluntary movements of patients with motor impairments. The control framework also serves as a 'substrate' of other robotic control behaviors for rehabilitation exercises by superimposing desired force or impedance profiles. A stability analysis is performed to examine the coupled stability between the robot and human. After designing the hardware and control, several experiments are carried out to test the

mobility and dynamic behavior of the robot. Lastly, a human subject study evaluates the effectiveness of the robot's shoulder mechanism and control algorithm in assisting the coordination around the shoulder. The results show that the robot induces desirable coordination in the presence of abnormalities at the shoulder.

Table of Contents

List of Tables

List of Figures

Chapter 1

Introduction

1.1 Background

1.1.1 Neuromuscular Disorders and Neural Plasticity

A substantial portion of the world population suffers from neuromuscular disabilities caused by neurological injuries or diseases such as stroke, traumatic brain injury (TBI), spinal cord injury (SCI), cerebral palsy (CP), or Parkinson's disease (PD), requiring intensive health care services including rehabilitation [20, 46]. For example, strokes as the leading causes of the neuromuscular disabilities affect around 800,000 people in the United States alone each year [1]. Approximately 80% of all stroke survivors experience some form of upper limb paresis, with only 18% of those gaining full motor recovery within the following year [155, 124, 25]. The forms of upper limb dysfunctions after strokes include control deficits, weakness, abnormal coordination and co-contractions, hyperactivity in reflexes, or delayed motor responses [52]. The severity and type of the deficits vary largely across individuals, depending on the lesion and time after the incidences.

For a few stroke patients, a part of the lost functionality is recovered spontaneously. However, in many cases, rehabilitation intervention is required to achieve any recovery or to stimulate further improvements. The functional recovery is neurologically explained by the reorganization and remodeling of the neural circuitry

in the damaged brain. Much evidence confirms that the brain keeps reorganizing its structure and function in response to the interaction with external stimulation and experiences including repetitive physical training [142, 31, 58]. This 'programmable' ability called neural or brain plasticity explains the mechanism of learning new behaviors and relearning the lost behaviors even in the damaged brain and is the underlying principle of rehabilitation [63, 87, 143]. In the damaged brain, learning and relearning are processed by plasticity mechanisms forming new connectivity in the neural network such as reinforcement of the functionality in redundant motor neurons and relocation of the function of the damaged part to the adjoining parts in the brain [11, 126]. Still, principles and mechanisms of the neural plasticity and motor learning are under vast exploration in neuroscience.

1.1.2 Potential of Robotic Rehabilitation

The goal of rehabilitation intervention is to restore an impaired mobility by stimulating the brain to encode new skills and remap the motor cortices [45, 107]. The intervention is also important in physical perspectives to prevent paralyzed body segments from joint stiffness, soft tissue and muscle contracture, or/and muscle spasticity, which otherwise would become principal obstacles to recovery [138, 108, 82]. Robotic rehabilitation, which utilizes robotic devices as a means of providing intervention, has been attracting a lot of attention from medicine, neuroscience, and engineering sectors because of the potential of delivering better rehabilitation outcome. Many studies have shown that robotic rehabilitation produces better or, at least, equivalent outcomes compared to conventional ther-

apy [117, 79, 92, 10], offering a number of benefits as follows;

- Sophisticated motion and force profiles that are designed based on the principles of motor learning and brain plasticity in neuroscience can be precisely and repetitively applied to rehabilitation exercises.

- Robotic rehabilitation can provide high-intensity, task-oriented functional trainings and massed passive range of motion exercises, which are critical for effective recovery, at low cost, for a longer duration, and without the physical labor of therapists.

- Robotic environment can effectively provide augmented feedback to users such as visual, haptic, and auditory ones that are potential to enhance motor learning. Virtual reality, for example, can be integrated into a user interface to motivate users and offer real-world like circumstances that enhance the transfer of acquired skills to the actual activities of daily life.

- A rehabilitation robot provides a precise and reliable platform that measure and evaluate the users' physical abilities. Quantitative values of motor abilities such as user's strength, quality of voluntary control, range of motion, or muscle tone that can be precisely measured by robots will allow clinical practitioners to accurately diagnose their customers and prescribe more appropriate and individual-specific rehabilitation protocols. Also, the robotic platform may serve as a data logging system to track the progress of patients so that the therapeutic exercises can be properly adjusted along their improvements.

- A robotic platform provides, needless to say, an automated environment where rehabilitation resources, can be effectively allocated in time and space. A therapist may be engaged in two or more rehabilitation sessions at a time, relying on automated exercises by the robots. Also, a portable robotic system can be delivered to the patient's place for remote rehabilitation when commute to a hospital is limited.

With these advantages, robotic rehabilitation has a potential to become an important addition to the conventional rehabilitation to deliver more effective and efficient practices. The efficacy of robotic rehabilitation, however, is largely determined by the features of a robotic system and its rehabilitation protocols.

1.1.3 Coordination and Potential of Exoskeleton Robots

Most activities of daily living (ADLs) consist of multi-joint movements, and coordination of multiple joints plays a key role in controlling such movements [30, 40]. Also, many ADLs exhibit stereotypical interjoint coordination in the arm and shoulder such as in a reaching motion [80]. Recovering from impairments means restoring the mobility as before the impairments including the normal coordination. However, conventional therapy focuses more on reinforcing compensatory movements that accompany alternative coordination in the impaired limb or alternative movements of the unimpaired side. This is because compensatory strategy is a natural reaction to impairments and usually results in quicker recovery, at least partially, of functional task performance while circumventing the impairments [75]. A compensatory movement learned during rehabilitation tends

to continue even after the impaired lesion is recovered and does not stimulate the damaged neural system, limiting long-term recovery [85, 128]. On the other hand, recovering an impaired mobility, referred as reacquisition or true recovery, may take longer to perform functional tasks but benefit long-term recovery with better outcome [2, 86]. In pursuance of true recovery, regeneration of lost interjoint coordination will be inevitably included in rehabilitation practices and an ability to control each joint for coordination may facilitate reacquisition of lost skills.

Movements of the upper arm are inherently coordinated with movements of the shoulder girdle, represented by the scapulohumeral rhythm (SHR). The inherent coordination in the shoulder affects the anatomical and biomechanical integrity, preventing impingement, securing a wide range of motion (ROM), and maintaining an optimal force-length relationship in the shoulder muscle groups [149]. Without attention to the coordinated motion of the shoulder, joint instability may occur, resulting in shoulder pain or injuries including irritation and impingement of the rotator cuff [32, 48]. Also, since the coordinated motion is a key functionality of the shoulder girdle and is a natural consequence of serial actuation by the muscles running from the thorax to the humerus via the shoulder girdle, it may be beneficial to include this coordinated motion in the rehabilitation process of the upper limb for better clinical results [57].

Two-handed manipulation from a therapist or an assistance from an end-effector type robot [89] may have difficulties in inducing an intended configuration of the arm and shoulder or joint torque composition in the multiple joints. A robotic exoskeleton worn around the upper body is capable of controlling the human joints

to guide an impaired limb for intended coordinated movements or applying torque at each joint independently. If an exoskeleton has a shoulder mechanism for full mobility of the shoulder, the inherent coordination around the shoulder can also be modulated. However, great caution is needed in designing an exoskeleton to ensure kinematic compatibility to the human body to prevent undesired stresses on the musculoskeletal system.

1.1.4 Human-Robot Interaction and Requirement for Rehabilitation Robots

Rehabilitation is recognized as a relearning process, and many investigators have recently emphasized that rehabilitation practices need to incorporate the principles of motor learning in designing therapeutic exercises and protocols [18, 75, 68, 156]. While some brain damages disable the capability of motor learning, the significant portion of strokes is believed to preserve the partial or full capability of motor learning and benefit from the principles [157, 27, 115, 131].

A prominent perspective on motor learning suggests that each movement in learning a motion should be involved in a problem-solving process recruiting all relevant motor cortex activities as a cognitive process rather than memorizing the sequence of muscle activation and replaying it [133, 83, 26, 75, 47]. A narrow implication of the perspective on robotic rehabilitation is that robotic assistance may have to focus on encouraging voluntary effort of participants as much as possible while movement deficits are minimally assisted in completing a goal. A simple effortless repetition based on a position control may not be sufficient because a rigid guidance from a position controlled robot discourages voluntary movements of

patients. In this perspective, allowing a dynamic interaction, which occurs through force and impedance, between robots and human would be essential to promote motor learning.

Dynamic interaction with a robot is also beneficial in assisting repetitive passive exercises. Regardless of motor learning principles, massed repetition is also essential in rehabilitation, especially for passive range of motion (ROM) exercises. Passive ROM exercises keep flexibility and range of motion, and prevent immobility, soft tissue and muscle contracture, or cartilage inflammation in the human body with paralysis, spasticity, muscle tone, or exaggerated stretch reflexes [138, 48]. Without accounting for the unexpected resistances to passive movements, position-controlled robots could injure subjects or impose an excessive pain because position control is robust to those 'disturbances' and proceeds with a given task regardlessly. Robots could also lead to over-extension and injuries in a joint at its limit of the range in passive exercises. While a certain level of resistance from the deficits needs to be overcome to complete the given passive exercise, forces applied by robots have to be under 'surveillance' all the time, and restricted to a certain level of values that depends on the physical condition of individuals if necessary.

To maximize voluntary movements of patients, a robot needs to be dynamically transparent as much as possible to let users take over the task when they can [53, 76, 78]. Dynamic transparency requires robots to have a good performance in force and impedance control, relying on the minimum impedance that robots can achieve. In passive exercises, impedance controlled robots can safely pull the subject's limbs with a regulative compliance while explicitly limiting the

maximum force. The controllability of force and impedance also enables a variety of therapeutic paradigms based on neurological hypotheses such as training with an error augmentation induced by a force field [111]. Therefore, rehabilitation robots with force and impedance controllability open up the possibility of developing advanced rehabilitation exercises based on motor learning principles and provide a safe environment for human-robot interactions.

1.2 Reviews on State-of-Art Robots for Upper-Body Rehabilitation

1.2.1 Review from Kinematic Perspective

Some existing upper-body exoskeletons support the mobility of the gleno-humeral joint, excluding that of the shoulder girdle [114, 44, 70, 151, 140]. These exoskeletons typically attach to the user's hand or wrist and not to the upper arm, and missing a connection to the upper arm makes the robots less sensitive to the kinematic compatibility around the shoulder allowing simplicity in robot design. Exoskeletons with a connection at the upper arm are beneficial in assisting upper limb motion with proper coordination at the shoulder but require careful attention in kinematic design to match with the anatomical structure including the mobility of the shoulder girdle to minimize undesirable residual force applied to the human joints.

Some exoskeletons are designed to partially support the mobility of the shoulder girdle: either elevation-depression [16, 104] or protraction-retraction [130]. Another design idea is to support shoulder girdle movements either with passive

joints [137] or with a combination of passive and active joints [123, 35]. These systems comply with full mobility of user-driven shoulder girdle movements with the advantage of self-alignment. The presence of passive joints, however, can limit active assistance to the shoulder girdle mobility. Also, the robots alone cannot fully control task-space forces at the end-effector or other locations while the robots worn by the human can partly control task-space forces using the human body as a leverage. The forces applied by the robot can induce reaction forces transferred to the human skeleton through the passive joints, which may cause undesirable stresses on the human joints. A 6-DOF end-effector connected to the upper arm also allows for full mobility of the shoulder [132], but the kinematic chain closed by the human shoulder can impose undesirable reaction forces on the shoulder joint in rehabilitation applications where usually large forces are required. One exoskeleton design supports both elevation and protraction with a 2-DOF mechanism that characterizes the kinematics of the shoulder girdle [5]. However, this idea has only been presented conceptually, and the proposed shoulder mechanism is bulky, limiting its extension to a bi-manual design with a wide range of motion.

Most upper-body exoskeletons for rehabilitation including MEDARM are unilateral, targeting uni-manual therapy. Those systems are interchangeable between the right and left configuration, enhancing cost effectiveness of the system. However, bilateral training is considered as an essential part of upper-body rehabilitation as positive evidence is discovered [135, 153, 19]. Some designers assume a bimanual robot can be achieved by a mirror-copying of their uni-manual robot. However, a mirror-copying can cause interference problem between the right and

left sides of shoulder mechanisms at a high abduction especially when the mechanism has a shoulder girdle mobility.

Some upper-body exoskeletons for rehabilitation are designed to be attached to fixed frames partially due to relatively large-sized shoulder mechanisms. An exoskeleton with a stand-alone structure and a compact form factor will be beneficial in installation at clinical facilities and providing remote rehabilitation. Also a stand-alone structure is expendable for an additional mobility when necessary such as the torso movement.

1.2.2 Review from Dynamic Perspective

The ability to control force and impedance is essential for providing natural and safe dynamic interactions between patients and exoskeletons [53, 76, 78] and for implementing novel therapy interventions.

Several end-effector type devices are capable of high performance of force and impedance control thanks to low inertial linkages driven by direct-drive motors equipped with torque sensors [76], but such a configuration is difficult to implement in an exoskeleton due to its three-dimensional kinematic structure with large degrees of freedom. Although a cable-driven actuation with a direct-drive or low gear reduction is one solution [114, 5], friction from complex cable routing and highly coupled cable tension reduce the quality of force and impedance control. Position control-oriented actuation with a force feedback from a rigid force sensor such as a load cell usually uses admittance control scheme; however it exhibits limited performance in low impedance behaviors [147]. When the force sensors

are located in an interaction port, the non-collocation issue further limits force control [34].

A series elastic actuator (SEA) is well known as an actuation configuration that is beneficial for controlling force/torque and impedance behavior [118, 150, 127]. Several rehabilitation robots have adopted SEAs for their actuation and exhibited satisfactory behaviors. To date, however, no full-size upper-body exoskeleton robot has adopted SEAs. This may be partly because it is difficult to secure a wide range of motion in many degrees of freedom structural design with a relatively larger size of SEA compared to general geared electric motors.

1.3 Goal and Scope of Work

The goal of the work in this dissertation is to develop an upper-body exoskeleton with its control framework that supports natural coordination with a wide range of motion and serves as a substrate for developing advanced robotic rehabilitation exercises based on motor learning principles. To achieve the goal, the exoskeleton is designed to be equipped with an anatomical structure, especially around the shoulder that supports the full mobility of the upper limb, and a torque-controllable actuation unit that controls force and impedance delicately. The control baseline is designed to achieve a minimum impedance behavior to promote dynamic transparency in user's voluntary movements. The framework serves as a platform of other robotic behaviors for advanced exercises by superimposing desired impedance behaviors while a coupled stability between the robot and human is guaranteed. Also, a control for assisting the coordination of the shoulder is im-

plemented in the framework, which can be applied to support other interjoint coordination. The mobility and dynamic behavior were evaluated to confirm the design goals, and a human subject study was performed to assess the effectiveness of the robot's shoulder mechanism and control algorithm in assisting the coordination in the shoulder.

1.4 Dissertation Outline

This dissertation presents a bi-manual upper-body exoskeleton, called HARMONY, with an anatomical shoulder mechanism that provides a natural mobility around the shoulder with a wide range of motion, powered by series elastic actuators. First, the hardware design is described after reviewing the human shoulder anatomy, followed by a description of a dynamic modeling process. The following chapters present the baseline control and stability analysis. The next chapter shows an experimental evaluation of the exoskeleton in kinematic and dynamic perspectives. Lastly, a human subject study is described, followed by discussion and conclusion.

Chapter 2

Human Shoulder Kinematics for Exoskeleton Design

2.1 Shoulder Biomechanics and Coordinated Motion

The skeletal structure of the shoulder complex consists of the scapula, clavicle, and humerus as shown in Fig. 2.1. The humerus articulates with the scapula via the glenohumeral (GH) joint, and the scapula is connected to the clavicle via the acromioclavicular (AC) joint. The clavicle is grounded to the thorax via the sternoclavicular (SC) joint. The clavicle and the scapula form the shoulder girdle, which is the foundation of the GH joint. Although the scapulothoracic (ST) joint is not a bony articulation, the scapula slides and rotates with constraints to the scapulothoracic gliding plane [146], where the scapula floats on muscles. Consequently, the shoulder girdle connecting the ST, SC and AC joint forms a closed kinematic chain and provides a stable base for the GH joint with the aid of muscles and ligaments [71]. Note that, from the kinematic point of view, the only bony connection from the shoulder girdle to the thorax is the connection along the clavicle with the AC and SC joint.

The shoulder complex is cooperatively actuated by a number of muscle groups with a variety of insertion points. For the process of shoulder abduction, for example, a significant amount of torque on the GH joint to abduct the humerus

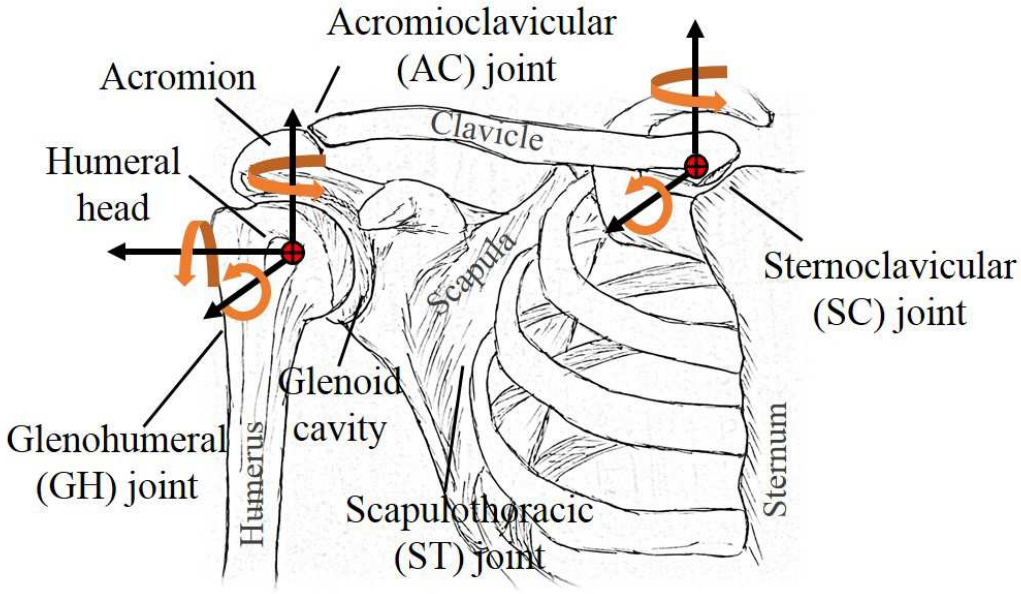

Figure 2.1: Skeletal anatomy of the shoulder complex.

is provided by the rotator cuff and deltoids, which originate from the shoulder girdle and are inserted into the humeral head and humerus, while the rotator cuff secures the humeral head in the glenoid cavity. Simultaneously, the trapezius and serratus anterior, which originate from the thorax and are inserted into the scapula, rotate the scapula upwards, and the levator scapula and rhomboid assist the upper trapezius in elevating the scapula [36, 57, 41]. Thus, the load from the arm transfers to the shoulder girdle and to the thorax in a cascade via muscles and tendons. This process underlies the coordinated motion of the shoulder girdle that is strongly coupled to the motion of the upper arm. Figure 2.2 illustrates an example of a coordinated motion during shoulder abduction. The coordinated motion is called the scapulohumeral rhythm (SHR), where the motion of the humerus accompanies the scapula's internal-external rotation, downward-upward rotation, and anterior-

posterior tilt. The SHR is characterized by the ratio of the humeral elevation to the scapular upward rotation. The ratio was originally believed to be 2:1, but recent studies show it to be nonlinear and to vary not only across individuals but also by situations such as a load on the arm [96, 91, 72]. Besides the coupled scapular upward rotation, protraction-retraction is also coupled with the motion of the arm. For example, a reaching movement of the arm is accompanied by protraction of the scapula [128]. The coordinated motions of the shoulder are essential for shoulder muscle function and joint stability and significantly affect recovery of upper limb mobility [29, 42].

The wide range of motion of the upper extremity is partly due to the coupled motion between the humerus and the shoulder girdle. The glenohumeral (GH) joint approximates a ball-and-socket joint providing a wide range of motion while the rhythmic motion of the shoulder girdle further enhances mobility [116, 42]. For example, the upward rotation of the scapula, which itself is a result of the rhythmic motion, contributes to the wide range of motion during shoulder abduction by preventing impingement of tendons on the humeral head to the acromion and by keeping an optimal muscle force-length relation for the primary humeral elevators [97].

2.2 Approximation of the Shoulder Girdle Kinematics

Movements of the shoulder girdle result in translational motions of the glenohumeral (GH) joint such as elevation-depression and protraction-retraction. For kinematic compatibility of an exoskeleton, the shoulder mechanism of an ex-

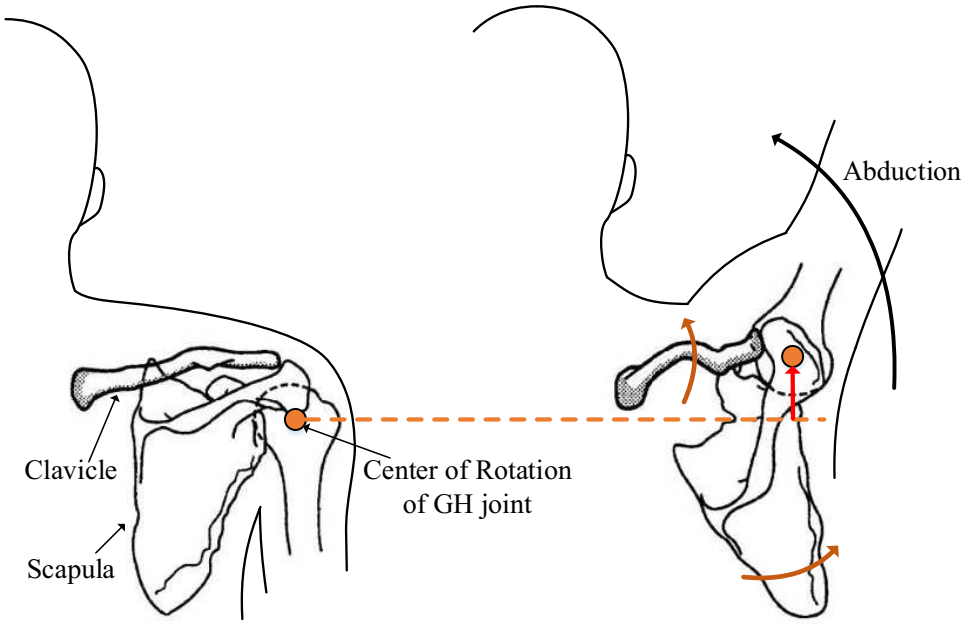

Figure 2.2: An example of the coordinated motions: the shoulder girdle, consisting of the scapula and clavicle, rotates and elevates in accordance with humeral elevation. As a result, the center of rotation of the glenohumeral (GH) joint shifts (the figure is adapted and modified from [145]).

oskeleton needs to follow the translational motion of the GH joint so that the center of rotation of the mechanism matches that of the GH joint.

During movements of the shoulder girdle, the scapula exhibits a complex motion consisting of three-dimensional rotation and translation along the curved plane while the clavicle performs a pivot motion. We assume that the translational motion of the GH joint mainly results from the pivot motion of the clavicle with respect to the sternoclavicular (SC) joint because the clavicle is the only bony connection from the GH joint to the thorax. Although the humeral head sits on the glenoid

of the scapula, the relative motion of the glenoid with respect to the clavicle is small because the end of the clavicle is attached close to the glenoid through the acromioclavicular (AC) joint and the motions of the AC joint are very small [84, 129]. If the clavicle with the sternoclavicular (SC) joint delivers the majority of translation of the GH joint, we could design the shoulder girdle mechanism by replicating the simple kinematic structure of the clavicle.

In case the glenohumeral (GH) joint is translated by a pivot motion of the clavicle, the trajectory of the translation would be a circular arc. To verify this assumption, we recorded the trajectory of the acromion of a healthy subject, which is located right above the GH joint, during repetitive shoulder elevation-depression and protraction-retraction using a motion capture system (PhaseSpace, Inc.). The markers were attached on the sternum, sternoclavicular (SC) joint, and acromion. The trajectory of the acromion with respect to the SC joint was fitted to a circle based on least squares. The results in Figure 2.3 show that the trajectory of the glenoid falls on a circular arc. Therefore, it is possible to translate the GH joint by a link pivoting around the center of rotation of the circular arc, and the shoulder girdle mechanism can be simplified as a link with two revolute joints. Although the clavicle-like shoulder girdle mechanism may not provide all the mobility of the scapula, the mechanism may promote motor recovery of the scapula by translating the lateral angle of the scapula. For example, elevating the lateral angle area provides moment and force to cause upward rotation and elevation of the scapula.

The experimental results indicate that the center of rotation of elevation-depression and protraction-retraction in the shoulder girdle motion shifts away from

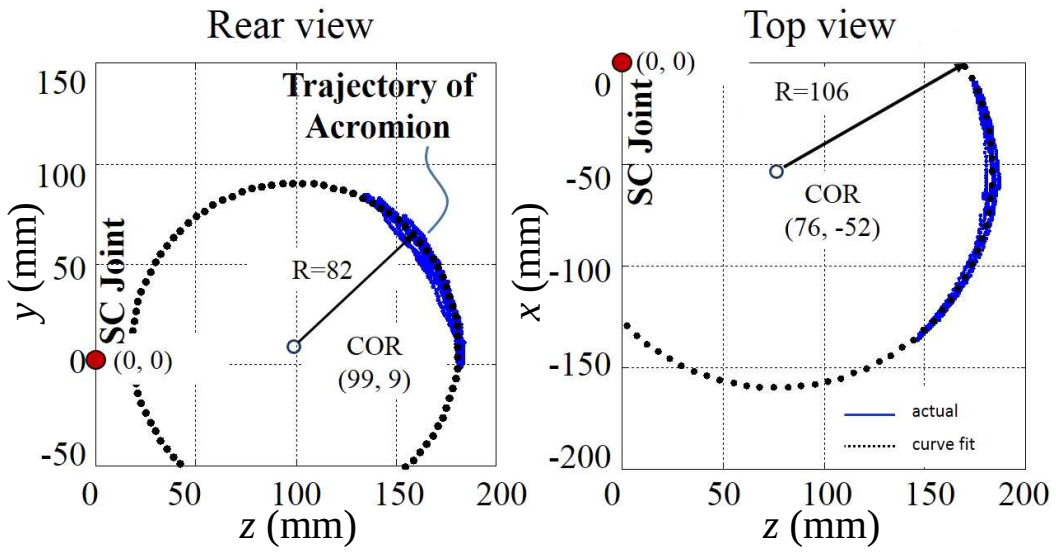

Figure 2.3: The trajectory of the acromion during the right shoulder girdle motion of a healthy subject: (a) elevation-depression and (b) protraction-retraction. Axes x, y, and z are aligned with the sagittal, longitudinal, and frontal axis, respectively.

the sternoclavicular (SC) joint. This shift probably occurs when the distance between the glenohumeral (GH) joint and the SC joint is reduced as muscle contraction around the shoulder girdle increases during shoulder elevation or protraction. As a result, the curvature of the trajectory is deformed and causes the shifted center of the approximated circle. Constraints from ligaments around the SC joint are also partly responsible for shifting the center of rotation away from the SC joint [84]. The amount of shifting and shortening may vary across individuals by their body size and flexibility around the shoulder. To support the shifted center of rotation with the shortened radius, a shoulder girdle mechanism requires an adjustable location of the pivot point and a link with an adjustable length.

The pivot motion of the clavicle, the sternoclavicular motion, consists of elevation-depression, protraction-retraction, and anterior-posterior axial rotation. The mobility of anterior-posterior axial rotation of the clavicle can be safely ignored during the design of the shoulder girdle mechanism because the functionality of anterior-posterior axial rotation widens the range of motion of the glenohumeral joint but does not add another degree of freedom. For example, during forward flexion of the humerus, the posterior axial rotation of the clavicle with the posterior tilt of the scapula opens up the acromion to prevent impingement of tendons of the rotator cuff, and consequently, the range of motion of the forward flexion becomes wider. In place of axial rotation of the clavicle, we can design the ball-and-socket joint itself to provide a sufficiently wide range of motion.

Chapter 3

Robot Design

Based on the findings on the biomechanics of the human shoulder, the first goal of this study is to design a kinematic structure that supports natural mobility and a wide range of motion of the upper body especially around the shoulder. For kinematic compatibility, a shoulder mechanism must include mobility of the shoulder girdle as well as that of the glenohumeral joint. HARMONY's shoulder kinematics has five main degrees of freedom (DOFs) composed of three DOFs at the glenohumeral joint and two DOFs at the shoulder girdle.

The design also aims at a bi-manual structure for a bilateral training that enhances rehabilitation results depending on the clinical status of patients [154]. Designing a bi-manual structure requires more than a mirror-copy. Both sides of shoulder mechanisms must be designed to avoid interference with each other during shoulder abduction. A controller also needs an algorithm to avoid a self-collision between arms. Also, the design pursues a stand-alone configuration without a large fixed frame on the floor or wall for extensibility. For example, a reaching movement of the arm is accompanied by an inclination of the torso in healthy subjects [128]. A stand-alone system can be easily extended to be combined with a back-support mechanism to generate motion of the torso.

The final design of the exoskeleton robot consists of a 14 degrees of freedom (DOFs) bi-manual structure with five DOFs on each shoulder, one DOF for each elbow, and one DOF for each forearm, arranged in a stand-alone structure. The shoulder mechanism is fully actuated by five active joints attached to a kinematic structure of a set of revolute joints and a parallelogram, which provides a good kinematic compatibility and a wide range of motion. The design details are described in the following subsections.

3.1 Shoulder Mechanism

The glenohumeral (GH) joint can be approximated as a ball-and-socket joint because the humeral head rotates inside the glenoid fossa of the scapula with negligible translation [148]. A ball-and-socket joint is kinematically equivalent to a serial chain with three rotational joints whose axes intersect at a single point. When the serial chain is placed alongside the shoulder, kinematic compatibility requires that the intersection point of the serial chain co-locates with the center of rotation (COR) of the GH joint. This constraint is critical for minimizing undesirable joint stresses that may cause pain or facilitate subluxation of the GH joint.

3.1.1 Shoulder Girdle Mechanism

A scapula-like mechanism, as illustrated in Figure 3.1, could translate the ball-and-socket mechanism. The scapula-like supporter attached to the outside of the scapula follows the scapular rotation and translation. However, the scapula-like supporter requires many degrees of freedom to connect to the ground because

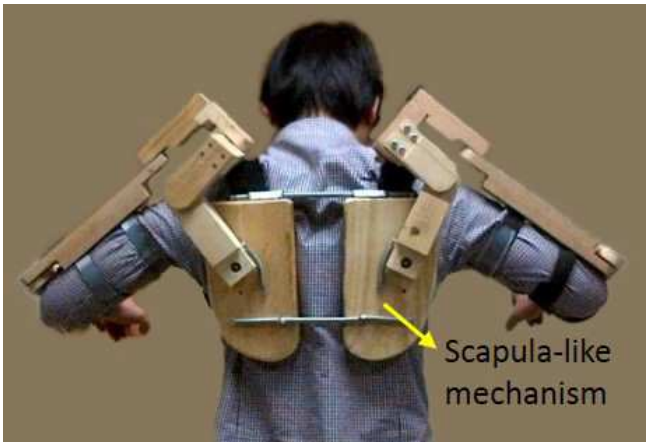

Figure 3.1: A prototype with a scapula-like shoulder girdle mechanism, which follows scapular motion well, but requires excessive degrees of freedom to connect the ground

of the complexity of the motion: three-dimensional rotation and three-dimensional translation along the curved scapulothoracic gliding plane. In addition, it is difficult to connect the supporter to the scapular securely because only the posterior surface of the scapula is exposed and there is little room to connect the mechanism.

The ball-and-socket joint mechanism must follow the translational motion of the glenohumeral joint induced by the motion of the shoulder girdle to match the center of rotation of the ball-and-socket mechanism with that of the glenohumeral joint. A clavicle-like kinematic structure is potentially a simple solution because it needs only two revolute joints as shown in Figure 3.2a. The first joint, $J1$, duplicates the shoulder elevation and depression and the second joint, $J2$, duplicates the shoulder protraction and retraction. A prototype with the clavicle-like shoulder girdle mechanism (Figure 3.2b) was built and tested to validate its kinematic compatibility. The mechanism provided enhanced mobility along shoulder eleva-

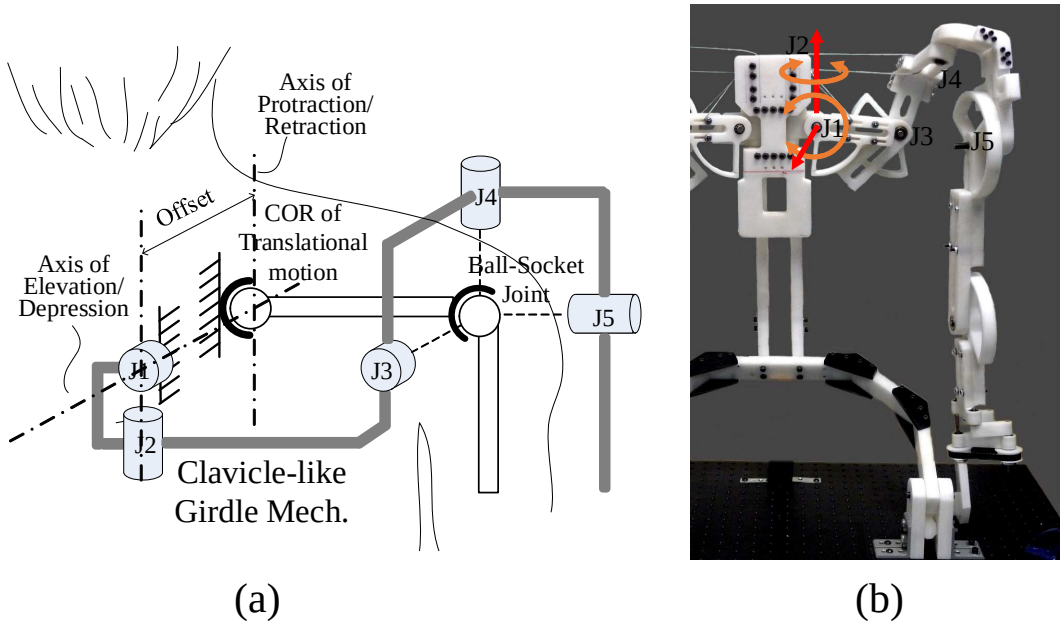

Figure 3.2: A clavicle-like shoulder girdle mechanism: (a) schematic view of the mechanism, and (b) a prototype. Kinematic tests with the built prototype revealed that motion in J2 did not match with protraction and retraction of the shoulder.

tion and depression; however, shoulder protraction and retraction was limited due to the constraint from the girdle mechanism. This constraint stems from the kinematic discrepancy between the shoulder and the mechanism caused by the offset between the center of rotation of the shoulder and that of the mechanism as shown in Figure 3.2a. $J2$ may locate above the head to coincide with the axis, but this configuration restricts the range of motion of bi-manual abduction because of the collision between joint $J2$s at both sides.

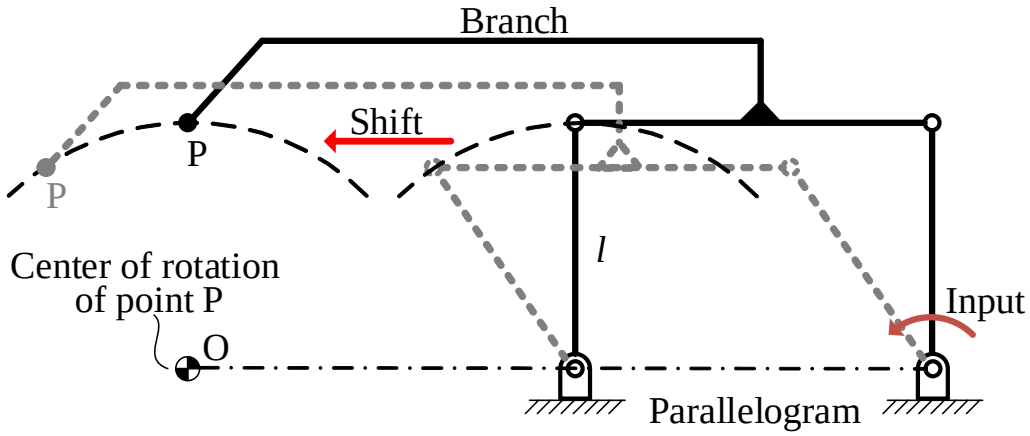

Figure 3.3: A parallelogram shifts a circular arc motion. The input can be considered as the motor input, point P as the center of the GH joint, and point O as the center of rotation for protraction and retraction.

3.1.2 Parallelogram in the Girdle Mechanism

To resolve the kinematic discrepancy in protraction and retraction, we developed a shoulder girdle mechanism equipped with a four-bar parallelogram linkage, which is capable of shifting circular motions. Figure 3.3 shows the principle of the shifting with a parallelogram mechanism. The circular motion of point P can be shifted in any direction depending on the shape of the branch while the radius of the circular motion remains unchanged, which is the same as length l of the link in the parallelogram. If the ball-and-socket joint is connected to the branch, point P can be considered the center of rotation (COR) of the ball-and-socket joints. By replacing axis $J2$ in Figure 3.2a with the parallelogram $J2\ J2'\ J2''\ J2'''$ in Figure 3.4, the whole ball-and-socket mechanism translates so that the COR of the ball-and-socket joint follows a circular trajectory with respect to the actual COR of

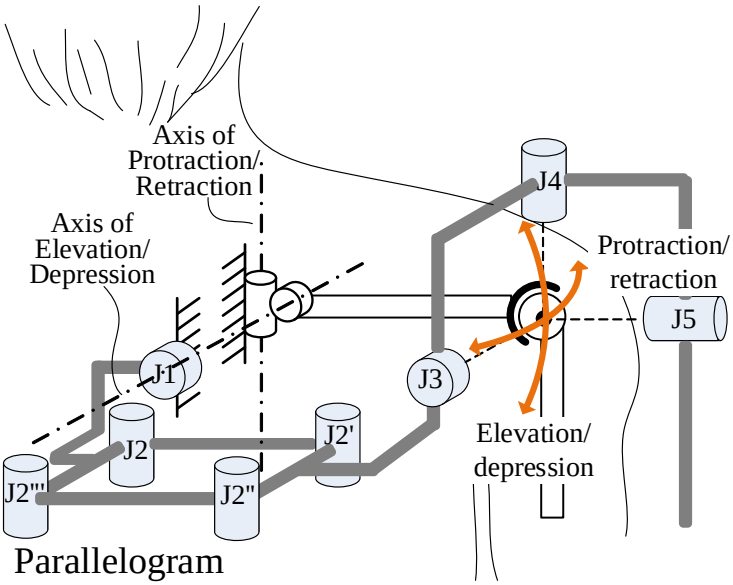

Figure 3.4: Schematic view of a shoulder girdle mechanism combined with a parallelogram.

the shoulder for protraction and retraction. Consequently, a compact form factor is maintained; the shoulder girdle mechanism provides both protraction-retraction and elevation-depression with a good kinematic compatibility.

3.2 Ball-and-Socket Joint

For a ball-and-socket joint, many exoskeleton robotic systems have adopted a serial chain with three revolute joints (Figure 3.5a, b) or two revolute joints with a large circular bearing that encircles the upper arm (Figure 3.5c) [5, 16, 114, 104]. Each configuration has different mechanical characteristics in terms of singularity and range of motion (ROM). For example, the ROM of shoulder abduction in the first configuration is limited mainly by a collision between joint $J4$ and the shoul-

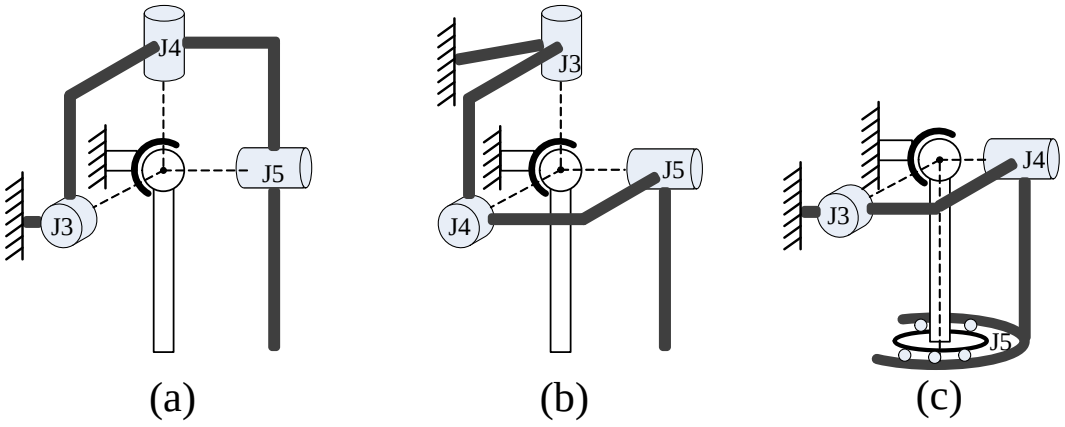

Figure 3.5: Examples of the serial chains representing motions of ball-and-socket joint.

der or the head, while the second configuration is limited mainly by a collision between joint $J3$ and $J5$. The third configuration (Figure 3.5c) could provide a larger range of motion for shoulder abduction than the two above but the encircled structure around the upper arm may cause interference with the upper torso during various arm movements when the upper arm comes closer to the torso. In all three cases, mechanical singularity occurs when the three axes lie in the same plane although the arm configuration is different in each case. In Figure 3.5, the first mechanism approaches singularity at extreme shoulder horizontal flexion with shoulder internal rotation that is already out of the range of motion for activities of daily life (ADL) [94]. Similarly, the second mechanism approaches singularity at extreme shoulder adduction with shoulder external rotation that also rarely occurs. On the other hand, the third mechanism approaches singularity with shoulder forward flexion at 90 degrees.

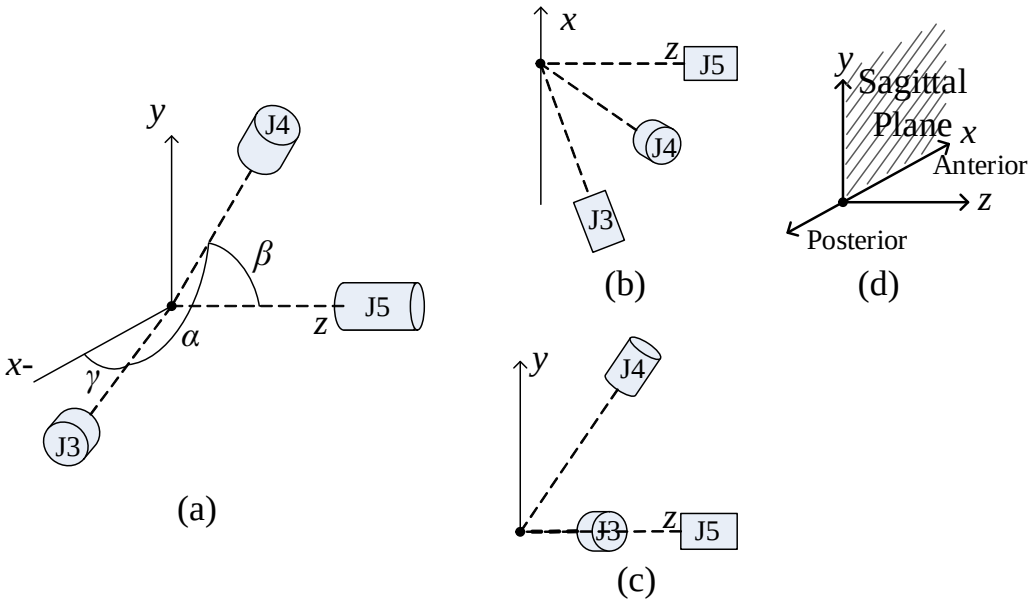

Figure 3.6: The optimized mechanism for the GH joint in the right shoulder: (a) isometric view, (b) top view, (c) rear view, and (d) plane definition.

We adopted the first configuration (Figure 3.5a) because of its ability to provide a wide range of motion. To further enhance the range of motion while avoiding singularity, three axes are positioned with an acute angle to each other instead of a perpendicular arrangement (Figure 3.6).

Accordingly, the joint at the top of the shoulder, $J4$, is aligned to the vertical axis with an angle outwards and backwards. In addition, axis $J3$ is aligned to the sagittal axis $x - x$ with an angle outwards, so that joint $J4$ is leaning toward the back side of the shoulder during shoulder abduction and avoids collision with the shoulder or the head. For design simplicity, the orientation of joint $J5$ at the default pose with relaxed arms points in the direction of the transverse axis $z - z$.

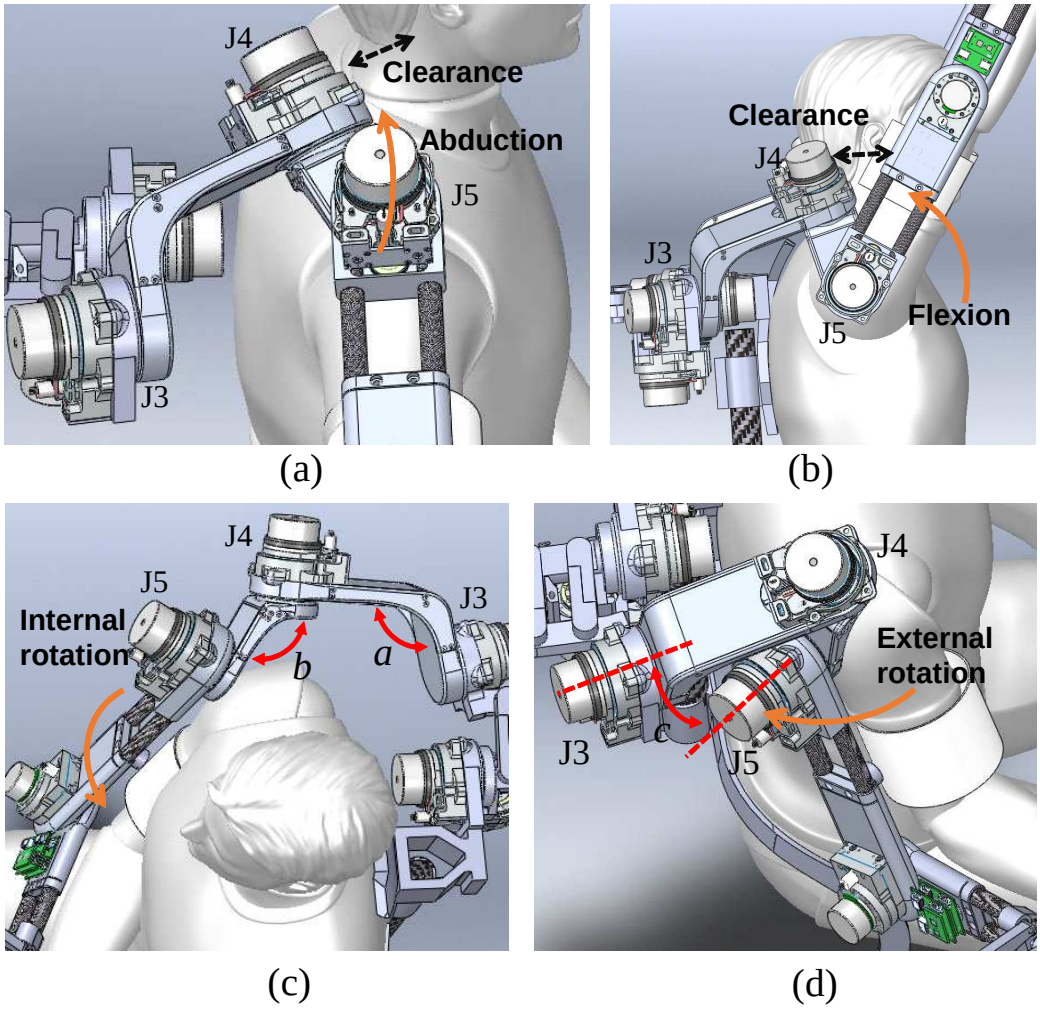

Figure 3.7: The 3-DOF ball-and-socket joint. An oblique arrangement of joint $J4$ provides a clearance with the head during abduction (a), and also a clearance with the upper arm during forward flexion (b). The bigger values of the angles *a* and *b* (smaller α and β in Figure 3.6), the smaller the range of motion of the internal rotation due to the singularity among $J3$, $J4$, and $J5$ (c). In the case of very large γ in Figure 3.6 (less margin at angle c), the range of motion of the external rotation is limited by the interference or singularity between the joint $J3$ and $J5$ (d).

Angles $\alpha,\ \beta$ and γ are determined based on the shape and volume of the actuators on the joint, and on the trade-off between a large abduction angle and avoidance of singularity. Figure 3.7 shows an example of the relationship between those angles, range of motion and singularity. When angle α and β are smaller, axis $J4$ lies further outwards and backwards from the shoulder, where more clearance is ensured between $J4$ and the shoulder at high abduction angles (Figure 3.7a) and between $J4$ and the upper arm at high forward flexion angles (Figure 3.7b). However, a smaller angle restricts the range of motion of the arm posed in front of the torso (Figure 3.7c). A larger angle of γ in Figure 3.6 secures more clearance for axis $J4$ during the abduction, but the larger angle limits the range of external rotation because of the interference or singularity between joint $J3$ and $J5$ (Figure 3.7d). With the angles between the axes, the distance between the intersecting point and each joint also affects the range of motion. Especially, ROM of bilateral abduction is mainly limited by a collision between both sides of $J4$, which is facilitated by the increased angle of $J1$ during the coordinated motion of the shoulder girdle mechanism. ROM of unilateral abduction is mainly limited by the interference between $J4$ and the ipsilateral shoulder. A higher position of $J4$ increases the angle where the interference in the unilateral abduction occurs, but reduces the angle where the collision in the bilateral abduction occurs.

The 3D interactions between complex surfaces of the human body, actuator units, and linkages are impossible to model accurately, making it difficult to use a numerical optimization technique. So, we used a number of 3D-printed mock-ups to determine the parameter values for the mechanism that result in a large range of

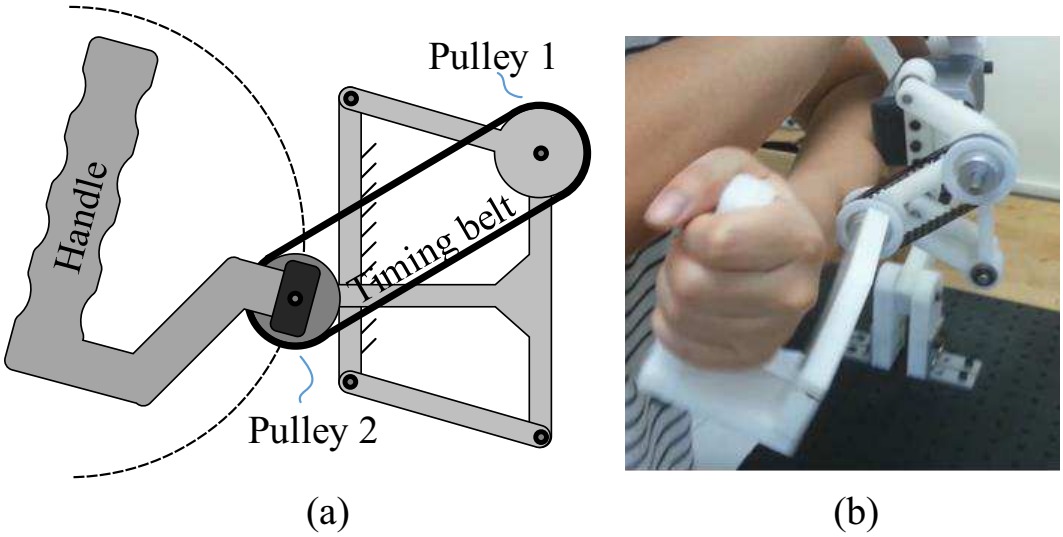

Figure 3.8: A new mechanism for supporting pronation and supination of the forearm: (a) the kinematic diagram, and (b) the prototype of the mechanism.

motion.

3.3 Forearm Mechanism

To support rotational motion along the longitudinal axis in the body segment, such as pronation and supination of the forearm, we developed a new mechanism with a light and compact structure. In many wearable robots, such rotational motions are generated by a curved rail bearing [114] surrounding the arm segments. However, this bearing is generally bulky and heavy, and could possibly restrict the range of motion of the arm in a situation where the upper arm moves close to the torso. Figure 3.8 shows our new mechanism that generates the same motion with a curved linear bearing. This mechanism consists of a parallelogram and a transmission that transfers the rotation of the link in the parallelogram to the handle. Pulley

1 rotating with the link in the parallelogram drives the timing belt connecting pulley 2. Pulley 2 is grounded via a bearing to the branch extruding from the other link in the parallelogram. Then, a handle or a wrist mechanism attached to pulley 2 revolutes along a circular path and simultaneously spins about the axis of pulley 2. The transmission can be either a timing belt, a gear train or an auxiliary parallelogram as long as it delivers the same rotational direction with a 1-to-1 gear reduction ratio. This mechanism is potentially light and easy to build. Another mechanism for supporting rotation along longitudinal axis has been presented previously [137] but the underlying kinematics of our design is distinct resulting in a more compact structure.

3.4 Final Kinematic Design and Alignment

In the final kinematic design of the shoulder mechanism (Figure 3.9), joints $J3$, $J4$, and $J5$ consisting of the ball-and-socket joint are arranged at an oblique angle to each other, thus increasing the range of motion while avoiding mechanical singularity within the workspace of the upper limb. The ball-and-socket joint connects the shoulder girdle mechanism, consisting of one revolute joint $J1$ and parallelogram $J2$, which translates the ball-and-socket joint along the trajectory of shoulder protraction-retraction and elevation-depression. The distance between both sides of $J1$ and length of the link in the parallelogram are adjustable to match shoulder size and radius of the shoulder girdle motion. The upper-arm and forearm segments are also adjustable for a wide range of subject body dimensions.

Alignment between the robot and the human body is important since mis-

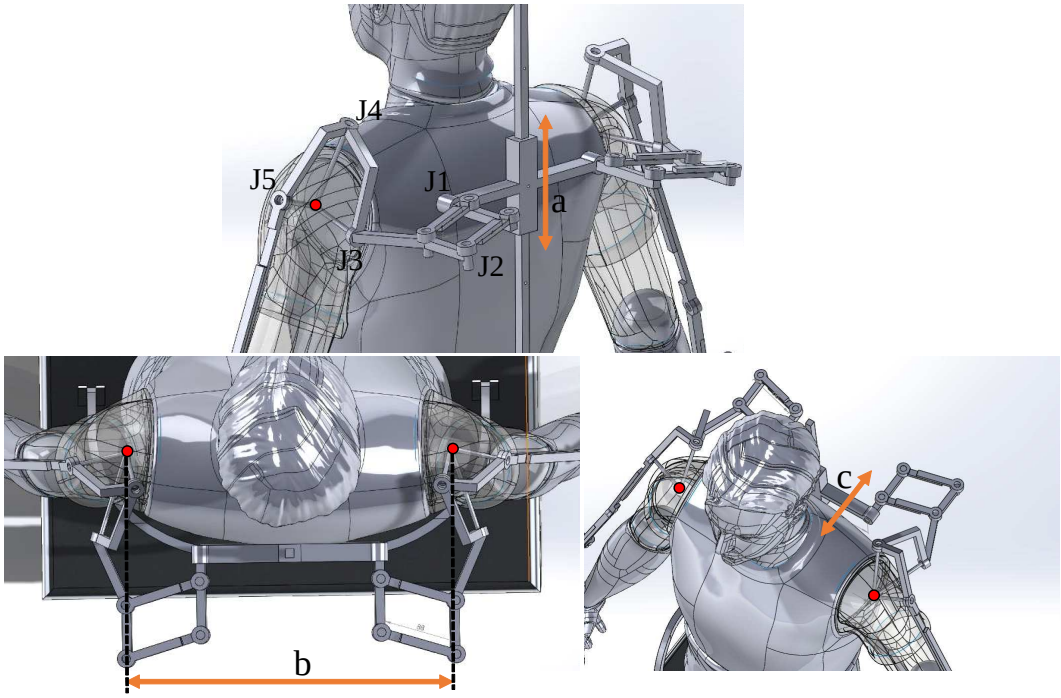

Figure 3.9: The final kinematic design of the shoulder mechanism. The three adjustment parameters a, b, and c allow to align the center of rotation of the *ball-and-socket joint* with that of the subject's glenohumeral joint.

alignment may cause undesirable stress on the subject's musculoskeletal system. The center of rotation (COR) of the ball-and-socket joint matches that of the glenohumeral joint in terms of three parameters: 'a' elevation of the shoulder mechanism, 'b' distance between both sides of $J1$, and 'c' gap between the back and the shoulder mechanism. Adjustment for parameter 'a' and 'c' is relatively straightforward if a therapist recognizes the COR of the glenohumeral joint by palpation and visual observation. The shoulder width is also easily adjustable by fitting the both-side upper-arm cuff to the body. However, the ratio between the length of parallelogram and subject's shoulder width needs to be investigated through a human

subject study. For example, around 60% of the distance between the sternoclavicular and acromioclavicular joints was acceptable for a good kinematic compatibility throughout a number of individuals in our trials. Using such a ratio, adjustment of shoulder width and parallelogram length can be done by one-time measurement of subject's shoulder dimension. The adjusting mechanism in the current system is realized by a sliding mechanism with a lock, but a quick adjustment mechanism may need to be developed to reduce setup time in the clinical application.

Adjustment process requires to measure subject's body size including shoulder width and sitting height at the beginning of rehabilitation process. The torso of a hemiparesis patient is usually lopsided, and both sides shoulders are unleveled. So, body size measurement needs to be done carefully for hemiparesis patients. The torso needs to be fixed with respect to the ground of the shoulder mechanism for alignment, and a harness is required to support the torso to be erected.

3.5 Actuation Type

Rehabilitation robots frequently provide force or impedance-based therapeutic trainings such as impedance-based resistant exercises [3] and force field-based trainings [6, 111]. For example, robots with force control can render an aquatic therapy-like environment with an active gravity compensation for the weight of the robot and full or partial weight of users while allowing user-driven free motions with or without viscous-like resistance [74]. An electrical motor permits quality of force or torque control with several configurations such as the direct-drive, a geared motor with a torque sensor, or a series elastic actuator (SEA). The direct-

drive does not satisfy our design goal because of the requirement for a large-size motor. A geared motor offers a compact size but usually needs for force feedback through a load-cell or spring. We adopt series elastic actuators (SEAs) to generate various force and impedance-based therapeutic exercises because SEAs offer precise and stable force control with robustness to impulsive external disturbances [118]. SEAs are also capable of producing a very low impedance [161], which is essential to encourage user's voluntary movements.

3.6 Fully Constructed System

Figure 3.11 shows the final CAD design of HARMONY and the constructed system. The robot is equipped with series elastic actuators (SEAs) at all 14 axes, linkages with an adjustable length, and four multi-axis force/torque sensors at the interaction ports of the wrist and upper arm. A wrist cuff and handle are commonly grounded at the force/torque sensor in the wrist. A chest harness attached to the frame is used to support the torso. Each actuator is a compact rotary SEA designed previously [33] and modified with a torque-type brushless DC motor (Maxon Motor, EC Flat series) and a Harmonic Drive (Harmonic Drive LLC, CSD Series). Specifications including continuous torque of SEA appear in Table 3.1.

The robot is operated by a real-time control system running at Linux patched with RT-Preempt (Figure 3.12). The customized motor drivers run the motor of the SEA, communicating with the Linux system via EtherCAT. A server program on the Linux system manages the EtherCAT communication with all motors and sensors, and low-level controls such as torque control. The server program runs simultane-

Figure 3.10: The CAD drawing of the upper body exoskeleton robot worn by a user

ously with a C++ code that contains a high-level control by communicating via a shared memory interface.

Safety is ensured mechanically by emergency stop buttons for the user and the operator and by hard stops at every joint. Additional safety features are added at a software level to limit a range of motion, avoid self-collision, limit joint velocity, or stop the robot at an excessive interaction force/torque.

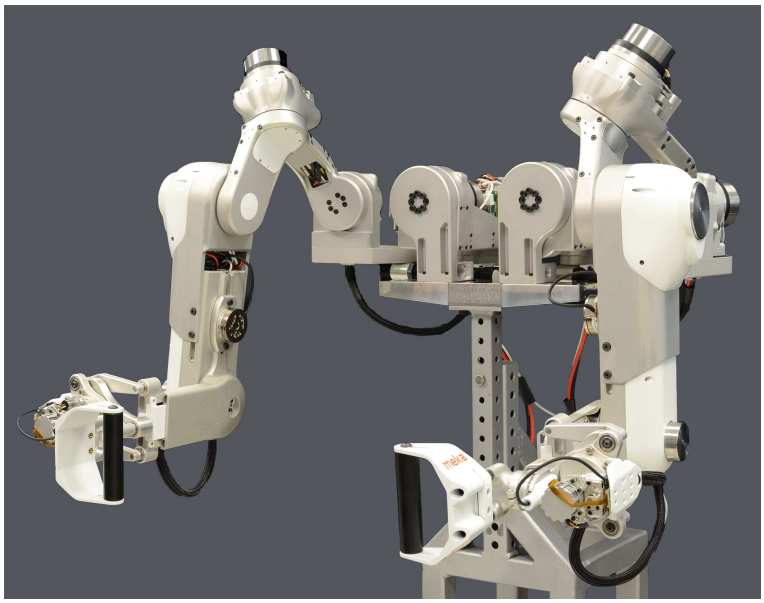

Figure 3.11: The upper body exoskeleton robot

Table 3.1: Specifications of HARMONY.

List	Value
Continuous Torque	34.4 Nm @ shoulder
	13 Nm @ elbow
	1.25 Nm @ wrist
Torque Bandwidth	7 Hz
Backdrivability	less than 0.3 Nm @ 0.6 rad/s
Robot Weight	31.2 kg excluding the frame
Control Frequency	Up to 2000Hz

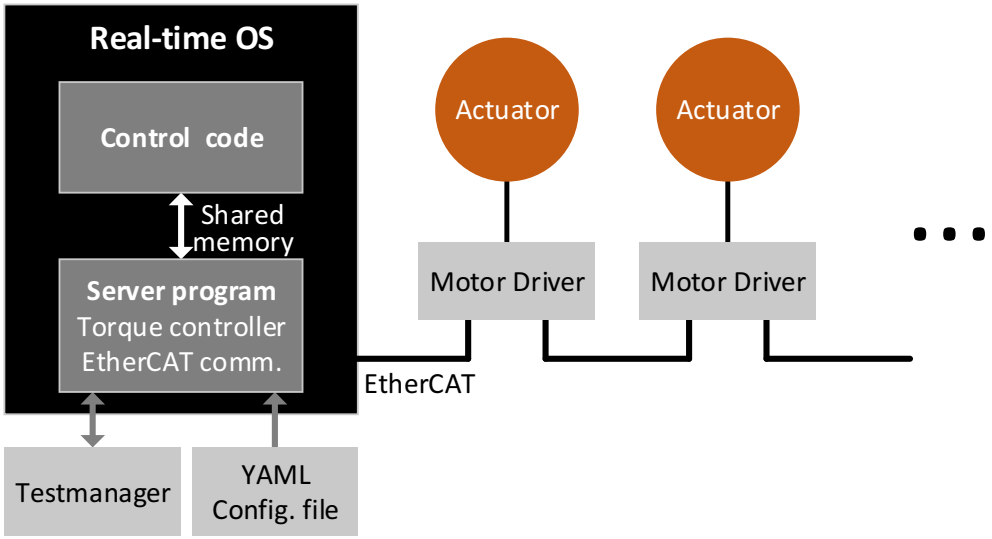

Figure 3.12: The software platform controlling the upper-body exoskeleton. A GUI interface (Testmanager from EtherLab®) to visualize parameters and a C++ environment is available. A YAML file is used to configure parameters at the start of the server program.

Chapter 4

Robot Modeling

In order to develop a control algorithm involving a feed-forward torque that compensates for the robot dynamics, an inverse dynamic model of the robot needs to be formulated. We present a methodology for modeling kinematics and dynamics of the robot that includes the unconventional parallelogram joint and adjustable-length links. Before the robot modeling, the dynamics of the series elastic actuator is first formulated.

4.1 Dynamics of SEA

In an SEA, usually a spring locates between its output shaft and a load so that the deflection of the spring directly measures output force or torque. However, the SEA in our robot adopts a flipped configuration in which a spring lies between and the stator of the motor and the ground as illustrated in Figure 4.1a. This configuration has the advantage of constructing a compact-sized SEA unit [110] and a compact actuation unit is critical for a large range of motion, avoiding interferences between actuators and links. In this configuration, the deflection of the spring does not directly measure the output torque due to the dynamics of the motor unit. The brushless DC motor with Harmonic Drive is grounded to the base via the ro-

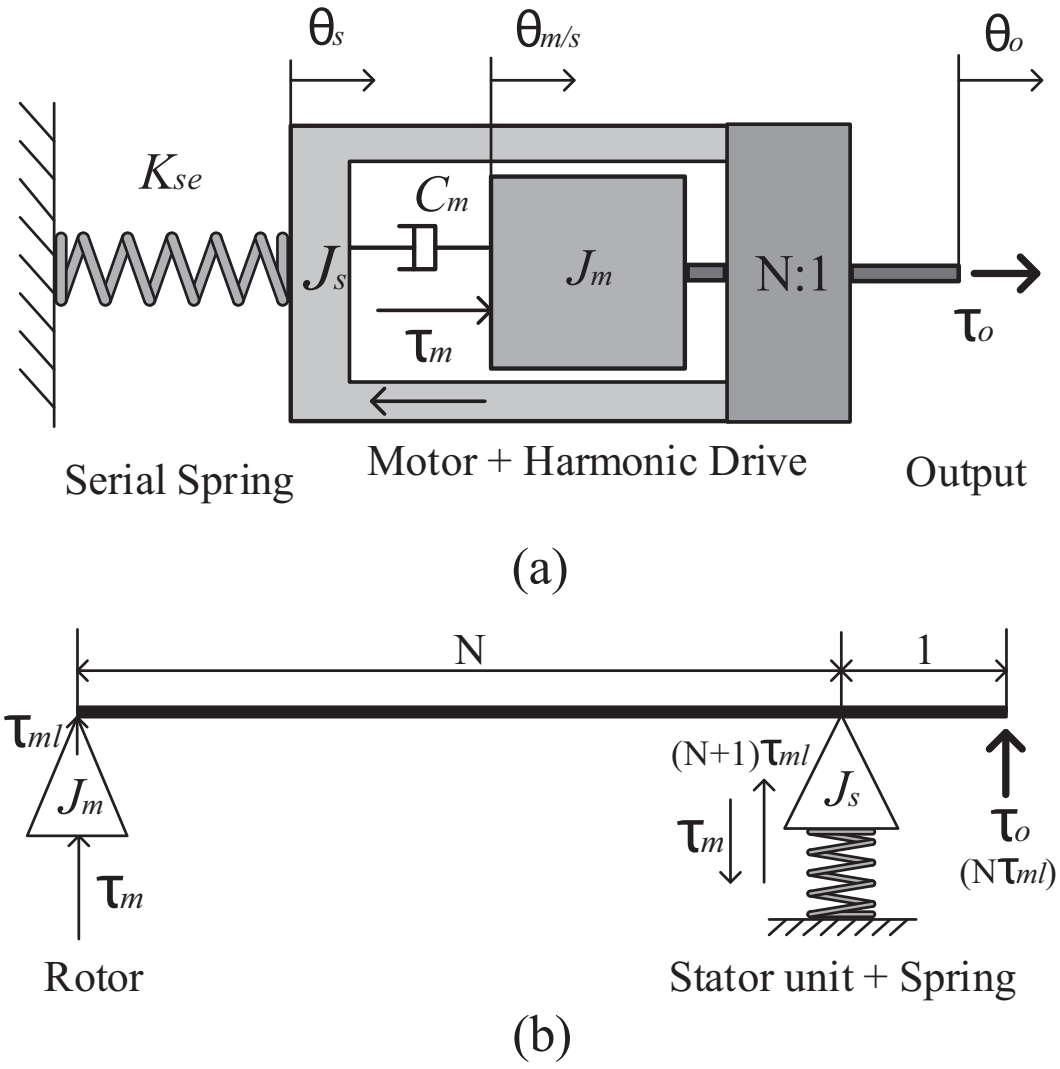

Figure 4.1: The flipped configuration of the series elastic actuator: (a) the illustration of the SEA, (b) the equivalent mechanical system

tary spring and two encoders measure the deflection of the spring and the position of the output shaft with respect to the ground, respectively. Figure 4.1b shows a dynamically equivalent mechanical system. The compliance and the mass of the

stator unit of the SEA is analogous to those of the fulcrum of the level system. At a static equilibrium, the deflection of the spring directly indicates the output torque, but movement of the masses in the input and the fulcrum adds a dynamic force to the torque output.

The deflection of the spring does not directly indicate torque output in the flipped SEA because of a dynamic force from movement of the motor unit. At a low frequency, however, the spring torque would approximate the output torque. To compare the measured torque from the spring deflection and the actual torque output, the dynamic equation of the SEA is formulated to calculate the actual torque output. Dynamics of the rotor and the stator of the motor are as follows:

$$J_m(\ddot{\theta}_{m/s} + \ddot{\theta}_s) + C_m\dot{\theta}_{m/s} + f_{hd} + \tau_{ml} = \tau_m \tag{4.1}$$

$$J_s\ddot{\theta}_s + K_{se}\theta_s = (N+1)\tau_{ml} - \tau_m \tag{4.2}$$

$$N\tau_{ml} = \tau_o \tag{4.3}$$

$$\theta_{m/s} = N(\theta_s - \theta_o) \tag{4.4}$$

where θ_s and θ_o represent the displacement of the stator and output shaft with respect to the ground, respectively and $\theta_{m/s}$ is the relative displacement of the rotor with respect to the stator. The rotation of the output of the Harmonic Drive is in the opposite direction to that of the input. Motor torque τ_m delivers a load torque τ_{ml} to the Harmonic Drive, overcoming the acceleration of the rotor with moment of inertia J_m, damping C_m, and friction f_{hd} in the Harmonic Drive. The load torque amplified by gear ratio N is transferred to the output τ_o while accelerating the stator unit J_s and deforming the spring with stiffness K_{se}. When the output shaft is fixed

($\theta_o = 0$), the output torque can be expressed as

$$\tau_o = -(J_{eq}\ddot{\theta}_s + C_{eq}\dot{\theta}_s + f_{hd} + K_{se}\theta_s) \tag{4.5}$$

where J_{eq} and C_{eq} are the equivalent moment of inertia and damping coefficient for the rotor and the stator unit. The negative sign of the torque is due to the opposite directional output of the Harmonic Drive. 4.5 indicates that the output torque differs from the spring torque because of the dynamic force of the motor unit, but the difference would be negligible when the frequency of the torque command is low. The difference is shown in Section 6.

4.2 Forward and Inverse Kinematics of the Shoulder Mechanism

The shoulder mechanism contains a parallelogram, which is a multi-link structure but still provides a motion of one degree of freedom, so that it can be treated as a joint with one joint variable. However, a parallelogram is not defined as a joint such as a revolute or prismatic joint in the conventional robotic kinematics; therefore, we need to define forward and inverse kinematics across the parallelogram. The oblique arrangement of the ball-and-socket joint also complicates the calculation of inverse kinematics. To address these problems, we have developed a methodology that includes attaching frames and performing coordinate transformations across the parallelogram and the ball-and-socket joint.

Figure 4.2 shows the coordinate representation of the shoulder mechanism. For the simplicity of calculation and angle representation, coordinate 2 is placed

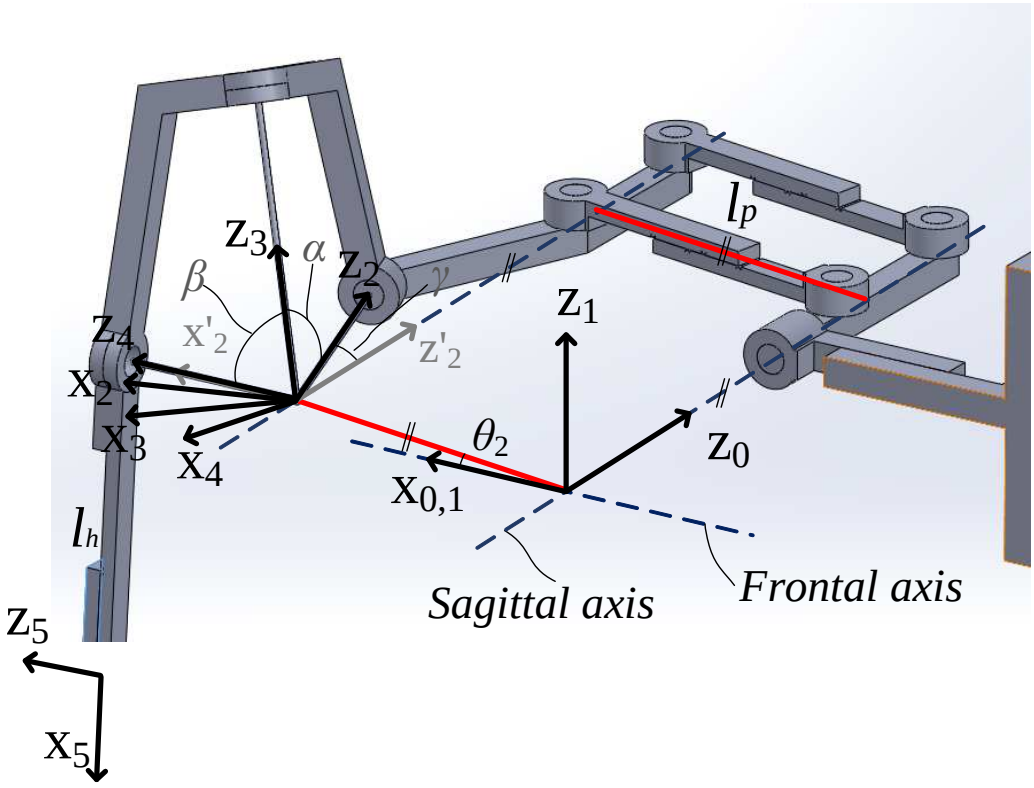

Figure 4.2: The coordinate representation of the kinematics of the shoulder mechanism. The i-th axis (z_{i-1}) is aligned to joint Ji and frame 0 is grounded. Axis x_2 of frame 2 locates at the center of rotation of the ball-and-socket joint instead of at the common normal of axis z_1 and z_2. Values of α, β, and γ are 60, 60, and 18 degrees, respectively.

at the center of the ball-and-socket joint. This is a deviation from the standard Denavit-Hartenberg (DH) convention with which coordinate 2 would be off the center of rotation of the ball-and-socket joint while the other coordinates follow the DH convention. In this case, a rotational transformation with respect to axis $y_{2'}$ by angle γ is added to transform coordinate 2 to the intermediate coordinate system of $x_{2'}$, $y_{2'}$, and $z_{2'}$, which is attached to the third link of the parallelogram where

axis z_2 is connected. Table 4.1 represents the DH parameters and the intermediate coordinate transformation for coordinate 2′.

Table 4.1: Denavit-Hartenberg parameters and the rotation for the intermediate transformation for coordinate 2.

i	a_i	d_i	α_i	θ_i
1	0	0	-90	θ_1 (variable)
2′	l_p	0	-90	θ_2 (variable)
2	rotation with respect to $y_{2'}$ by γ			
3	0	0	-α	θ_3 (variable)
4	0	0	β	θ_4 (variable)
5	l_h	0	0	θ_5 (variable)

Kinematics of a parallelogram is different from that of a revolute joint. Rotation of a parallelogram changes position but not orientation of the following linkage. Transformation between frames 2 and 1 is as follows:

$$ {}^{1}P = \begin{bmatrix} 1 & 0 & 0 \\ 0 & c\alpha_2 & -s\alpha_2 \\ 0 & s\alpha_2 & c\alpha_2 \end{bmatrix} {}^{2'}P + \begin{bmatrix} c\theta_2 & -s\theta_2 & 0 \\ s\theta_2 & c\theta_2 & 0 \\ 0 & 0 & 1 \end{bmatrix} \begin{Bmatrix} l_p \\ 0 \\ 0 \end{Bmatrix} \tag{4.6} $$

$$ {}^{2'}P = \begin{bmatrix} c\gamma & 0 & s\gamma \\ 0 & 1 & 0 \\ -s\gamma & 0 & c\gamma \end{bmatrix} {}^{2}P \tag{4.7} $$

${}^{i}P$ represents the position of point P with respect to coordinate i. Transformation of the others axes is expressed as

$$ {}^{i-1}P = \begin{bmatrix} c\theta_i & -s\theta_i & 0 \\ s\theta_i & c\theta_i & 0 \\ 0 & 0 & 1 \end{bmatrix} \left(\begin{bmatrix} 1 & 0 & 0 \\ 0 & c\alpha_i & -s\alpha_i \\ 0 & s\alpha_i & c\alpha_i \end{bmatrix} {}^{i}P + \begin{Bmatrix} a_i \\ 0 \\ d_i \end{Bmatrix} \right) \tag{4.8} $$

Therefore, the rotational and position transformation from coordinate 5 to 0 can be expressed as

$$ {}^0_5R = Z_{\theta_1}X_{\alpha_1}X_{\alpha_2}Y_{\gamma}Z_{\theta_3}X_{\alpha_3}Z_{\theta_4}X_{\alpha_4}Z_{\theta_5}X_{\alpha_5} \tag{4.9} $$

$$ {}^0P =^0_5 R({}^5P + [l_h\ 0\ 0]^T) + Z_{\theta_1}X_{\alpha_1}Z_{\theta_2}[l_p\ 0\ 0]^T \tag{4.10} $$

${}^0_5R$ is the total rotational matrix from coordinate 5 to 0. Z_{θ_i} and X_{θ_i} represent the rotational matrix with respect to z_i and x_i by angle θ_i and α_i, respectively. The intermediate transformation, Y_{γ}, is a rotation matrix with respect to $y_{2'}$ by angle γ for the transformation between frame 2 to 2′. ${}^0P$ and ${}^5P$ are the position vectors with respect to coordinate 0 and 5, respectively. Note that there is no rotational transformation by angle θ_2 in the total rotational matrix. The rotation by angle θ_2 (rotation in the parallelogram) affects only the positional calculation in 4.10.

Inverse kinematics for the shoulder mechanism converts the origin and the angle of coordinate 5 into the angles of the joints.

$$ {}^0O_5 - {}^0_5R[l_h\ 0\ 0]^T =^0 O_{2,3,4} = Z_{\theta_1}X_{\alpha_1}Z_{\theta_2}[l_p\ 0\ 0]^T \tag{4.11} $$

$$ Y_{\gamma}^T X_{\alpha_2}^T X_{\alpha_1}^T Z_{\theta_1}^T {}^0_5R = Z_{\theta_3}X_{\alpha_3}Z_{\theta_4}X_{\alpha_4}Z_{\theta_5}X_{\alpha_5} \tag{4.12} $$

${}^0O_5$ and ${}^0_5R$ are the position of the origin and the angle of coordinate 5, respectively and are the known values for an inverse kinematics problem. The left side of the 4.11 indicates the position of the center of rotation of the ball-and-socket joint (the origin of coordinate 2, 3, 4) with respect to the fixed frame. Since origin ${}^0O_{2,3,4}$ is a known vector, $\theta_{1,2}$ on the right side of the 4.11 can be calculated from the three equations of the vector components. With the value of θ_1 and θ_2 known; θ_3 ,θ_4, and θ_5 can be calculated by 4.12.

4.3 Inverse Dynamics

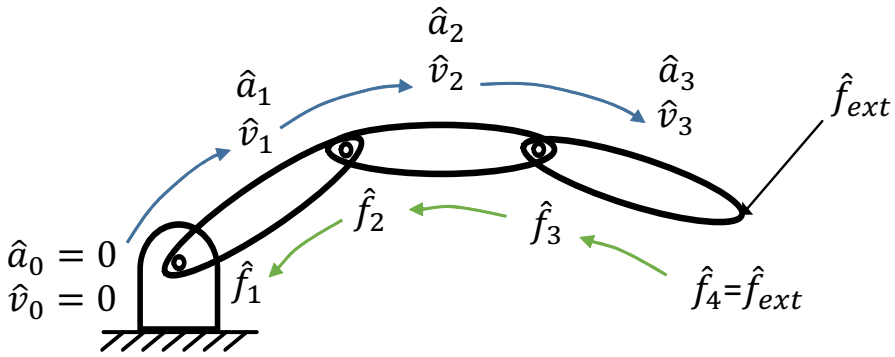

Figure 4.3: A schematic of kinematic and force recursion in a serial chain

The unconventional arrangement of the parallelogram joints and adjustable-length links in HARMONY make it difficult to utilize general dynamic libraries. Instead, in this study we formulate the dynamic model using a recursive Newton-Euler method with spatial dynamics representation, which provides efficient calculation suited for a real-time control environment [39]. The inverse dynamic modeling process consists of kinematic recursion and force recursion described in Figure 4.3. Kinematics is calculated through forward recursion from the base to the end-effector of a robot, expressed as

$$ {}^0\hat{v}_i = {}^0\hat{v}_{i-1} + {}^0\hat{s}_i\dot{\theta}_i \tag{4.13} $$

$$ {}^0\hat{a}_i = {}^0\hat{a}_{i-1} + {}^0\dot{\hat{s}}_i\dot{\theta}_i + {}^0\hat{s}_i\ddot{\theta}_i \tag{4.14} $$

where ${}^0\hat{v}_i$, ${}^0\hat{a}_i$, and ${}^0\hat{s}_i$ are 6×1 spatial vectors of velocity, acceleration, and joint axis, respectively. The left superscript of the parameters refers to the reference frame, and frame '0' indicates an inertial reference frame. The right subscript is

link and joint number in ascending order from the base link to the end-effector and the hat indicates spatial quantities. Both spatial velocity and acceleration at the base link are zero in the case of base-grounded robots. Feed-forward torques are calculated through backward recursion from the end-effector to the base and expressed as

$$ {}^0\hat{f}_i = {}^0\hat{f}_{i+1} + {}^0\hat{I}_i{}^0\hat{a}_i + {}^0\hat{v}_i \hat{\times} {}^0\hat{I}_i{}^0\hat{v}_i \tag{4.15} $$

$$ \tau_i = {}^0\hat{s}_i \,\hat{\cdot}\, {}^0\hat{f}_i \tag{4.16} $$

where ${}^0\hat{f}_i$, ${}^0\hat{I}_i$, and ${}^0\tau_i$ are 6×1 spatial force, 6×6 spatial inertia matrix, and scalar joint torque or force, respectively. Spatial force is a joint quantity, and an external force at the end-effector is equivalent to the force at the last virtual joint at the end-effector as shown in Figure 4.3. $\hat{\times}$ and $\hat{\cdot}$ express spatial cross and dot product and details are found in [38].

4.3.1 Jacobian and Static Equilibrium

From 4.13, the spatial velocity of the n–th link can be expressed in a matrix form as

$$ {}^0\hat{v}_n = \left[{}^0\hat{s}_1 \cdots {}^0\hat{s}_n\right] \{\dot{\theta}_1 \cdots \dot{\theta}_n\}^T \tag{4.17} $$

$$ {}^0\hat{J}_n = \left[{}^0\hat{s}_1 \cdots {}^0\hat{s}_n\right] \tag{4.18} $$

and the concatenation of the spatial joint vectors is the Jacobian (${}^0\hat{J}_n$) of the transformation between the robot's joint velocities and the spatial velocity of the n–th link. From the virtual work principle between joint space and task space, the static

equilibrium between external spatial force ${}^0\hat{f}_e$ applied at the n–th link and the joint torques from '1' to 'n' is given as

$$\tau^T = {}^0\hat{J}_n{}^T \begin{bmatrix} 0_3 & I_3 \\ I_3 & 0_3 \end{bmatrix} {}^0\hat{f}_e \tag{4.19}$$

or

$$\tau_i = {}^0\hat{s}_i \hat{\cdot} {}^0\hat{f}_e \tag{4.20}$$

where τ and τ_i are the joint torque vector and scalar, and i runs from '1' to 'n'.

To apply a desired force or impedance at the interaction port attached on the n–th link in task space, the velocity of the interaction port needs to be calculated from the spatial velocity of the link, which is given by 4.13, and the desired force needs to be converted into the spatial form to be used in 4.20. When point $\vec{P}$ is attached at the n–th link and point $\vec{O}$ is the origin of the local reference frame of the link, the velocity of point $\vec{P}$ is given by

$${}^0v_P = {}^0v_O - \vec{OP} \times {}^0\omega \tag{4.21}$$

$${}^0\hat{v}_n = \left[{}^0\omega^T \; {}^0{v_o}^T\right]^T \tag{4.22}$$

${}^0v_P$ is the velocity of point $\vec{P}$ with respect to the global reference frame. ${}^0\omega$ and ${}^0v_O$ are the first and the last three components of spatial velocity ${}^0\hat{v}_n$ of the n–th link, and are the angular velocity of the link and the linear velocity of point $\vec{O}$ with respect to the global reference frame, respectively. $\vec{OP}$ is the vector from point $\vec{O}$ to point $\vec{P}$ with respect to the global reference frame.

The transformation of an external force or moment into a spatial form is given by

$$ {}^0f_e = \left[{}^0\hat{s}_F \ {}^0\hat{s}_M \right] \left[F \ M \right]^T \tag{4.23} $$

, where

$$ {}^0\hat{s}_F = \left[{}^0\omega_F{}^T \ \left({}^0\rho_F \times {}^0\omega_F \right)^T \right]^T \tag{4.24} $$

$$ {}^0\hat{s}_M = \left[\vec{0}^T \ {}^0\omega_M{}^T \right]^T \tag{4.25} $$

F and ${}^0\hat{s}_F$ are the magnitude of the external force and the spatial vectors that describe the line of action and the point of application of the external force, respectively. Similarly, M and ${}^0\hat{s}_M$ are the magnitude of the external moment and the spatial vectors that describe the line of action of the external moment. ${}^0\omega$ and ${}^0\rho$ is the direction vector of the line of action and the location vector of any point on the line of action.

4.3.2 Spatial Joint Vector of the Parallelogram Joint

Spatial dynamics combines linear and rotational dynamics into one expression and simplifies overall modeling process and calculation. Spatial joint vector, which is a key parameter in the modeling process, defines the direction and location of a given axis, and well defined previously for a rotational and prismatic joint but not for a parallelogram. Spatial joint vector is derived in the process of describing spatial velocity of a rigid body, which is originated from screw theory [4]. Spatial velocity of a rigid body is described by its angular velocity and linear velocity of a point on the rigid body that is instantaneously coincident with the origin of a

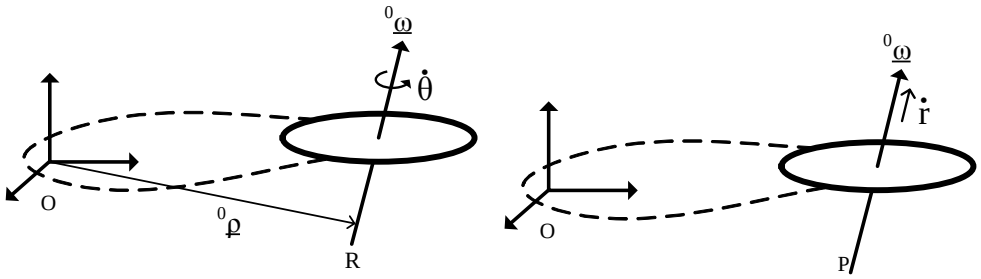

(a) Rotary Joint (b) prismatic joint

Figure 4.4: Spatial velocity of (a) a rotary joint and (b) prismatic joint.

reference frame, expressed as

$$ {}^0\hat{V}_B = \begin{pmatrix} {}^0\underline{\omega}_B \\ {}^0\underline{\mu}_B \end{pmatrix} \tag{4.26} $$

where ${}^0\hat{v}_B$ is the spatial velocity of body B with respect to frame 0. ${}^0\omega_B$ and ${}^0\mu_B$ are the 3×1 vectors of angular velocity and linear velocity of the instant point on body B, respectively.

For example, the spatial velocity of a rotary joint can be expressed as

$$ {}^0\hat{V}_B = \begin{pmatrix} {}^0\underline{\omega} \\ {}^0\underline{\rho} \times {}^0\underline{\omega} \end{pmatrix} \dot{\theta} \tag{4.27} $$

where ${}^0\underline{\omega}$ and ${}^0\underline{\rho}$ are the direction and location vectors of the rotational axis with respect to frame 0 in Figure 4.4a, respectively. $\dot{\theta}$ is the angular velocity of the link with respect to the rotational axis. The spatial velocity of a prismatic joint can be expressed as

$$ {}^0\hat{V}_B = \begin{pmatrix} \underline{0} \\ {}^0\underline{\omega} \end{pmatrix} \dot{r} \tag{4.28} $$

where $\underline{0}$ and ${}^0\underline{\omega}$ are the 3×1 zero vector and the direction vector of the linear axis with respect to frame 0 in Figure 4.4b, respectively. $\dot{r}$ is the linear velocity of the link along the sliding axis. In the serial linkage with N links in Figure 4.5, the spatial velocity of the N-th link is simply a summation of all spatial velocities of the links as

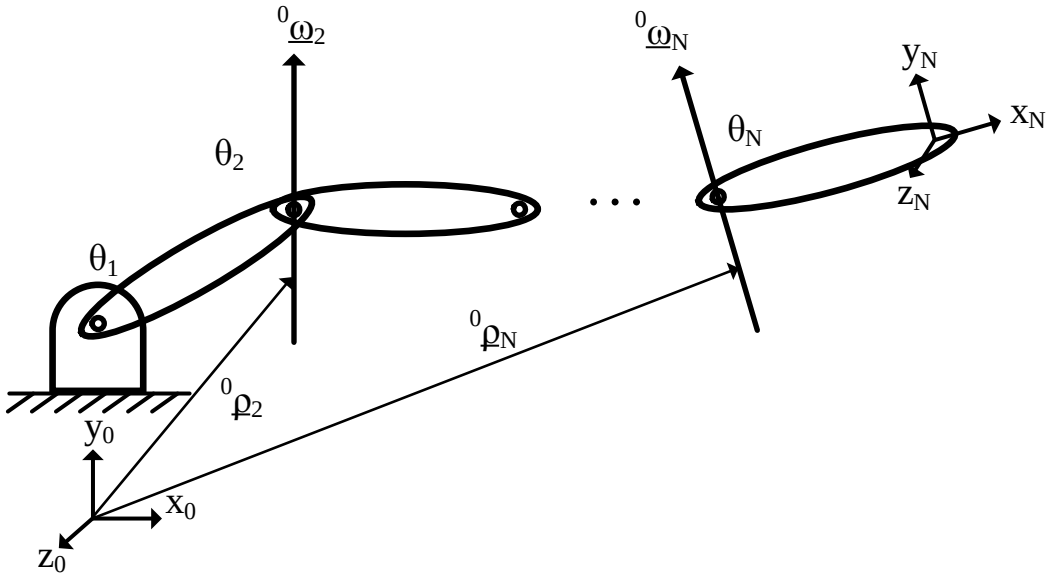

Figure 4.5: An example of a serial chain

$$ {}^0\hat{V}_N = \begin{pmatrix} {}^0\underline{\omega}_1 \\ {}^0\underline{\rho}_1 \times {}^0\underline{\omega}_1 \end{pmatrix} \dot{\theta}_1 + \begin{pmatrix} {}^0\underline{\omega}_2 \\ {}^0\underline{\rho}_2 \times {}^0\underline{\omega}_2 \end{pmatrix} \dot{\theta}_2 + ... \begin{pmatrix} {}^0\underline{\omega}_N \\ {}^0\underline{\rho}_N \times {}^0\underline{\omega}_N \end{pmatrix} \dot{\theta}_N \quad (4.29) $$

where ${}^0\hat{V}_N$ is the spatial velocity of N-th link with respect to reference frame $x_0y_0z_0$. ${}^0\underline{\omega}_i$, ${}^0\underline{\rho}_i$, and $\dot{\theta}_i$ are the direction and location vectors of the rotational axis with

respect to the reference frame, and angular velocity with respect to the rotational axis of link 'i', respectively.

Although a parallelogram is a multi-link mechanism, it acts as a joint with single degree-of-freedom and the spatial velocity of its moving body can be derived. Figure 4.6 shows decomposition of the spatial velocity of body B of the parallelogram. The spatial velocity of body B can be expressed as a combination of the spatial velocity of body B' caused by the angular motion in axis a and the spatial velocity that brings body B' to B induced by the angular motion in axis b, where the two angular motions are opposite in direction with an identical magnitude. Therefore, the spatial velocity of the parallelogram can be expressed as

$$\begin{aligned} {}^0\hat{v}_B &= \begin{pmatrix} {}^0\omega_a \\ {}^0\rho_a \times {}^0\omega_a \end{pmatrix} \dot{\theta} + \begin{pmatrix} {}^0\omega_b \\ {}^0\rho_b \times {}^0\omega_b \end{pmatrix} (-\dot{\theta}) \\ &= \begin{pmatrix} \underline{0} \\ ({}^0\rho_a - {}^0\rho_b) \times {}^0\omega \end{pmatrix} \dot{\theta} \\ &= {}^0\hat{s}_i \, \dot{\theta} \end{aligned} \tag{4.30}$$

where ${}^0\hat{v}_B$ is the spatial velocity of body B with respect to frame 0 and ${}^0\omega_a$, ${}^0\rho_a$, ${}^0\omega_b$, ${}^0\rho_b$ are the direction and location vectors of axis a and b with respect to frame 0, respectively. $\dot{\theta}$ and $-\dot{\theta}$ are the angular velocity in axis a and b, respectively. Since axes a and b are aligned in the same direction (${}^0\omega_a = {}^0\omega_b$) the spatial velocity of body B can be reduced in the form of ${}^0\hat{s}_i\dot{\theta}$ in 4.30. Therefore, ${}^0\hat{s}_i$ becomes the spatial joint vector of the parallelogram to be used in the modeling process.

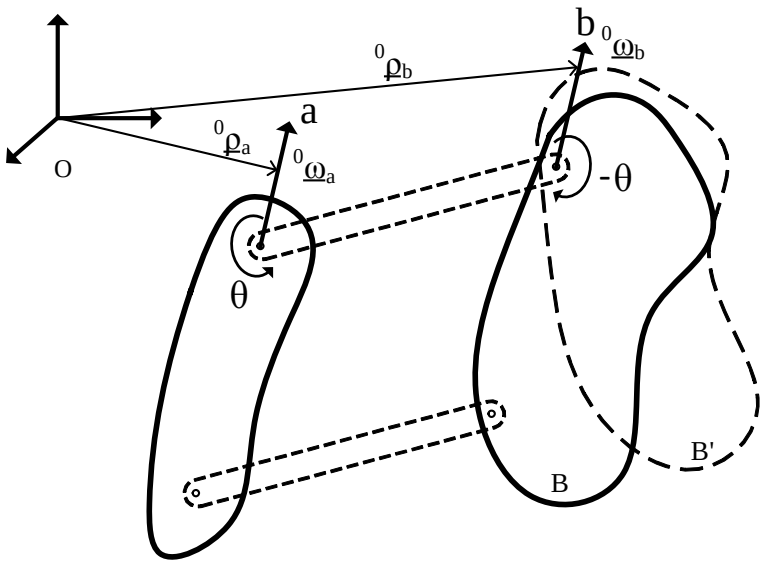

Figure 4.6: Spatial joint vector for the parallelogram joint.

4.3.3 Spatial Inertia Matrix of an Adjustable-Length Link

HARMONY consists of adjustable-length links for various body sizes. In non-spatial dynamics, the inertia matrix of an adjustable link with a complex 3D shape requires a calculation from a CAD software at every link length or complicates dynamic modeling process despite of the parallel axis theorem. However, in spatial dynamics, the total inertial matrix of an adjustable-length link can be easily updated at variable length without an extra calculation, utilizing the feature of spatial inertia matrix that supports arithmetic summation in a common coordinate frame.

$$ {}^0\hat{I}_i = {}^0_{i1_c}\hat{X}\left({}^{i1_c}\hat{I}_{i1}\right){}^{i1_c}_0\hat{X} + {}^0_{i2_c}\hat{X}\left({}^{i2_c}\hat{I}_{i2}\right){}^{i2_c}_0\hat{X} \tag{4.31} $$

The 6×6 spatial inertia matrix of adjustable-length link 'i' ($^0\hat{I}_i$) with respect

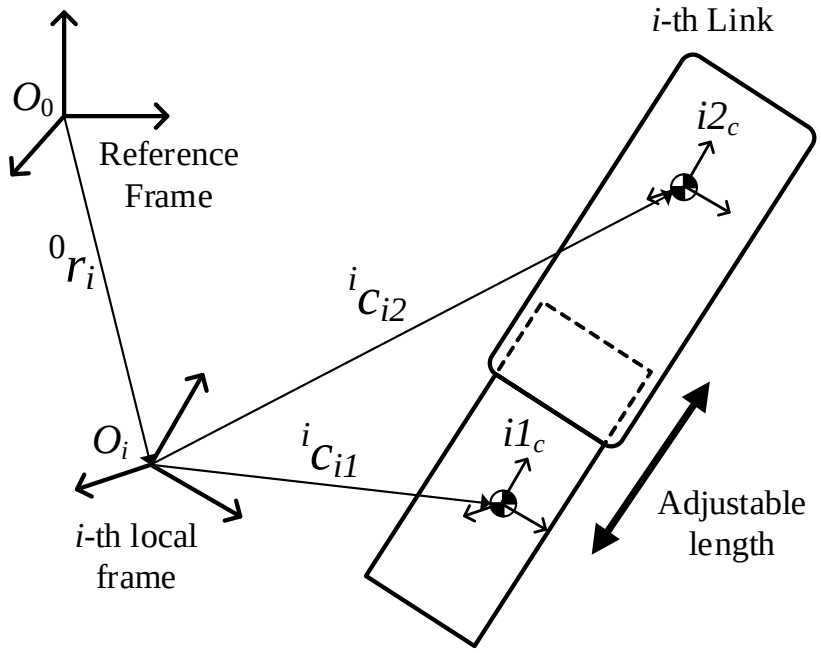

Figure 4.7: Coordinate systems and location vectors for calculating the spatial inertia matrix of an adjustable-length link

to reference frame '0' is a sum of the spatial inertia matrices of the two consisting rigid bodies with respect to the same reference frame as shown in 4.31. ${}^{i1_c}\hat{I}_{i1}$ and ${}^{i2_c}\hat{I}_{i2}$ are the two inertia matrices of the two consisting bodies with respect to each local frame, '$i1_c$' and '$i2_c$', which are located at each center of mass and parallel to the local frame of link 'i' as shown in Figure. Spatial inertia matrix is transformed by spatial transformation and its inverse transformation. ${}^{0}_{ij_c}\hat{X}$ is for transformation from frame 'ij_c' to '0' and expressed as

$$ {}^{0}_{ij_c}\hat{X} = \begin{bmatrix} {}^{0}_{i}R & \mathbf{0}_{3\times3} \\ ({}^{0}r_{ij_c}\times)\,{}^{0}_{i}R & {}^{0}_{i}R \end{bmatrix} \tag{4.32} $$

where ${}^{0}_{i}R$ is the rotational matrix from local frame 'i' to reference frame '0'. ${}^{0}r_{ij_c}$

is the location vector of the center of mass of body ‘j’ of link ‘i’ with respect to the reference frame, and calculated as

$$^{0}r_{ij_c} = ^{0} r_i + {}^{0}_{i}R \, ^{i}c_{ij} \tag{4.33}$$

where $^{0}r_i$ is the location vector of the origin of local frame ‘i’ with respect to the reference frame. $^{i}c_{ij}$ is the location vector of the center of mass of body ‘j’ of link ‘i’ with respect to local frame ‘i’ and contains the length value of the adjustable link. Therefore, by changing the value of the link length in $^{i}c_{ij}$, the spatial inertia matrix of adjustable-length link ‘i’ can accordingly be updated in the dynamic model.

Chapter 5

Robot Control Design and Stability Analysis

5.1 Design of Robot Control

5.1.1 Control for Baseline Behavior

Voluntary movements of patients in rehabilitation training are critical to effectively provoke neuromuscular recovery [99]. To facilitate patient's voluntary movement without imposing a physical load to the patients in therapeutic training, rehabilitation robots need to be highly backdrivable and weightless to the patients during patient-driving movements. Due to the torque controllability of the SEAs of HARMONY, the joints in the robot are highly backdrivable when the zero-torque value is commanded to the each actuator. However, a patient would still carry all the physical load from the robot dynamics including its weight during patent-driving free motion unless the robot dynamics is not properly compensated. Also, a major portion of patients with neuromuscular insults lack the strength to support even their own body weight in performing a variety of voluntary motions. Partial or full supports to their body weight encourage them to move their body voluntarily with a wider range of motion as do in aquatic therapy [9].

For effective controls during rehabilitation intervention, our plan is to model the robot dynamics and then compensate for the weight and frictional forces of the

robot, thus making the robot appear weightless and minimally resistive to the voluntary movements of patients. An assistive or resistive force including gravity compensation for the patient body weight, then, can be added to this baseline behavior without major distortion from the robot dynamics.

Another component of the baseline behavior is the coupling torque for achieving scapulohumeral rhythm (SHR). In rehabilitation practice for patients with abnormal SHR, movements from the robot without a coordination with the shoulder girdle can cause pain, impingement, or injuries on the shoulder. HARMONY's mechanism allows for powering of the SHR. We have developed an impedance controller that calculated the coupling torque for achieving the SHR [66]. Having the reference angles of the shoulder girdle with respect to the angles of the upper arm, an impedance controller induces coordinated movements of the shoulder girdle while the movements are compliant to external disturbances such as spasticity to prevent injuries. Therapists might set the stiffness value in the impedance control to be small at the beginning of therapy for safety and increase the value depending on patient's shoulder condition.

Figure 5.1 shows the control block diagram to achieve baseline behavior of HARMONY and 5.1 gives the controller terms.

$$
\begin{aligned}
M(\theta)\ddot{\theta} &+ C(\theta,\dot{\theta})\dot{\theta} + F\dot{\theta} + G(\theta) = \tau + \tau_I \qquad (5.1)\\
\tau &= \tau_{comp} + \tau_{SHR} + \tau_{task}\\
\tau_{comp} &= \hat{G}(\theta) + f\dot{\theta}\\
\tau_{SHR} &= K_{sh}(\theta_{ref} - \theta) - D_{sh}\dot{\theta}
\end{aligned}
$$

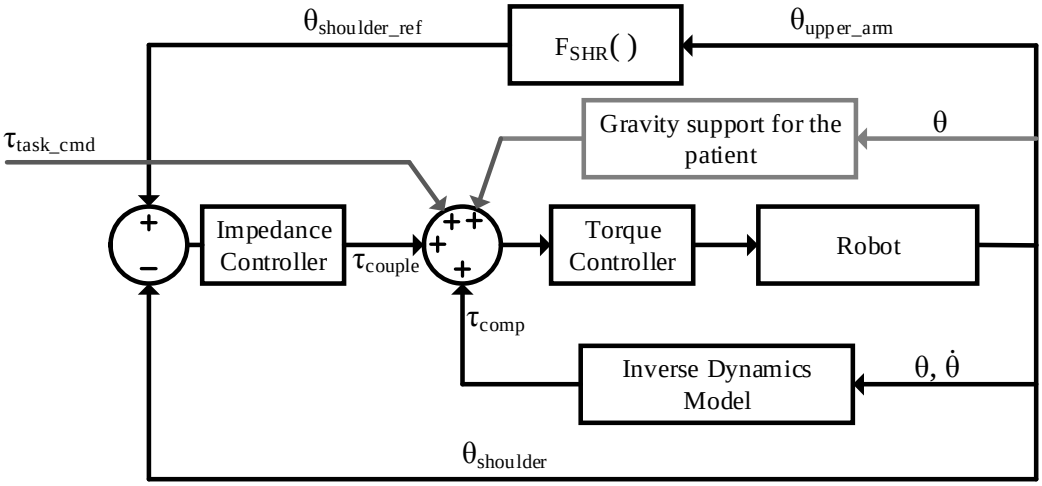

Figure 5.1: Block diagram of the controller for baseline behavior of HARMONY. Nonlinear function $\mathrm{F_{SHR}}()$ calculates the reference position (θ_{sh_ref}) of the shoulder girdle mechanism from the angle of the upper arm (θ_{upper_arm}). $\mathrm{F_{SHR}}()$ can be formulated from a curve fitting of data collected in the exoskeleton worn by healthy subjects.

where $M(\theta)$, $C(\theta, \dot{\theta})$, F, and $G(\theta)$ are the inertia matrix, the Coriolis and centrifugal force matrix, joint friction matrix, and the gravitational force vector, respectively. We assume the joint friction is linear viscous damping and can be expressed as a positive definite diagonal matrix. τ and τ_I are the command torque and interaction torque between the robot and human, respectively. The interaction torque, τ_I, is the sum of the user-robot interaction forces (F_i) transformed by their corresponding Jacobians (J_i) at the interaction ports ($\tau_I = \sum {J_i}^T F_i$). τ_{comp} is a compensatory torque for gravity and joint friction, and $\hat{G}(\theta)$ is the estimated gravitational force vector. f is a friction compensation matrix of which elements are positive and smaller than the corresponding elements in the joint friction matrix. τ_{SHR} is the coupling torque that induces a normal scapulohumeral rhythm. K_{sh} and D_{sh} are

the spring and damping coefficient matrices, where only the first and second diagonal components for the shoulder girdle joints are non-zero. The coupling torque can be set to zero when a patient does not need the SHR assistance. Assistive or resistive forces for therapeutic training are added to task torque τ_{task}, which is zero in the baseline behavior.

At the baseline behavior, a user can perform voluntary movements with minimal muscle effort that is just enough to overcome the residual forces including the inertial forces and remaining frictional forces. In robotic rehabilitation exercises, movements are usually designed to be slow, where the effect from all dynamic terms is insignificant compared to that of gravity [56]. The inertia forces of HARMONY are further diminished because of the series elastic actuators that decouple the effect of the reflected inertia of the motor rotor [144], which usually produces a major portion of the inertia forces in a robot rigidly connected to high-ratio geared motors.

Compensating more for the residual forces may further enhance the dynamic transparency in the baseline control, but may also increase the possibility of violating stability criteria. Remaining frictional forces after the compensation help in ensuring the stability of the robot. Inertia compensation can make the robot into a non-passive system that can jeopardize the coupled stability of the human-robot system when, for example, a user introduces a high stiffness by co-contractions [67]. The inertia compensation during user-driven free movements requires for estimation of acceleration introducing additional dynamics that can adversely affect the stability.

5.1.2 Control of Coordinated Motion

During scapulohumeral rhythmic motion, the kinematic relationship between the shoulder girdle and the humerus is nonlinear, and varies based on dynamic conditions such as a load on the hand. Therefore, the shoulder girdle mechanism needs to follow the humeral motion with a variable ratio, while supplying sufficient force to support the shoulder girdle for the rhythmic motion. The reference position of the shoulder girdle mechanism is determined by humeral angle. However, very low impedance may result in insufficient supportive force for the rhythmic motion, allowing excessive variance in the coupled motion. In contrast, very high impedance may generate excessive reaction force in case of kinematical mismatch.

The key idea of the control strategy is to introduce a coupling torque to the shoulder mechanism so that the angular position of the humerus induces corresponding elevation/depression or protraction/retraction of the shoulder girdle mechanism. A simple way of constraining might be to control position of the shoulder girdle mechanism with respect to the humeral angle. However, with this scheme even a small amount of kinematic variation in the coordinated motion would cause an excessive residual force leading to undesirable stresses on the musculoskeletal system around the shoulder with the risk of injury. On the other hand, low coupling torque would not be sufficient to induce the coordinated motion because of force requirement to overcome robot dynamics, including gravity force.

Coupling torque τ_{couple} for the rhythmic motion is generated based on elastic and damping force with respect to the reference trajectory (θ_{sh_ref}). The damping

coefficient (D) for a critical or slightly over damped behavior in the shoulder girdle mechanism would be preferable for comfortableness without vibratory behaviors. The stiffness (K) of the elastic force is opened to regulation within a limited range depending on patient's conditions or clinical progress. While the maximum stiffness value in the controller level is limited to avoid an excessive induced force to a patient, therapists may set a low value at the beginning and increase it, monitoring patient's pain during trial movements of the upper arm. Function F_{SHR} defines the angular relationship of the scapulohumeral rhythm between the angular position of the robot's upper arm (θ_{upper_arm}) and the reference position of the shoulder girdle mechanism (θ_{sh_ref}), we adopt the previous experimental data and modify it for the exoskeleton to match with a normal scapulohumeral rhythm of a healthy subject.

5.1.2.1 Angular Position Corresponding to Scapulohumeral Rhythm

To calculate the reference angle of the shoulder girdle mechanism, this research adopts the angular relation between the humerus and the shoulder girdle during humeral elevation from the previous study [7] with the modification of the angular representation for our robot and update the coefficients for better comfortableness. The angle of the elevation and depression of the shoulder girdle with respect to the elevation of the humerus is

$$\beta_c = 0.0036\beta_h^2 + 0.085\beta_h \tag{5.2}$$

where, β_h and β_c are the angle of the humerothoracic elevation and the shoulder girdle elevation in degrees, respectively. Fig. 5.2 shows the conversion between the angular representation of the scapulohumeral rhythm, and the rotational matrix and

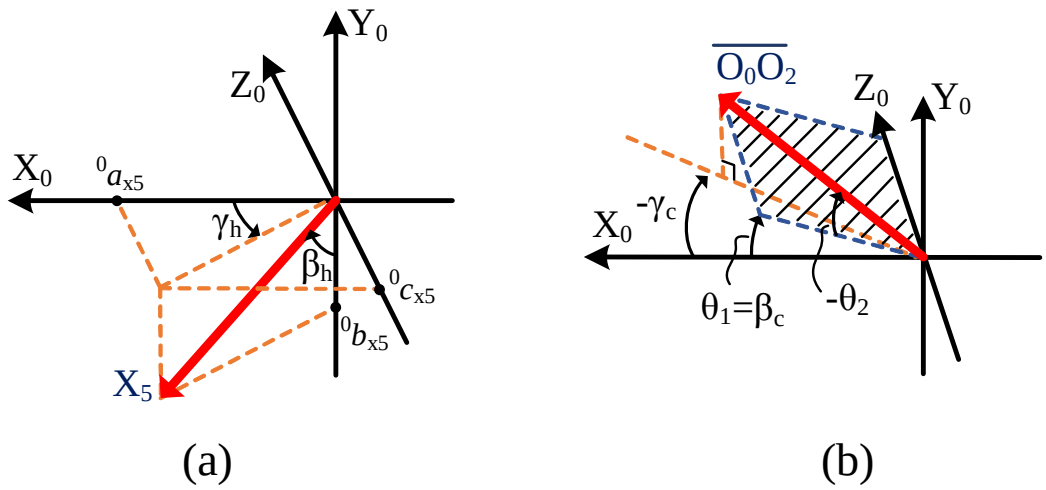

Figure 5.2: The angular conversion between the humerothoracic elevation and the position of the robot: (a) humerothoracic elevation, and (b) the position of the shoulder girdle with respect to the reference frame.

the angular representation of the robot. The conversion is expressed as

$$\beta_h = cos^{-1}({}^0b_{x5}) \tag{5.3}$$

$$\gamma_h = -sign({}^0c_{x5})cos^{-1}\left(\frac{{}^0a_{x5}}{\sqrt{1-({}^0b_{x5})^2}}\right) \tag{5.4}$$

$0° \leq \beta_h \leq 170°$, $-30° \leq \gamma_h \leq 150°$ where, γ_h is the angle of the humerothoracic elevation plane. $[{}^0a_{x5}\ {}^0b_{x5}\ {}^0c_{x5}]^T$ is the first column of the rotational matrix from frame 5 to 0 (${}^0_5R$). Once the humeral elevation is identified from the position of the robot, the reference angle of the shoulder girdle mechanism is calculated from the equation 5.2. From the fact that rotation of x-axis (which is initially coincident to

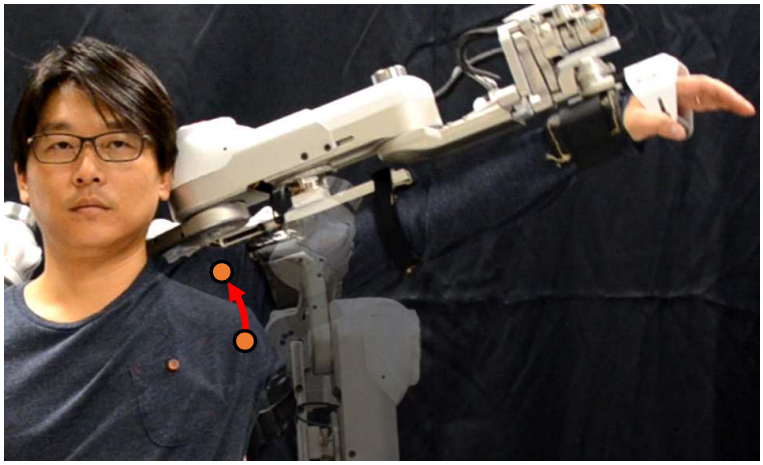

Figure 5.3: Scapulohumeral rhythm of the shoulder during abduction. The circular dots indicate the center of rotation of the glenohumeral joint before and after abduction

X_0) along the two passes are the same, that is $Y(\theta_2)Z(\theta_1)x = Z(\beta_c)Y(\gamma_c)x$.

$$\theta_1 = \beta_c \tag{5.5}$$

$$\theta_2 = sin^{-1}\left(\frac{sin(\gamma_c)}{cos(\theta_1)}\right) \tag{5.6}$$

where, γ_c is and the angle of protraction and retraction of the shoulder girdle. θ_1 and θ_2 are the reference angles of the shoulder girdle mechanism. The humeral position with respect to the thorax (humerothoracic elevation) is usually defined by as shown in Fig. 5.2a.

5.1.3 The Behavior of the Shoulder Mechanism

To evaluate the controller, we first confirmed that the feed-forward torque with zero-torque command compensated for the majority of the robot's weight against gravity in every configuration. This allows the user to feel weightless and

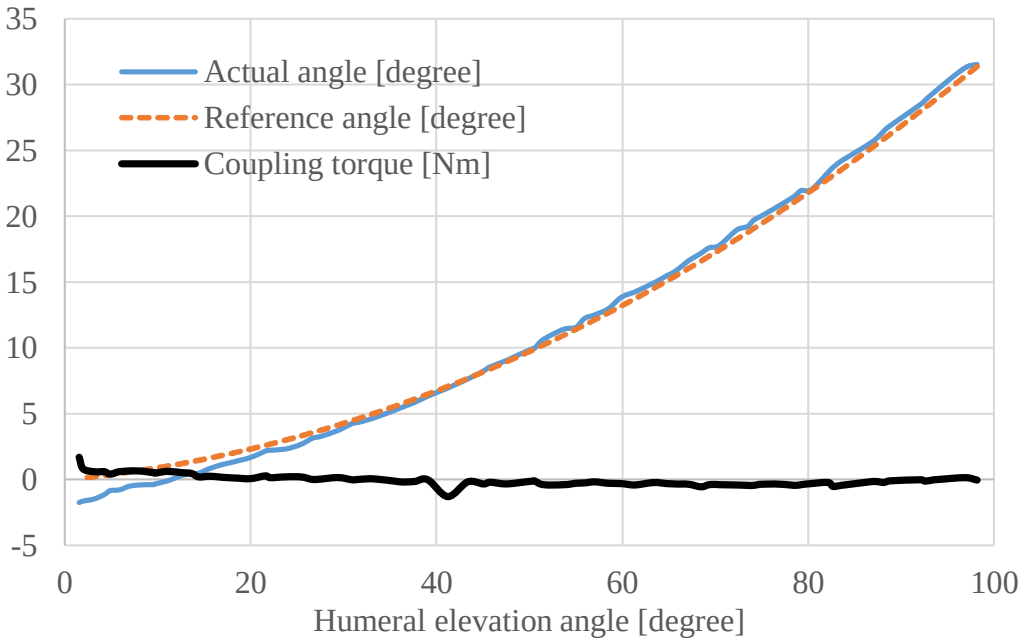

Figure 5.4: Coordinated motion and coupling torque on the shoulder girdle mechanism during shoulder abduction. A user moves the upper arm of the robot without applying force on any another part. The dotted line is the reference angle of the shoulder elevation and the solid line is the actual angle of the shoulder elevation. The heavy line is the coupling torque that induces the coordinate motion

very low resistance to drag the exoskeleton. Then, the coupling torque was added to constrain the shoulder mechanism to follow the upper-arm link with the given angular ratio. Fig. 5.3 shows the center of rotation of the glenohumeral joint shifting along with the humerus during shoulder abduction. Since the user has a normal scapulohumeral rhythm, the exoskeleton imposed no constraint to the user allowing the natural coordinated movements around the shoulder. The user reported comfortableness in interacting with the exoskeleton.

We measured the angular trajectory and coupling torque of the shoulder gir-

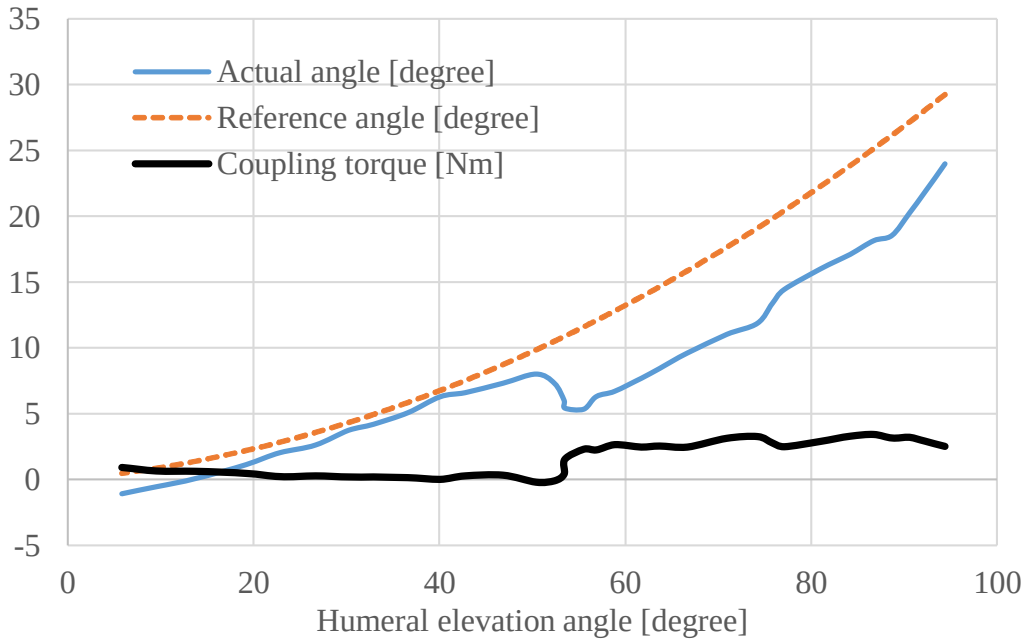

Figure 5.5: Coordinated motion and coupling torque during shoulder abduction with external force applied on the shoulder girdle mechanism. A user pushed down the shoulder girdle mechansim during elevating the upper arm link of the robot. Once the actual angle (the blue solid line) of the shoulder girdle mechanism is off from its reference trajectory (the dotted line), the coupling torque (the black heavy line) increases. The strength of the coupling torque with respect to the offset is open to be regulated based on patient's physical condition on the shoulder

dle mechanism while the operator elevated the upper-arm link externally. Only the coordinated motion during shoulder abduction is considered here. The coupling torque and the angular trajectory of the shoulder girdle mechanism are shown in Fig. 5.4. The shoulder mechanism tracks the reference trajectory closely with respect to the angle of the upper-arm link with a nearly zero coupling torque throughout the elevation. On the other hand, when the operator applied a force to the shoulder girdle mechanism with one hand while elevating the upper arm link with

another hand (replicating a situation that user's shoulder has an abnormal scapulo-humeral rhythm with spasticity or abnormal muscle tone in the shoulder girdle), the shoulder girdle mechanism exerts a gentle force to safely recover the normal coordinated angle as shown in Fig. 5.5. The amount of the coupling torque with respect to the angular offset of the shoulder girdle mechansim from the reference angle can be adjusted by changing the coefficients in the impedance controller. During therapy, a therapist might set a low amount of coupling torque at the beginning and gradually increase the amount depending on patients' conditions.

5.2 Stability Analysis

5.2.1 Coupled Stability at the Baseline Control

The coupled stability is fundamental to guarantee the safety in human-robot interaction systems. Although two subsystems are stable independently, a system consisting of the two subsystems that are physically coupled at an interacting port can be unstable. A coupled system is stable if all subsystems are passive [134]. Therefore, the coupled stability of a human-robot system is guaranteed if the interacting port of the robot behaves passively since the apparent dynamic behavior of the human limb is equivalent to that of a passive system [54, 24]. To examine passivity at the baseline control, an energy storage function is formulated as the sum of the kinematic energy and the shaped potential energy as follows:

$$V = \frac{1}{2}\dot{\theta}^T M \dot{\theta} + \frac{1}{2}\tilde{\theta}^T K_{sh} \tilde{\theta} \tag{5.7}$$

where V, M, and K_{sh} are the energy storage function, the inertia matrix of the robot, and the stiffness matrix of the impedance control in the SHR assistance, re-

spectively. $\dot{\theta}$ is joint velocity, and $\tilde{\theta}$ is the deviation of joint angles from its reference angles for the SHR assistance control, where only the first and second joint angles are used in the calculation. Having the control law as 5.1 with the assumption of $G(\theta) \simeq \hat{G}(\theta)$, the time derivative of the storage function at the baseline behavior is expressed as follows;

$$\dot{V} = \dot{x}_I^T F_I - \dot{\theta}^T \left((F - f) + D_{sh} \right) \dot{\theta} \tag{5.8}$$

where F_I and $\dot{x}_I$ are the vector of the forces and velocities at the interaction ports. Power between the human $(\dot{x}_I^T F_I)$ and the robot flows through the two interaction ports at each arm, and the combination of two subsystems with the dual ports for passivity formalism appears in the next section. Equation 5.8 shows a passive mapping from human force F_I to velocity $\dot{x}_I$ at the interaction ports because $(F - f)$ and D_{sh} are positive definite matrices.

Once the robot is shown to be passive, the stability of the robot alone can be easily examined by having 5.7 as a Lyapunov candidate function and taking null of the human input. The time derivative of the function ($\dot{V} = -\dot{\theta}^T \left((F - f) + D_{sh} \right) \dot{\theta}$) is negative semi-definite, and the invariant set theorem with the radially unbounded Lyapunov function shows the robot with the baseline control to be globally asymptotically stable with the invariant set where $\dot{\theta} = 0$ with all θ [134].

In practice, although the robot is controlled to be passive, the actual behavior may not be strictly passive, rather 'nearly' passive due to non-ideal factors such as actuator dynamics, model uncertainty, or time-delayed sensing and controlling. Such a nearly passive system can be destabilized when coupled with a rigid environ-

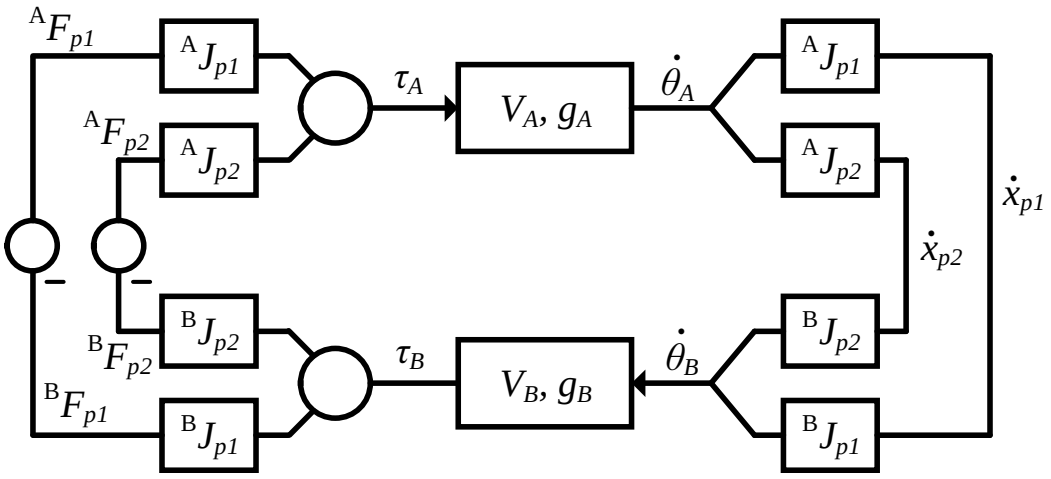

Figure 5.6: Input-output connectivity of two multi-body articulated subsystems interacting with each other at two ports. For example, subsystems 'A' and 'B' are the arms of the human and robot, and ports 'p1' and 'p2' are the physical connections in the cuffs at the upper arm and the wrist, respectively.

ment which is usually referred to the worst case [22]. However, the soft actuators on HARMONY increase the coupled stability margin because the combined stiffness in contact with a rigid environment is bounded by the compliance in the series elastic actuator [64, 125].

5.2.2 Proof of Passivity

5.2.2.1 Passivity Formalism with a Dual-Port Interaction

Since each robot arm is attached to the human arm through two interacting ports at the upper arm and the wrist, passivity formalism for such dual port system is described here based on energy conservation [134]. We assume that the robot and human have a rigid connection. Although the connection at the interaction port, in reality, is compliant due to the flesh and cuffs, the assumption of rigid connection

is valid for the proof of passivity of the human-robot coupled system [54] because the compliance in the interacting port can be safely assumed passive so omitting it makes the coupled stability analysis to be more conservative. Figure 5.6 shows the input-output connectivity of two subsystems interacting with each other at two ports in feedback combination. Power balances of subsystems A and B are expressed as,

$$\dot{V}_A = \dot{\theta}_A^T \tau_A - g_A \tag{5.9}$$

$$\dot{V}_B = \dot{\theta}_B^T \tau_B - g_B \tag{5.10}$$

where $\dot{V}_A$ and $\dot{V}_B$ are the time derivatives of stored energy of subsystems A and B, where the storage functions are positive. $\dot{\theta}$ and τ with subscriptions are the joint velocity and torque vectors of the corresponding subsystems, and the multiplication of two vectors indicates external power input to each subsystem. g_A and g_B are positive scalar functions indicating internal power generation. The joint torque vectors are the sum of two interaction forces transformed by corresponding Jacobians.

$$\tau_A = {}^A J_{p1}^T {}^A F_{p1} + {}^A J_{p2}^T {}^A F_{p2} \tag{5.11}$$

$$\tau_B = {}^B J_{p1}^T {}^B F_{p1} + {}^B J_{p2}^T {}^B F_{p2} \tag{5.12}$$

${}^S J_{pi}$ is the Jacobian of subsystem 'S' at port 'pi'. ${}^S F_{pi}$ is the force applied to subsystem 'S' from interaction port 'pi', having action-reaction pairs as,

$${}^A F_{p1} = -{}^B F_{p1} \tag{5.13}$$

$${}^A F_{p2} = -{}^B F_{p2} \tag{5.14}$$

The velocities of the ports are commonly shared by two subsystems, converting to joint velocities of two subsystems separately as,

$$\dot{x}_p 1 = {}^{A}J_{p1}\dot{\theta}_A = {}^{B}J_{p1}\dot{\theta}_B \tag{5.15}$$

$$\dot{x}_p 2 = {}^{A}J_{p2}\dot{\theta}_A = {}^{B}J_{p2}\dot{\theta}_B \tag{5.16}$$

Using 5.11-5.16, the sum of power balances of the two subsystems that the coupled system is shown to be dissipative as follows,

$$\begin{aligned}
\dot{V}_A + \dot{V}_B &= \dot{\theta}_A^T \tau_A + \dot{\theta}_B^T \tau_B - (g_A + g_B) \\
&= \left({}^{A}J_{p1}^{+}\dot{x}_{p1}\right)^T {}^{A}J_{p1}^{T\,A}F_{p1} + \left({}^{A}J_{p2}^{+}\dot{x}_{p2}\right)^T {}^{A}J_{p2}^{T\,A}F_{p2} \\
&+ \left({}^{B}J_{p1}^{+}\dot{x}_{p1}\right)^T {}^{B}J_{p1}^{T\,B}F_{p1} + \left({}^{B}J_{p2}^{+}\dot{x}_{p2}\right)^T {}^{B}J_{p2}^{T\,B}F_{p2} \\
&\quad - (g_A + g_B) \\
&= \dot{x}_{p1}^{T\,A}F_{p1} + \dot{x}_{p2}^{T\,A}F_{p2} + \dot{x}_{p1}^{T\,B}F_{p1} + \dot{x}_{p2}^{T\,B}F_{p2} \\
&\quad - (g_A + g_B) \\
&= - (g_A + g_B)
\end{aligned} \tag{5.17}$$

where J^+ indicates the pseudoinverse ($(J^T J)^{-1} J^T$) of each Jacobian. Having only the dissipative terms, the feedback combination of the two subsystems interacting with each other at the two ports holds for passivity formalism.

5.2.2.2 Passivity of the Baseline Behavior

To show that the robot with the baseline control is passive with respect to the power input by a user through the interaction ports, the time derivative of the

energy storage function in Equation (5.7) of the robot is derived.

$$\dot{V} = \dot{\theta}^T M\ddot{\theta} + \tfrac{1}{2}\dot{\theta}^T \dot{M}\dot{\theta} + \dot{\theta}^T K_{sh}\theta \tag{5.18}$$

Applying the robot dynamics equation and control law in Equation (5.1) to Equation (5.18) yields

$$\begin{aligned} \dot{V} &= \dot{\theta}^T \left(\tau + \tau_I - C\dot{\theta} - F\dot{\theta} - G(\theta)\right) + \frac{1}{2}\dot{\theta}^T \dot{M}\dot{\theta} + \dot{\theta}^T K_{sh}\theta \\ &= \dot{\theta}^T \tau_I - \dot{\theta}^T \left((F - f) + D_{sh}\right)\dot{\theta} + \frac{1}{2}\dot{\theta}^T (\dot{M} - 2C)\dot{\theta} \end{aligned} \tag{5.19}$$

Since $\dot{M} - 2C$ is skew-symmetric [109], we have

$$\dot{V} = \dot{\theta}^T \tau_I - \dot{\theta}^T \left((F - f) + D_{sh}\right)\dot{\theta} \tag{5.20}$$

Applying the Jacobians at the ports yields

$$\dot{V} = \dot{x}_I^T F_I - \dot{\theta}^T \left((F - f) + D_{sh}\right)\dot{\theta}$$

, where

$$\begin{aligned} \dot{x}_I &= \left[\dot{x}_{p1}^T \, \dot{x}_{p2}^T\right] \\ F_I &= \begin{bmatrix} F_{p1} \\ F_{p2} \end{bmatrix} \end{aligned}$$

$\dot{x}_{pi}$ and F_{pi} represent the velocity and force at interacting port 'pi'.

Chapter 6

Experiments with Robot

6.1 Evaluation of HARMONY

We present experimental procedure and results from two sets of experiments with HARMONY: i) first to test and quantify the range of motion of all the DOFs and test the kinematic compatibility around the shoulder, and ii) second to test dynamic performances of the robot. During both experiments, the baseline control was implemented.

6.1.1 Range of Motion

In order to quantify the range of motion, a user was asked to move the robot throughout its full possible range. The robot was connected to the user through the handle and the cuff at the upper arm. The cuff was securely connected to the upper arm at two points so that the robot followed the rotation and translation of the upper arm including the shoulder girdle motion. Figure 6.1 shows several poses at the limits of the range of motion. Figure 6.2 shows the range of three-dimensional workspace of the left arm. The outer cloud of dots indicates the locations of the center of the wrist measured by robot's position sensors during user-driven free movements. The inner small cloud of dots around the shoulder shows the locations of the center of rotation of the ball-and-socket joint translated by shoulder

protraction-retraction and elevation-depression during the free movements. The workspace covers almost the full range of motion necessary for activities of daily living, promising a sufficient range of motion in therapeutic training.

Table 6.1 compares the range of motion of our robot with the mean values of the maximum range of motions of activities of daily living (ADLs) reported in [94]. The range of motion of the abduction is lower than that of ADLs due to

Table 6.1: Comparison between the measured range of motions (ROMs) of the robot and those of activities of daily living (ADLs) reported in [94]. The value in the parentheses in abduction indicates the ROM of abduction with external rotation. In the case of external and internal rotation of the humerus, the maximum ROMs differ in accordance to arm configuration. The ROM of elbow flexion also moderately varies depending on the length of the forearm link. Values are in degrees.

Motion	ROM of Robot	ROM of ADLs
Abduction	118 (170)	131
Adduction	60	54.4
Forward flexion	160	130.5
Extension	45	50.5
External rotation	79 (62)	75.5
Internal rotation	80 (48)	61.7
Elbow flexion	150 (145)	148.1
Pro/supination	172	166.5

the interference between $J5$ and the head; however, the abduction with external rotation offers a larger range of motion as does the human shoulder. The novel forearm mechanism also provides a range of motion sufficient for pronation and supination. The two joints of the shoulder girdle mechanism have the range of

motion of 50° degrees in elevation, 5° in depression, 20° in protraction, and 45° in retraction. The range of motion of each joint is restricted by a mechanical hard stop for safety. During the bimanual operation, the range of motion of abduction in the absence of external rotation slightly decreases due to the interference of the shoulder mechanism itself (Figure 6.1c) but other shoulder motions maintain their wide range of motion unless both arms interfere each other.

The shoulder girdle mechanism was tested in various movements of the upper arm, including an independent shoulder girdle motion and a coordinated rhythmic motion. Figure 6.4 and 6.5 show the translated location of the ball socket joint during motions of the shoulder girdle mechanism. The mechanism follows protraction and retraction during forward flexion such as a reaching motion and a drive motion of rowing exercises (Figure 6.4), and follows elevation and depression (Figure 6.5).

6.1.2 Kinematic Compatibility Test

To evaluate the kinematic compatibility of the shoulder mechanism of HARMONY, parasitic residual force and torque at the upper-arm interaction port were measured during humerothoracic elevation. The upper-arm cuff is connected to the robot's bicep via a multi-axis force/torque sensor (ATI Industrial Automation, Mini 45), and the cuff is securely connected to the upper part and lower part of the human bicep with two stiff rings consisting of inelastic straps and rigid semicircular shells covered by leathers. The stiff cuff is less comfortable but provides a strict environment for evaluating the kinematic compatibility. The scapulohumeral assistance

was turned off to measure the parasitic forces only from the kinematic discrepancy. Force and torque were measured at several discrete positions during a user-driven humerothoracic elevation along the plane of elevation around at 70° from the frontal plane while the torso was fixed. Both shoulder protraction and elevation occur during the elevation along the plane of elevation that deviates from the frontal plane. The experiment was performed for two cases: i) the shoulder girdle mechanism was free to move as designed, and ii) the shoulder girdle mechanism was locked, and for each case five trials were conducted.

Figure 6.6 shows the measured forces and torques in the two cases. The forces and torques with the full mobility in the shoulder mechanism remain very low during the elevation. The low values confirm the kinematic compatibility of the shoulder mechanism. In contrast, in the case of the fixed girdle mechanism the forces keep increasing and it was impossible to raise the arm above 80°.

The low values of residual effects during shoulder elevation indicate a high kinematic compatibility. The residual forces are partly originated from imperfect backdriveability and errors in gravity compensation.

6.1.3 Joint-Space Torque Responses

A preliminary torque controller adopts PD control based on the feedback from the deflection of the spring. The torque output at several low frequencies are shown in Figure 6.7 in the time domain. A chirp signal was fed into the torque command, and the frequency response was estimated from the output torque measured by the deflection of the spring. Figure 6.8 shows the Bode plot of the torque output,

where the solid line is the torque measured by the spring and the dotted line is the actual torque estimated from Equation (4.5). The difference between the measured torque and the actual torque is unnoticeable at a low frequency so that the torque measured by the spring can be considered as the torque output. The magnitude of the output torque is almost equal to that of the command up to around 10 rad/s, and resonance occurs around 45 rad/s (7 Hz).

The SEA exhibits minimum impedance behaviors when the desired torque is set to zero in the torque controller. The minimum impedance indicates the back-driveability of the robot when a user moves the robot. To measure the minimum impedance at zero-torque command, a user was asked to rotate the output shaft of the SEA with various velocity. The input motion and the torque output of the SEA were measured while the velocity and acceleration of the position input were calculated in the post process, using a high-order midpoint derivative after filtering.

The results show that the resistive torque during the backdriving movements remains less than 0.4 N·m and even smaller when a friction compensation is applied. Figure 6.9 shows the torque output according to the motion input from the user in the time domain. To further reduce the resistive torque, while maintaining stability, a part of viscous frictional torque was positively fed back to the command input of the actuator. Figure 6.10 shows the backdriveability improved by the friction compensation. The joint velocity was conditioned using a first order filter to reduce the noise from the derivative of the quantized position data.

6.1.4 Task-Space Force and Impedance Responses

To evaluate the performance of force and impedance control of the overall system, the robot was commanded to produce task-space forces and impedances at the interaction port located at the middle of the wrist. The last joint for the pronation-supination of the wrist was locked leaving the arm to possess six degrees of freedom. A multi-axis force/torque load cell (ATI Inc., Nano 25) attached to the conjunction of the end-effector and the forearm link measured the forces while the joint position sensors with the kinematic model measured the position and velocity of the interaction port. Figure 6.11 shows the robot configuration and the task-space coordinate system used in the experiments.

To measure force responses, reference forces were given to the command input while the end-effector was fixed to the ground. Figure 6.12 shows step force responses measured by the load cell at the wrist. The force outputs were filtered by a moving average with 10 Hz cutoff frequency. The rise time of the step response in each direction was around 22-24 ms for the rise from 0 to 100%. The maximum steady-state errors were around 10% at the commanded input of 5 N and 13% at the commanded input of 10 N. A force gauge (OMEGA, DFG55) was used to measure the steady state errors and to offset the forces measured by the load cell because the measurement by the load cell exhibited drifts and creeps. Figure 6.13 shows sinusoidal force responses. The time delay of the sinusoidal response was around 0.1 seconds leading to 18 degrees of phase shift at 0.5 Hz input. The maximum amplitude error was around 13% for the commanded amplitude of 8 N.

To evaluate impedance responses, reference forces corresponding to the po-

sition and velocity of the interaction port were given to the command input, and the interaction port was pulled along straight trajectories in the Z-direction.

The interaction port exhibits a minimum impedance behavior (see Extension 1) as an indication of backdriveability when the desired task-space force at the port is set to zero. Figure 6.14 shows an example of the backdriveability of the interaction port in the task space when a user slowly pulls the port back and forth. The resistive force was around 1-2 N with the peak value of around 2.5 N at the moment when the direction of the movement was reversed.

A spring-like behavior at the interaction port was implemented where the resistive force was proportional to the travel distance of the port from a reference point. The relationship between the force and the position with respect to the reference point exhibits close to linearity, and the effective stiffness values are estimated through a linear regression and exhibit around 11% error or less as shown (Figure 6.15).

A damping-like behavior was implemented where the resistive force at the interaction port was proportional to the velocity of the port. The commanded damping coefficient was set to 100 N·s/m and a user pulled the interaction port back and forth in the Z-direction. The result in Figure 6.16 shows that the forces are correlated to the velocity with the coefficient of 0.96 and the effective damping coefficient exhibits around 5% error.

A trajectory control based on impedance was implemented for the interaction port to follow a linear trajectory back and forth repeatedly. The result shows

that the interaction port follows the trajectory with a small deviation while allowing compliant behaviors to external disturbances as shown in Figure 6.17.

Overall, the commanded task-space force and impedance behaviors were well reproduced across the six DOFs without a major distortion, promising various desired dynamic behaviors for rehabilitation exercises to be designed. Despite of some nonlinearities in the impedance responses, the user could clearly feel the intended spring-like and damping-like behaviors. The errors in the task-space responses mainly originate from the gravity compensation with uncertainty in the model. In the damping-like behaviors, other factors such as inertial forces of the robot, actuator dynamics, remaining joint frictions also contribute to the errors. The high-frequency noises in the data of the task-space experiment are mainly from the loadcell-type force sensor electromagnetically excited by the motors on but not from the robot's behaviors, and users feel smooth reactive forces during the interaction with the robot.

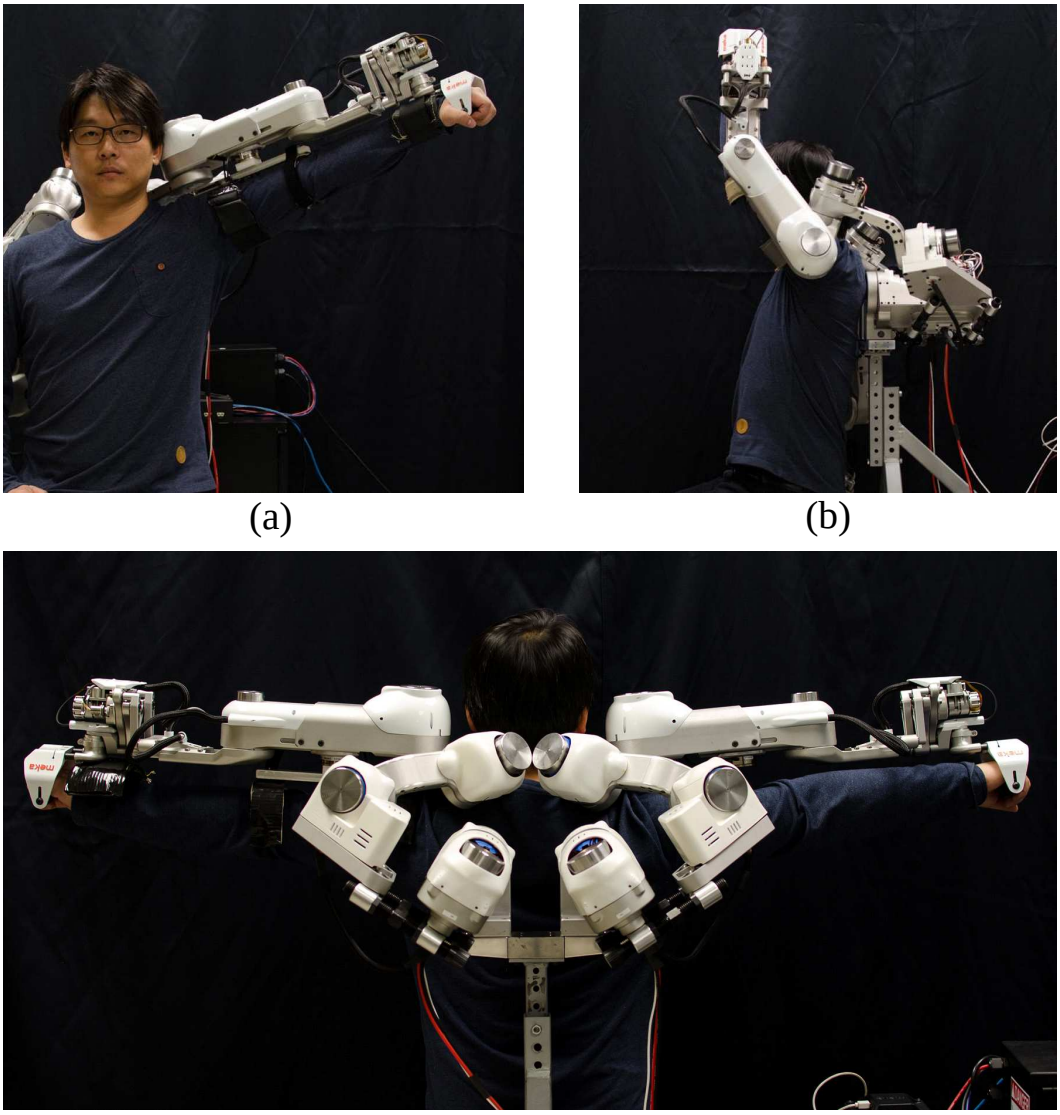

Figure 6.1: Examples of the range of motion of the exoskeleton: (a) maximum abduction without external rotation. The range becomes larger with an external rotation, (b) maximum forward flexion, (c) maximum bilateral abduction without external rotation where the range of motion is smaller than that of unilateral abduction because of the interference caused by the shoulder girdle mechanism. In all cases, humerothoracic elevation accompanies shoulder elevation.

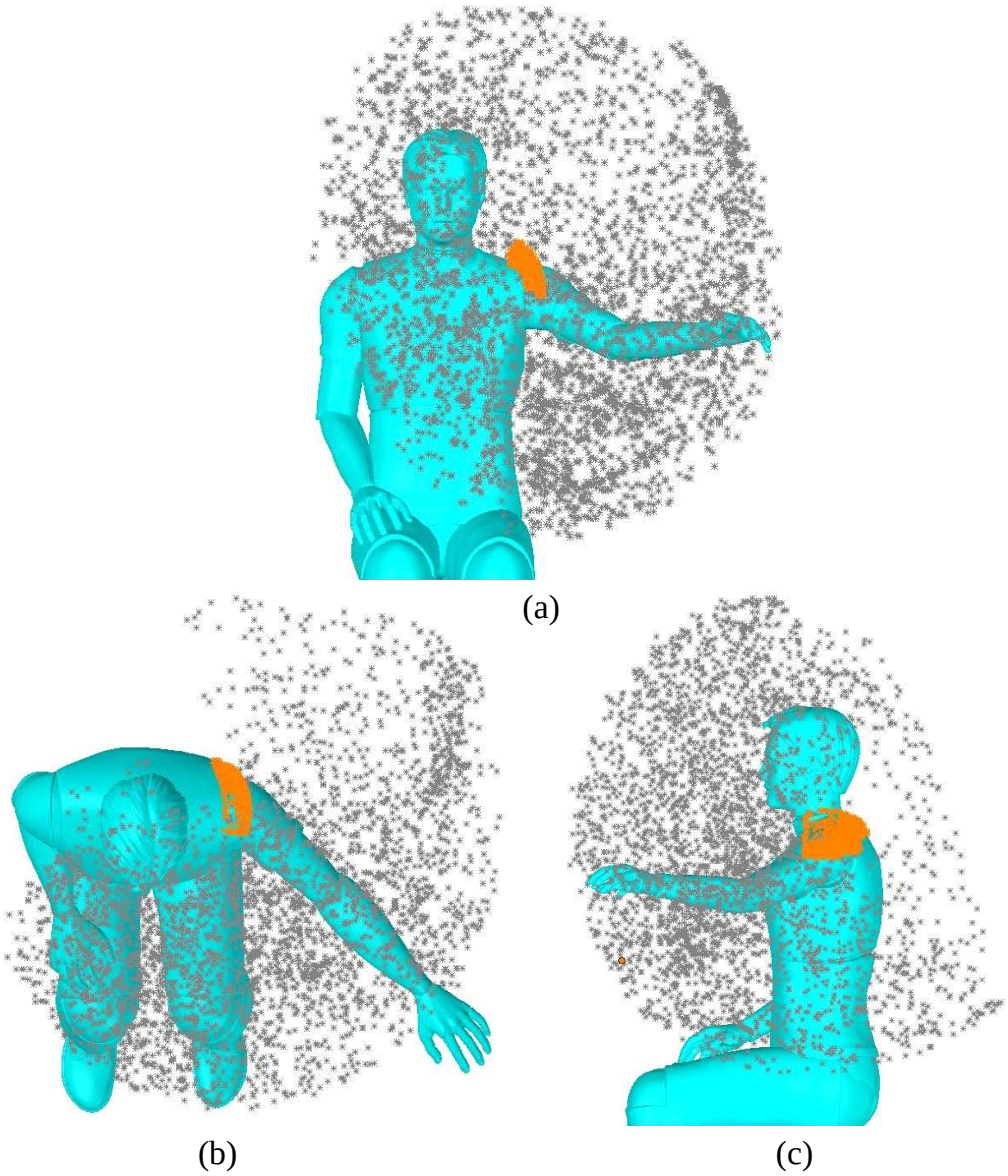

Figure 6.2: 3D workspace of the end-effector (center of the wrist) measured by the robot's position sensors during free motion by a user wearing the robot in the baseline mode: (a) front view, (b) top view, and (c) side view. The inner small point-cloud indicates the range of motion of glenohumeral joint translation.

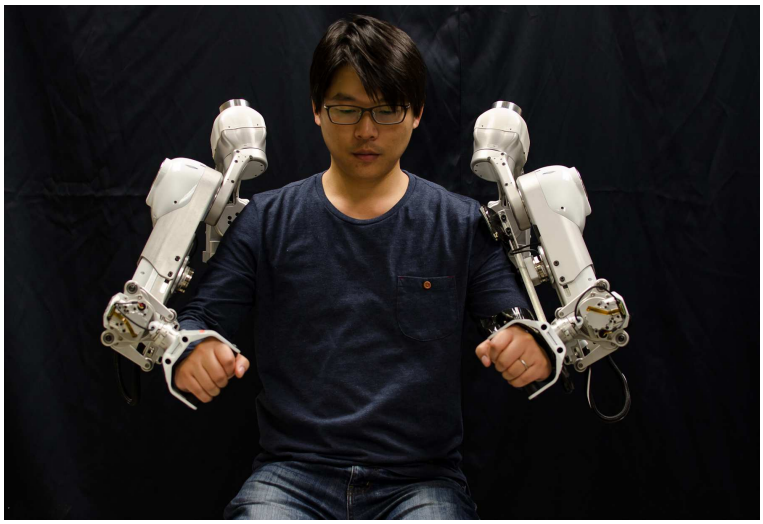

Figure 6.3: Example of a bi-manual operation

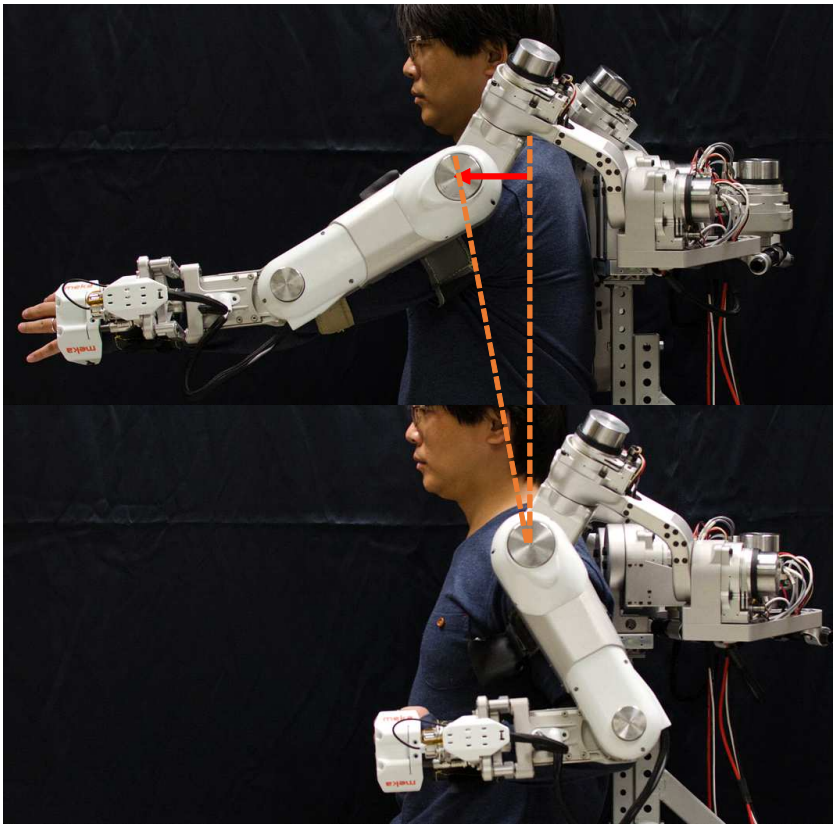

Figure 6.4: Coordinated protraction and retraction of the shoulder mechanism during a typical forward and backward arm motion

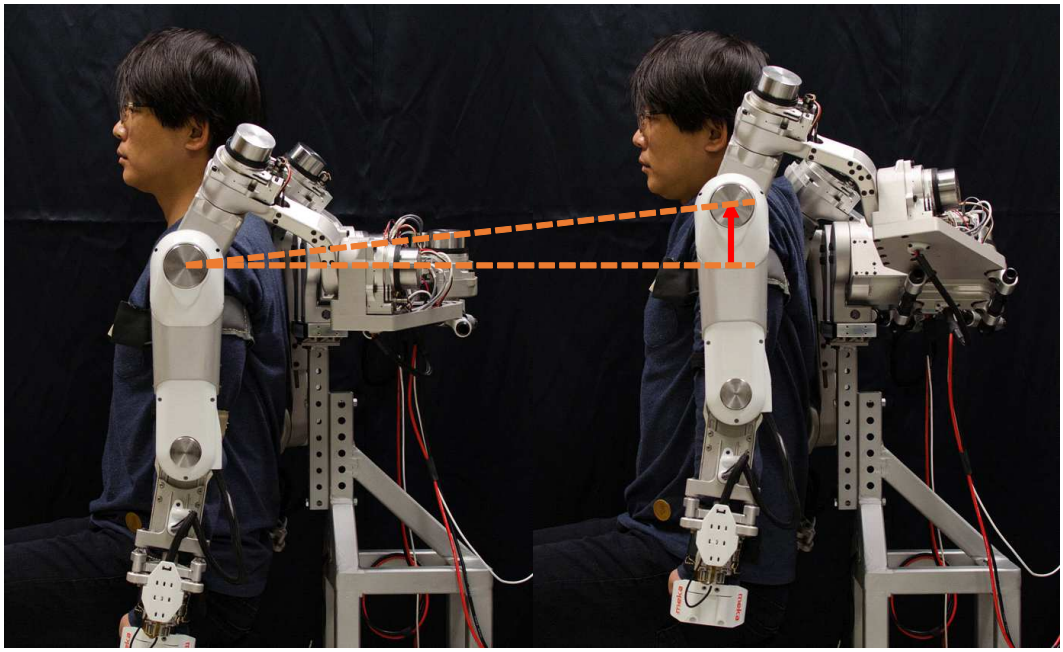

Figure 6.5: Independent depression and elevation of the shoulder showing that the mechanism follows the motion seamlessly.

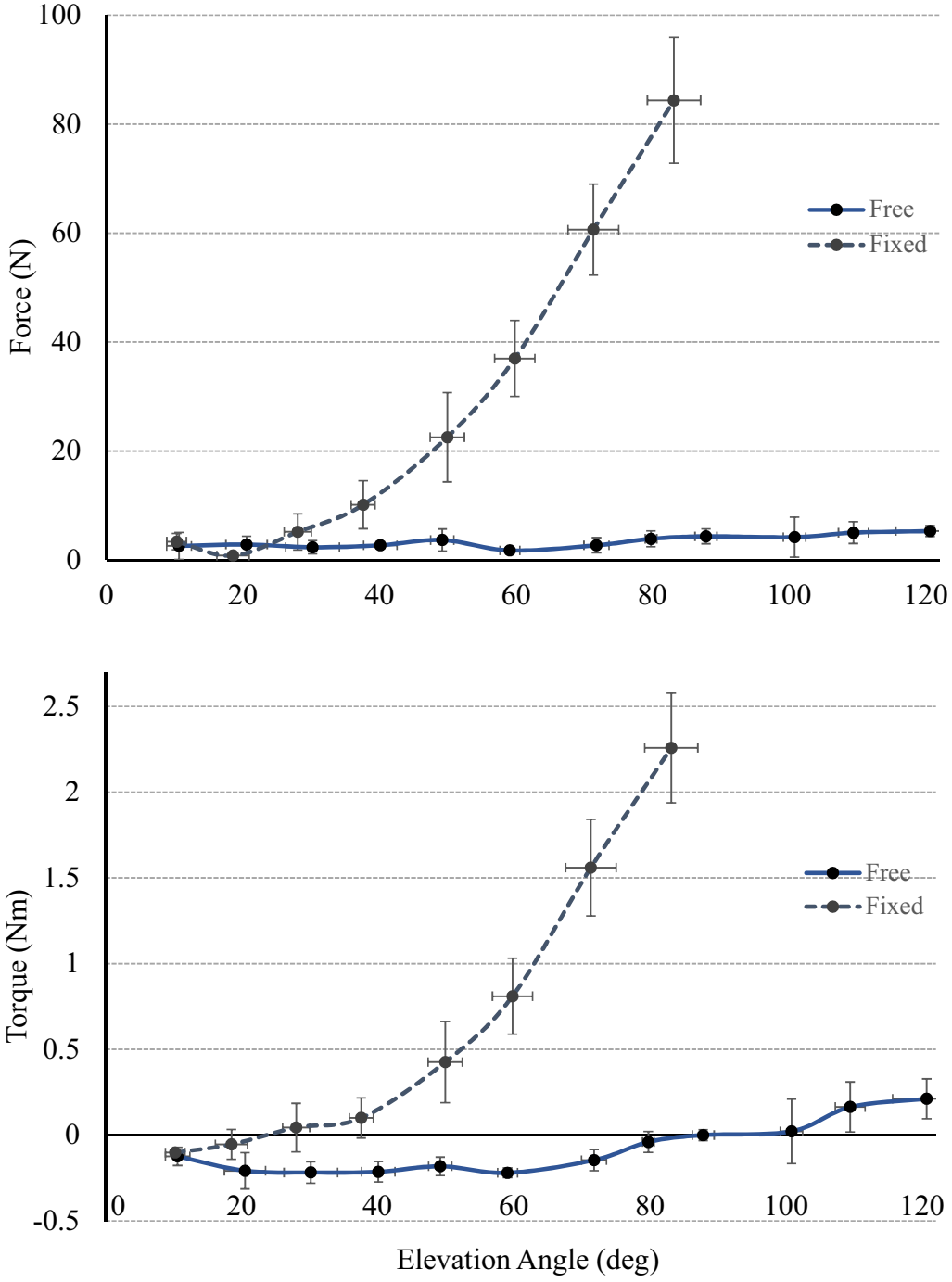

Figure 6.6: Residual forces and torques exerted on the upper arm during shoulder humerothoracic elevation.

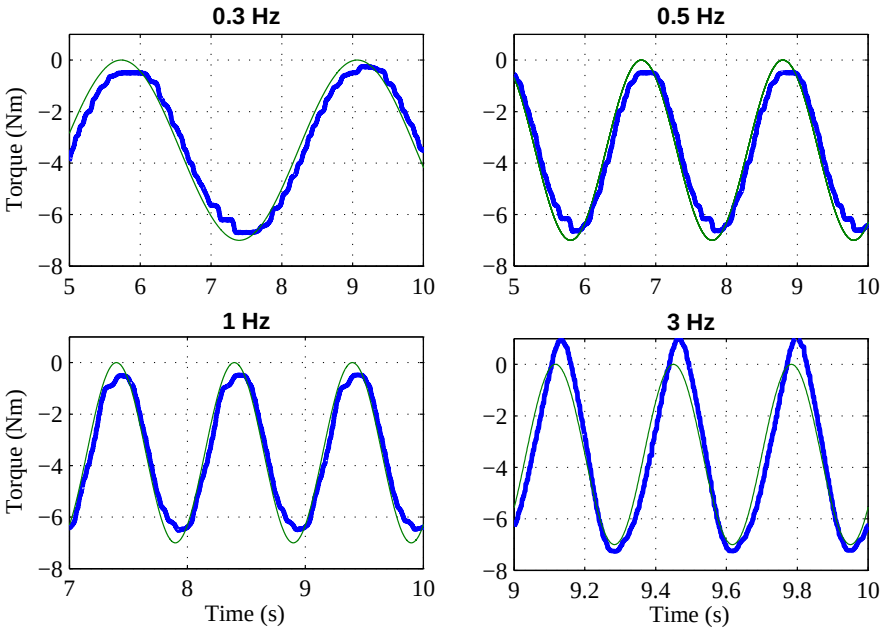

Figure 6.7: Torque responses of the SEA in time domain with several frequencies of sinusoidal reference input. The light and heavy line indicate the commanded and actual torque, respectively. The force fidelities are 95.3, 95, 94.2, and 92.3 % at 0.3, 0.5, 1, and 3 Hz, respectively.

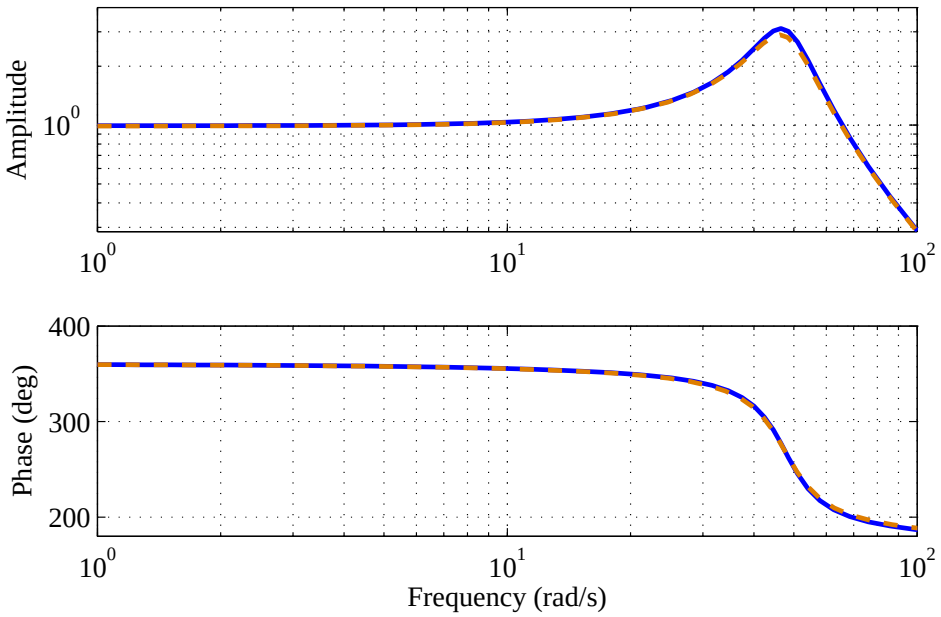

Figure 6.8: Frequency responses of the torque control. The torque output measured by the deflection of the spring in the SEA (the solid line) is very close to the estimated actual torque output (the dotted line) at low frequency.

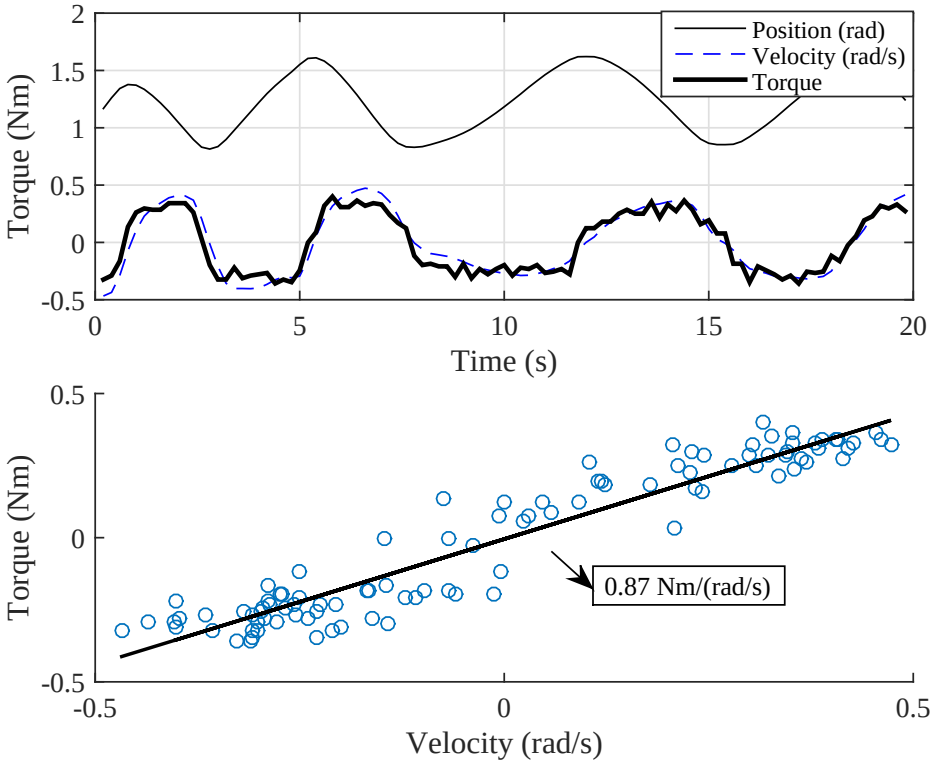

Figure 6.9: Torque output at the zero-torque command in time domain. At various velocities ranging from -0.5 to 0.5 rad/s, the resistive torque from the SEA ranges form -0.4 to 0.4 N·m with a strong tendency of linear viscous behaviors with 0.87 N·m/(rad/s) of friction coefficient.

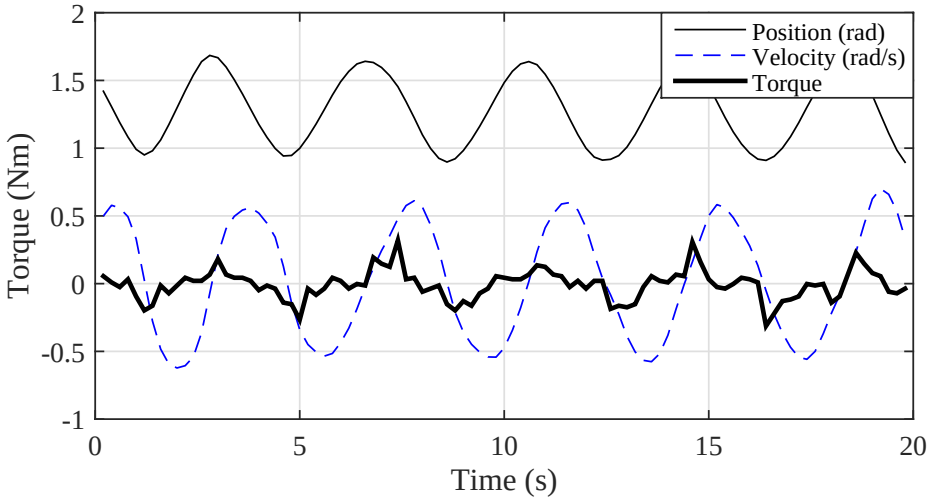

Figure 6.10: Torque output at the zero-torque command with a friction compensation. Around 70% of viscous frictional torque (0.6 N·m/(rad/s)) was positively fed back to the command input of the actuator. The resistive torque remains within 0.1 or 0.2 N·m except a peak value at the moment when the direction of the movement is reversed.

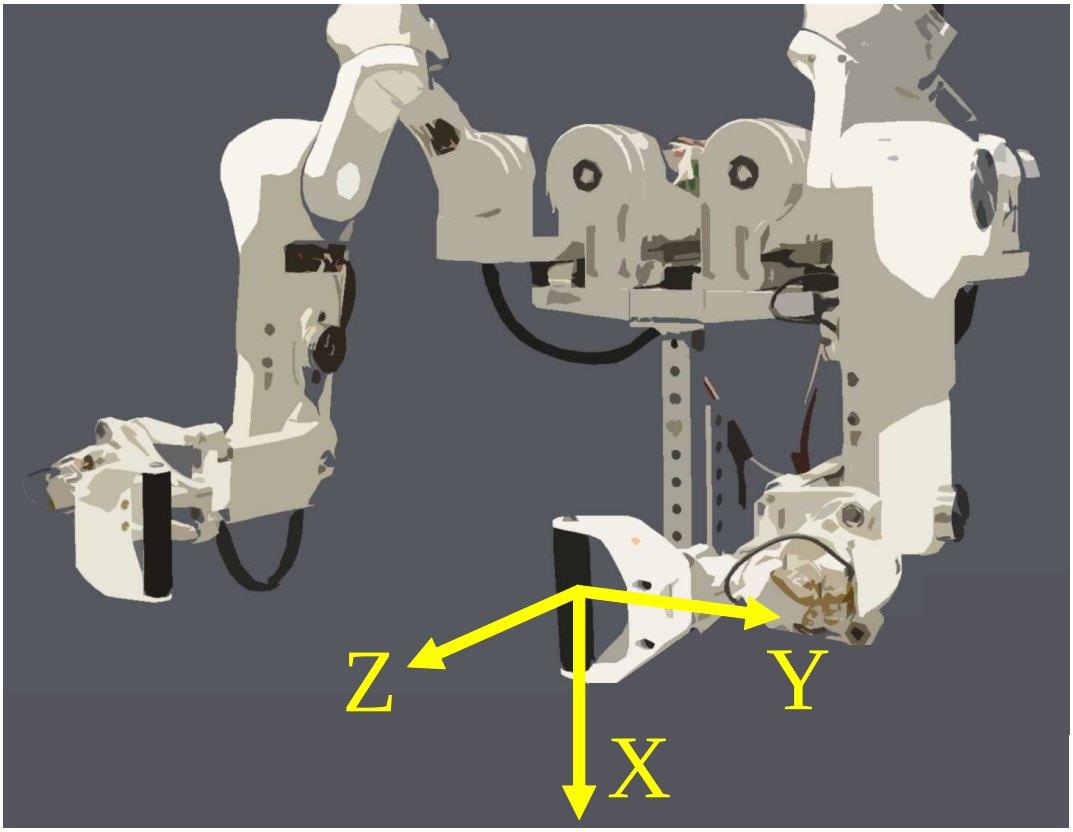

Figure 6.11: Task-space coordinate system.

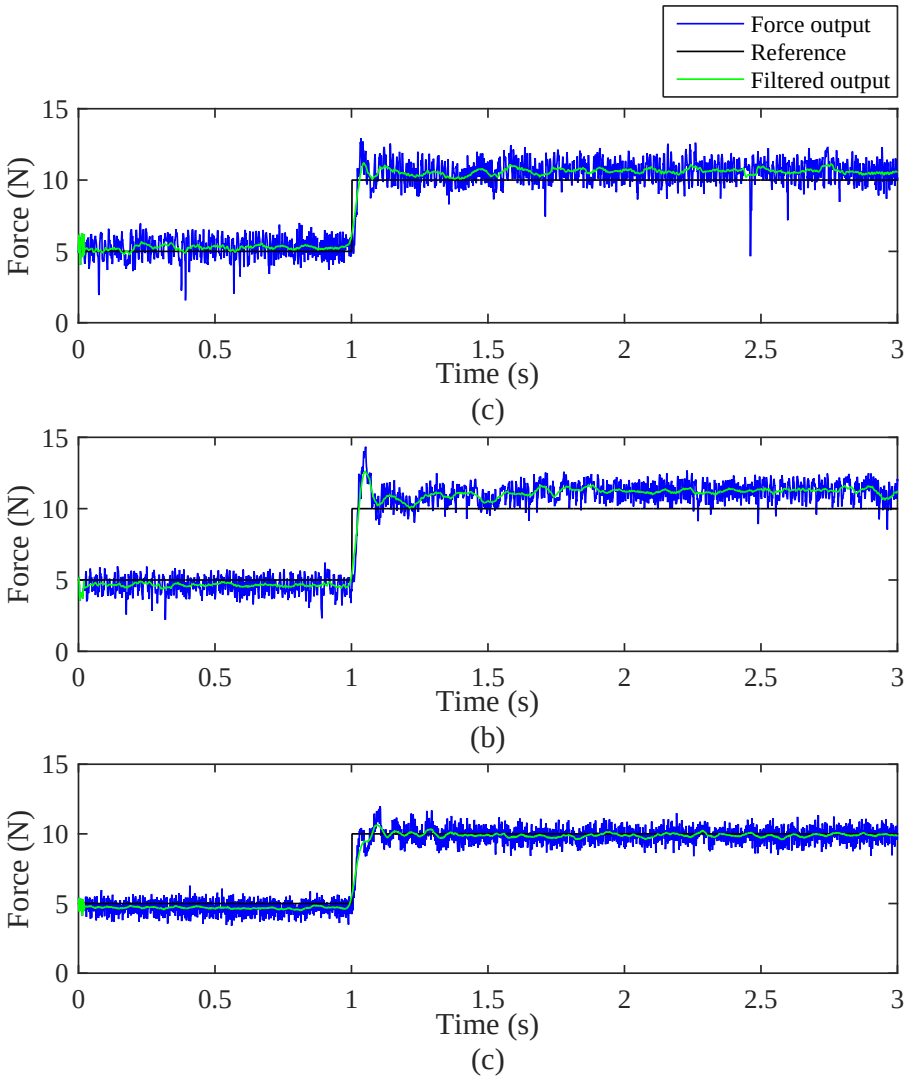

Figure 6.12: Task-space step force responses with the rise from 5 to 10 N. (a), (b), and (c) are the step responses at the interaction port of the wrist in the X, Y, and Z-direction in the task space, respectively.

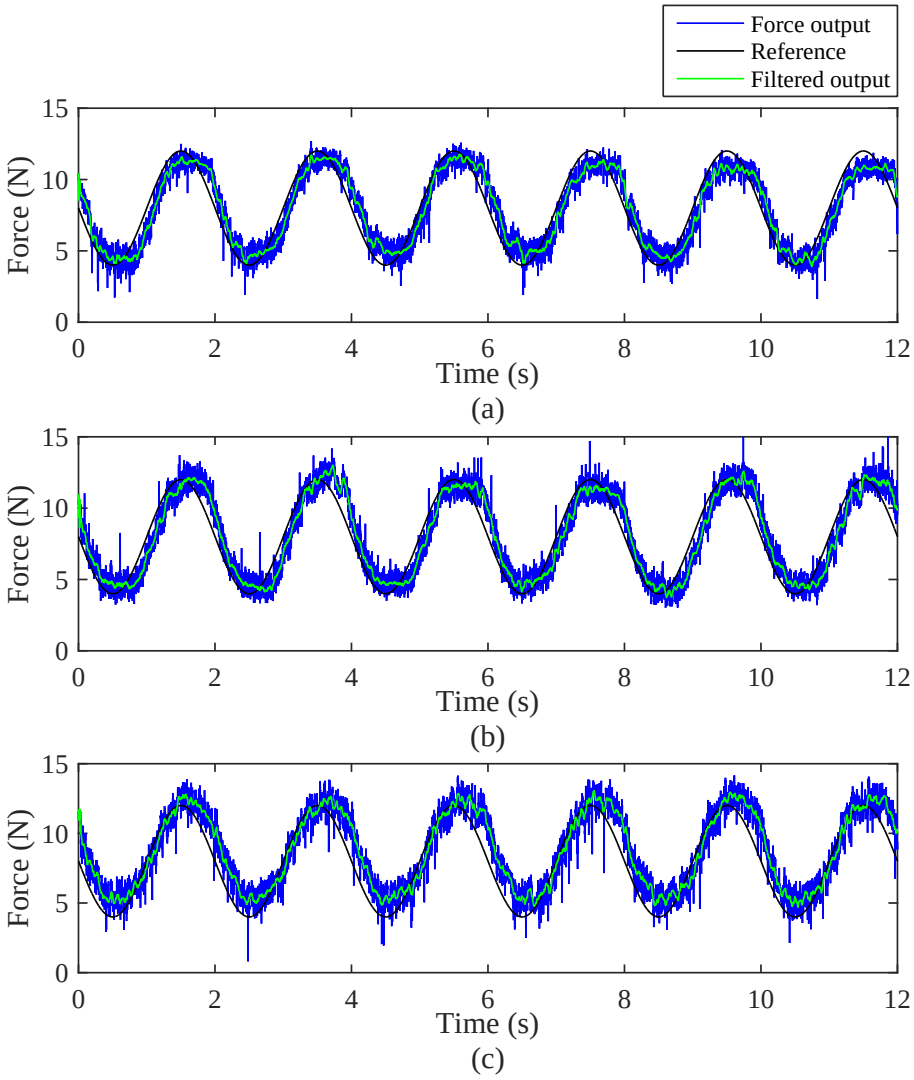

Figure 6.13: Task-space sinusoidal force responses. The frequency of the reference input is 0.5 Hz with the magnitude from 4 to 12 N. (a), (b), and (c) are the sinusoidal responses at the interaction port of the wrist in the X, Y, and Z-direction in the task space, respectively.

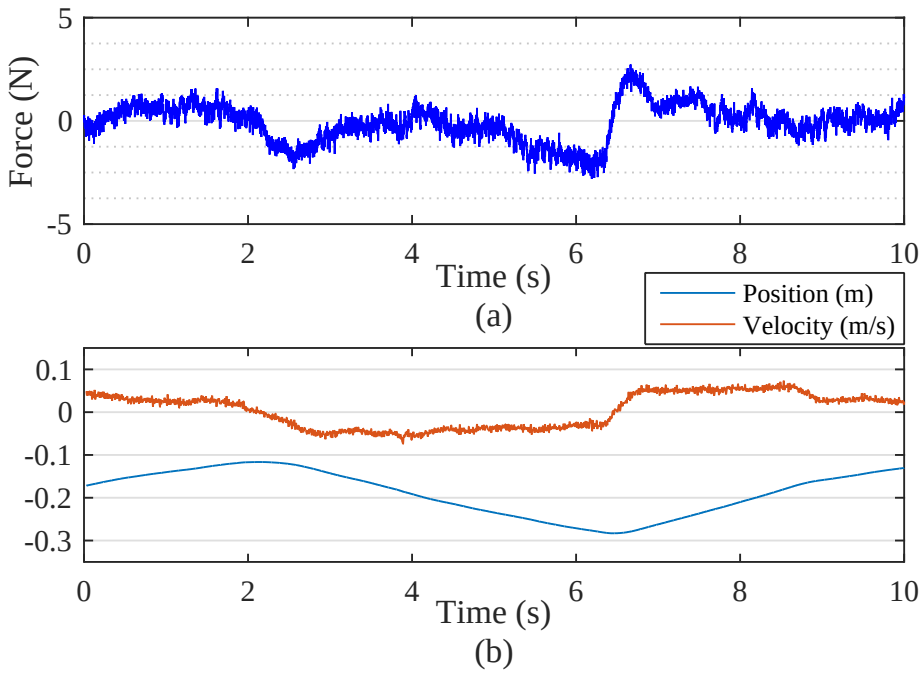

Figure 6.14: Resistive forces at the interaction port when the command force input at the interaction port of the wrist is set to zero and the port is pulled by a user in the Z-direction. (a) resistive forces with respect to time, (b) user-input position and velocity of the interaction port.

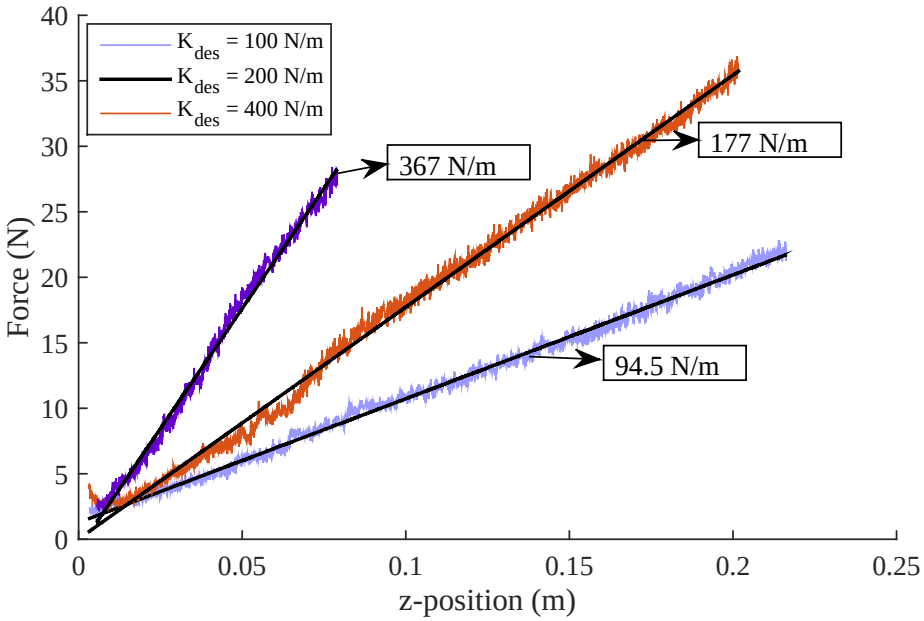

Figure 6.15: Stiffness control responses at the interaction port of the wrist in the Z-direction. The effective stiffnesses for the commanded values of 100, 200, and 400 N/m, are 94.5, 177, and 367 N/m, respectively.

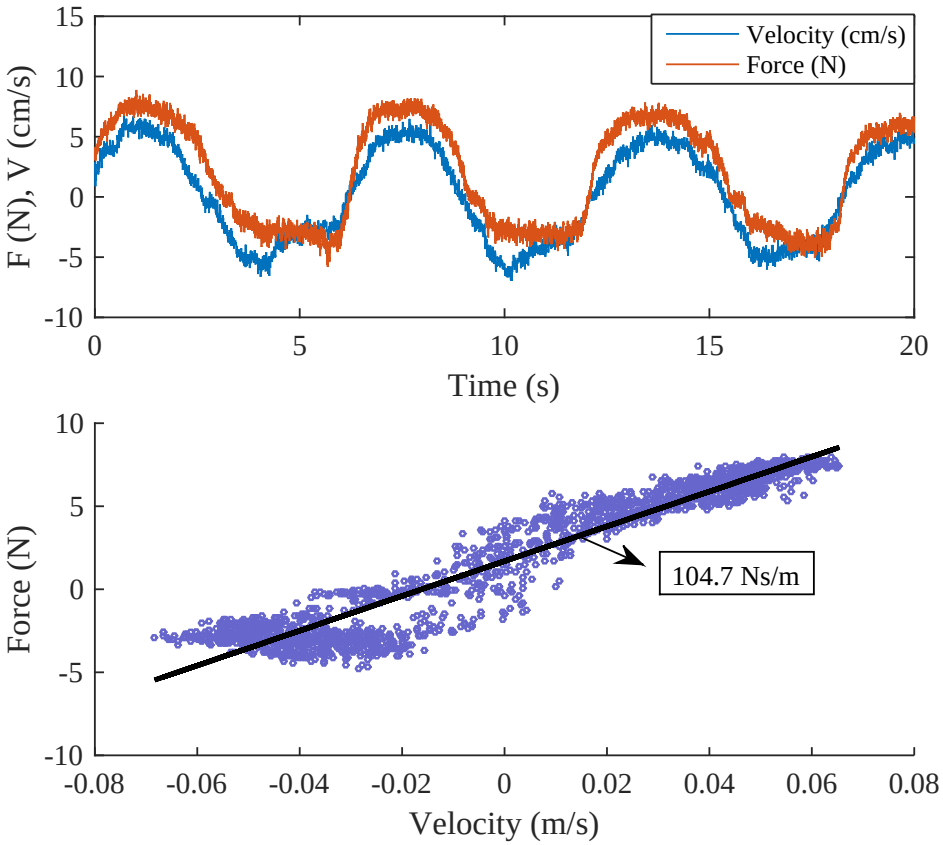

Figure 6.16: Task-space damping-like behavior at the interaction port of the wrist in the Z-direction. The effective damping coefficient for the commanded value of 100 N·s/m is 104.7 N·s/m.

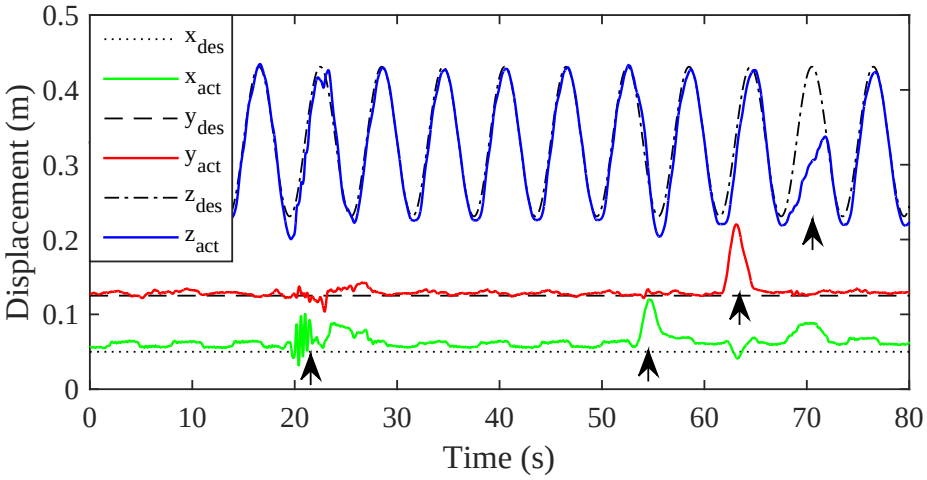

Figure 6.17: Impedance-based tracking performance and compliant responses to external disturbances at the interaction port of the wrist in the task space. The arrows indicate the points where the external disturbances are applied.

Chapter 7

Human Subject Experiment

7.1 Goal

Exoskeleton type rehabilitation robots intend to control each joint of the human body to correctly assist coordinated movements, expecting better therapeutic outcomes [90, 98]. However, so far, there is limited discussion on how to provide active assistance to the coordinated movements involving scapulohumeral rhythm around the shoulder in rehabilitation robotics studies. We have developed an upper-body exoskeleton that can actively support the full mobility of the shoulder and control algorithm that assists the coordinated motion around the shoulder. To confirm the benefits of the assistance, a human subject study has been conducted.

This chapter presents a study whose goal is to evaluate how the shoulder mechanism with its control strategy affects the coordinated movements in the human shoulder. We compare the biomechanics around the shoulder before and after the robot assistance in the presence of an abnormality. The result of this study will demonstrate the potential of the robot in correcting abnormal scapulohumeral rhythm (SHR).

7.2 Method

In this study, we simulate abnormalities in the healthy shoulder inspired by common pathology in stroke patients, namely, flaccidity and spasticity. The simulated abnormalities are not necessarily consistent with the stereotypical patterns of the pathology but are rather used to introduce an alteration in the biomechanics of the shoulder analogous to the abnormal patterns. The biomechanics of the shoulder before and after the robot assistance in terms of kinematics and muscle activities are compared to each other to verify whether the robot corrects the simulated abnormalities as intended.

7.2.1 Simulated Abnormality of the Shoulder

7.2.1.1 Overview of Common Pathologies of the Shoulder in Strokes

The majority of post-stoke patients with hemiplegia experience flaccid paralysis on the shoulder complex at early stages and spasticity at later stages, resulting in limited mobility, shoulder pain, and an abnormal SHR [101, 59, 21].

Flaccidity is characterized by the lack of voluntary muscle activation and therefore, with the loss of voluntary mobility at the affected side, the shoulder also loses its inherent coordinated motion and frequently exhibits subluxation by gravity pull. Passive range exercises in the early stage are known to prevent immobility and soft tissue contracture [82]. However, careless handling with disregard for coordinated shoulder movements such as in an overhead pulley exercise may cause impingement, rotator cuff rupture, or nerve injuries [103, 61]. During the humeral elevation, the upward rotation and posterior tilt of the scapula and the external rota-

tion of the humerus prevents the impingement of the supraspinatus or the long head biceps brachii between the undersurface of the acromion and the greater tubercle of the humeral head.

After a short period of flaccidity, spasticity usually develops with shoulder pain and an abnormal muscle tone around the shoulder. The muscle tone interferes with the coordinated motion around the shoulder including SHR and further increases a risk of impingement or nerve injuries if improper manipulation is performed during rehabilitation exercises. The muscle tone around the shoulder frequently induces retracted-depressed shoulder girdle and humeral adduction-internal rotation [138, 108].

7.2.1.2 An Abnormality Inspired by Flaccidity in the Shoulder: Passive Elevation

It would be difficult to suppress or change the kinematics of the normal SHR in an intact shoulder during a user-active motion, where a human subject voluntarily moves, because the highly activated muscles around the shoulder that overcome gravity forces from the arm and shoulder weight are difficult to constrain. Contrarily, if the arm is passively manipulated while the subject fully relaxes, the muscle groups around the shoulder would minimally engage in the coordinated motion so that an external force can alter the response of the shoulder girdle during humeral movements. The relaxed arm and shoulder may not capture the entire characteristics of paralysis but may provide an analogous environment for the robot assistance to change the posture of the shoulder girdle because the internal forces generated

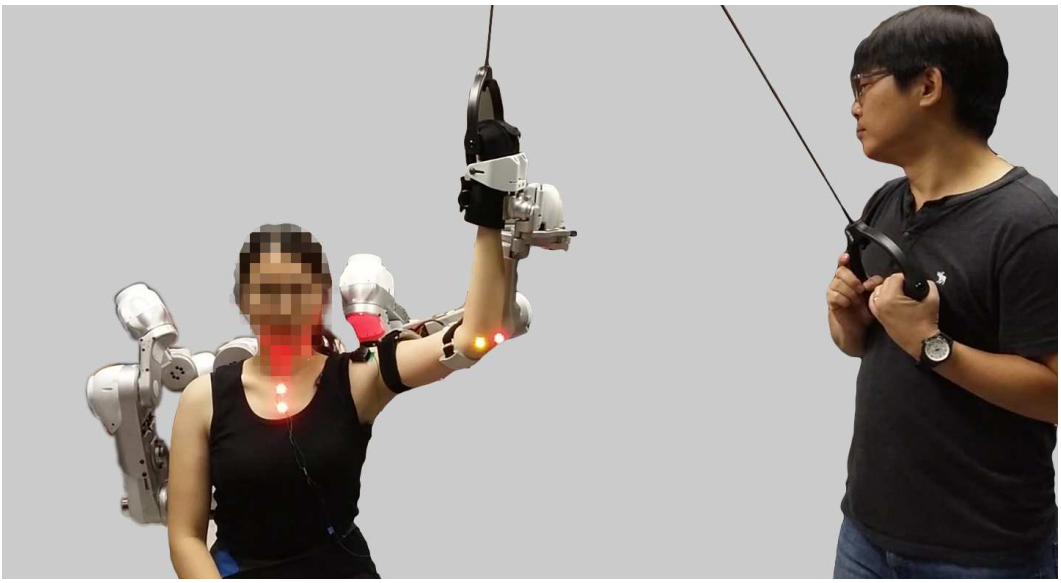

Figure 7.1: Passive elevation by a overhead pulley with robot assistance

by muscle activation stay low, and only a small resistance to passive stretches of muscles and tendons remains. The velocity of passive movements needs to be slow enough not to generate any stretch reflexes.

While passive ROM exercises are recognized as an essential intervention to prevent immobility or soft tissue and muscle contracture, careless handling must be avoided as it may cause shoulder pain or injuries. Overhead pulley exercises are known to be undesirable since they can cause shoulder pain, impingement, or even rotator cuff injuries due to ignorance of the support to shoulder coordination [103].

We assume that the totally relaxed shoulder in a healthy subject during overhead pulley exercises is analogous to the flaccid shoulder in a way that no significant muscle activity engages in the manipulation of the coordination around the shoulder. We investigate the ability of the robot to change the coordination of a

flaccid shoulder by comparing shoulder girdle movements during an overhead exercise with conventional overhead pulley and during the overhead pulley exercise with the SHR assistance from HARMONY.

The SHR assistant is tuned to increase the SHR ratio compared to the one during the passive elevation by the overhead pulley. We confirmed that the increased elevation of the shoulder girdle during the humeral elevation did not impose any pain or constraint to the healthy shoulder. We may expect that the increased shoulder girdle elevation would relieve the pressure between the undersurface of the acromion process and the humeral head. However, this study focuses on testing whether SHR is altered by the robot assistance during the overhead pulley exercise. We postulate a hypothesis as follows;

Hypothesis (H1): The elevation of the GH joint with the assistance of HARMONY is higher than that with the overhead exercise pulley ($P<0.05$).

In the experiment, we apply two different SHR ratios to examine whether the degree of the SHR changes by the robot can be even regulated.

Figure 7.1 shows the experimental setup for the overhead pulley exercise. While the subject is asked to fully relax, an operator pulls up the subject's hand using an overhead pulley, where the handle is securely connected to the subject's hand by a gripping glove (Active Hands, Ltd.) so that the hand and forearm can also be totally relaxed.

7.2.1.3 An Abnormality Inspired by Spasticity in the Shoulder: Active Elevation

Muscle tone during spasticity phases is partly responsible for the abnormal coordination around the shoulder. The force by the muscle tone constrains the shoulder girdle in several stereotypical patterns including the one that pulls the shoulder girdle to be retracted and depressed. If a constraining force that is similar to the one from the muscle tone acts on a healthy shoulder, the coordination of the shoulder may exhibit an abnormality in either kinematics or muscle activities that resembles a part of the abnormality in the spastic shoulders. Once an abnormality is introduced, by measuring whether the robot recovers the altered biomechanics of the shoulder, we may assess the potential of the robot to assist the rehabilitation for the shoulder with muscle tone. However, any excessive constraints on the activated shoulder would impose undesirable stresses and must be avoided in the experiment for the safety of human subjects. The constraints have to allow the inherent coordinated movements while applying the least necessary force to change the biomechanics of the shoulder coordination. In this experiment, differences in kinematics and muscle activation are investigated during active elevation with and without the constraints, and the robot assistance in the presence of the constraints. Also, we do not include the effect of spasticity, which is velocity-dependent resistance to passive stretch.

We adopted kinesiology tapes such as Kinesio Taping® and applied it to a healthy subject to constrain the shoulder against protraction and elevation. The direction, tension, and number of layers of the taping were decided based on trial

and error to effectively constrain the shoulder girdle to be retracted and depressed at rest. Two groups of tapes were applied in vertical and horizontal manner. The subjects were asked to maintain the posture of retracted and depressed shoulder during taping. The origin of the vertical tapes starts from the frontal surface of the shoulder and covers the acromion and lateral end of the clavicle across the acromio-clavicular joint. While the tension of the tape is kept at almost its maximum, the insertion points of the vertical tapes ran from the middle of thoracic spine to the lumbar. The vertically applied tapes provide pull-down forces that induce shoulder depression and some of shoulder retraction. The horizontally applied tapes that starts from the upper rib cage under the armpit and ends at the other armpit running over the inferior angle of the scapula provide more constraints for shoulder retraction. Figure 7.2 shows an example of a shoulder constrained by the taping, and the effect of constraining forces that pull down and back the shoulder girdle. Also, the maximum range of motion in abduction and forward flexion are reduced by the tapes, implying a change in the coordination which is being investigated in the experiment.

With a healthy subject with taping, the purpose of the experiment is to evaluate whether the biomechanics of the shoulder is changed or not, and if changed, to check if the robot assistance recovers the altered biomechanics. We postulate hypotheses as follows;

Hypothesis 2 (H1): the constraint by the tape imposes a difference in the kinematics or muscle activities of the shoulder during active elevation compared to those during active elevation without any constraint ($P<0.05$).

Figure 7.2: The shoulder constrained by kinesiology tapes.

Hypothesis 3 (H1): There is a difference in kinematics or muscles activities between during active elevation without any constraint and during active elevation with the constraints and the robot assistance ($P<0.05$).

The first hypothesis verifies whether the constraint by the tape introduces an abnormality in the shoulder biomechanics. The second hypothesis evaluates whether the SHR assistance from the robot properly recovers the altered kinematics or muscle activities. Here 'recover' means that there are no meaningful differences in both kinematics and muscle activities between the baseline active elevation and the active elevation with the constraint and the robot assistance.

7.2.2 Participants

11 healthy adults (age: 23 ± 3.5, range: 19.7-30.2, five females, nine right-handed) with no history of injuries or neurological disorders in the shoulder participated in the study. The experimental procedure was approved by the Internal

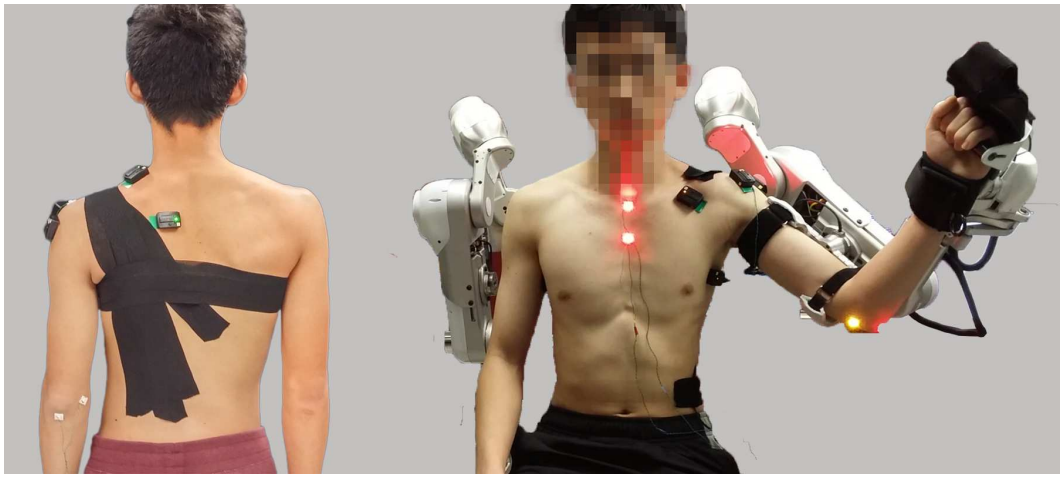

Figure 7.3: The shoulder constrained by taping and an active arm elevation with the SHR assistance by the robot.

Review Board (IRB) organized by the Office of Research Support in The University of Texas at Austin, and the participants provided written informed consent that was reviewed by the board.

7.2.3 Experiment Protocols

7.2.3.1 Protocol for Passive Elevation

In the passive elevation case, three conditions were applied: a baseline passive elevation and passive elevations with two conditions of the robot assistance. For the baseline passive elevation, an operator elevated the arm of the participants using an overhead pully while the participants were asked to relax their arm and shoulder as much as possible. The participants were seated upright, and the operator pulled up subjects left hand, which was securely attached to the handle of the overhead pulley. The range of elevation was from around 20 degrees to around 120

degrees of upper arm elevation angle along the plane of elevation that was deviated from the frontal plane by 45 degrees. The upper arm was externally rotated (in lateral rotation) while the forearm was kept vertical to the ground at all time during the elevation. The speed of elevation was maintained very low (around 10 seconds to the maximum elevation) to suppress any velocity-related effects from muscle stretch of the participants. In the case of the robot assistance, while the subjects were connected to the robot in the baseline control with the SHR assistance, the operator pulled up the robot handle that was securely connected the subject's hand, using the overhead pulley in the same way of the previous case to preserve the experiment condition except the shoulder assistance from the robot. Two ratios between the humeral angle and the shoulder girdle angle in the SHR assistance were applied to confirm whether the SHR assistance could regulate the shoulder coordination with different SHR ratio values in the controller. The three conditions for passive elevation are as follows:

- Condition 1: passive elevation by an overhead pulley.
- Condition 2: passive elevation by an overhead pulley in the presence of the SHR assistance with a relatively high SHR ratio (C1) from the robot.
- Condition 3: passive elevation by an overhead pulley in the presence of the SHR assistance with a relatively low SHR ratio (C2) from the robot.

7.2.3.2 Protocol for Active Elevation

In the active elevation experiment, three conditions were applied: a baseline active elevation, an active elevation with a constraint on the shoulder girdle, and an active elevation with the SHR assistance from the robot in the presence of the constraint on the shoulder girdle. For the baseline active elevation, while seated upright, the participants were asked to elevate their arm along the plane of elevation that was deviated from the frontal plane by 45 degrees. The range of elevation was from around 20 degrees to around 120 degrees of upper arm elevation angle. The participants were asked to maintain the forearm vertical to the ground at all time during the elevation to keep the upper arm in lateral rotation. After applying kinesiology tapes to the shoulder girdle, the elevation was proceeded as in the baseline active elevation except an reduced range of elevation. To minimize any risk of pain or injury around shoulder by the constraint, the participants were asked to elevate their arm only in the range where they did not feel any discomfort or pain. The same procedure was applied to the elevation with the tape applied and the SHR assistance by the robot. The three conditions for active elevation are as follows:

- Condition 1: active elevation.
- Condition 2: active elevation in the presence of the constraint from the kinesiology tape on the shoulder girdle.
- Condition 3: active elevation in the presence of the constraint and the SHR assistance from the robot.

7.2.4 Measurement

We measured kinematic and EMG data around the shoulder. In the passive elevation experiment, the kinematic data was used to compare the shoulder coordination in the three conditions while EMG data was used to confirm that there was not a prominent muscle activation during the passive elevation. In the active elevation experiment, both the kinematic and EMG data were used to compare the shoulder biomechanics in the three conditions.

To measure the kinematics around the shoulder, a motion capture system (Phasespace Inc., Impulse X2) was used with three landmarks at the upper sternum (between the two sternoclavicular joints), acromion process, and olecranon (at the point where the extension line of the humerus meet at 90 degrees of elbow flexion). We assume that the line from the upper sternum to a point below the acromion process represents the position of the shoulder girdle and the line from the point under the acromion process to the olecranon represents the position of the humerus. The point under the acromion process was assumed to be the center of glenohumeral joint since the point was selected in a way that the defined humeral length was minimally changed during the humeral elevation. Figure 7.4 shows the angle representations of the humeral and shoulder elevation. θ_1 indicates the angle between the humeral line and the global vertical line with respect to the humeral elevation plane. θ_1 represents the angle between the shoulder girdle line and the global horizontal line with respect to the frontal plane of the body. The coordination around the shoulder was defined as the ratio between θ_1 and θ_1.

An EMG data acquisition system (Delsys Inc., Trigno Wireless EMG) mea-

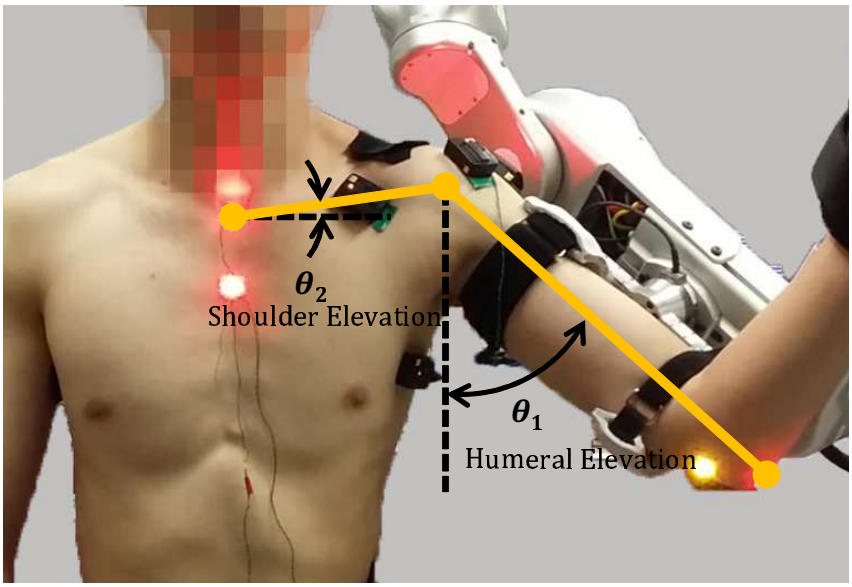

Figure 7.4: Angle measurement from a Motion Capture System. θ_1 and θ_2 represent the humeral elevation angle and shoulder girdle elevation angle, respectively.

sured muscle activation at the upper and middle trapezius, anterior and middle deltoid, pectoralis major, and serratus anterior (Figure 7.5). EMG signals were filtered by a fifth order low-pass Butterworth filter at 5 Hz and normalized using an MVC method. In the analysis, only two data groups at the upper trapezius and anterior deltoid were used since only the upper trapezius, anterior and middle deltoid were evidently activated during humeral elevation, and the anterior deltoid exhibited similar patterns with the middle deltoid with higher activation levels.

Synchronization between the motion capture data and EMG data was ensured in the post process using a spike signal that was generated by a brief voluntary movement prior to every measurement.

Figure 7.5: EMG sensors attached on a participant.

7.2.5 Dependent Variables and Data Analysis

The goal of this experiment was to compare the kinematics and muscle activation before and after the robot assistance to the shoulder coordination with simulated abnormalities. To statistically compare the results, we took one dependent variable for each case. For the kinematics, we adopted a mean slope of the curve of the shoulder elevation (θ_2) with respect to the humeral elevation (θ_1). The mean slope was calculated from the data points at every 10 degrees from 40 degrees to 100 degrees in humeral elevation angle.

For the dependent variable in muscle activation, we mapped the time-base EMG data to an EMG curve with respect to the humeral elevation angle and adopted an integration value of the EMG curve with respect to the humeral elevation, analogizing work done by force and displacement. The range of the integration was between 40 to 100 degrees of humeral elevation angle.

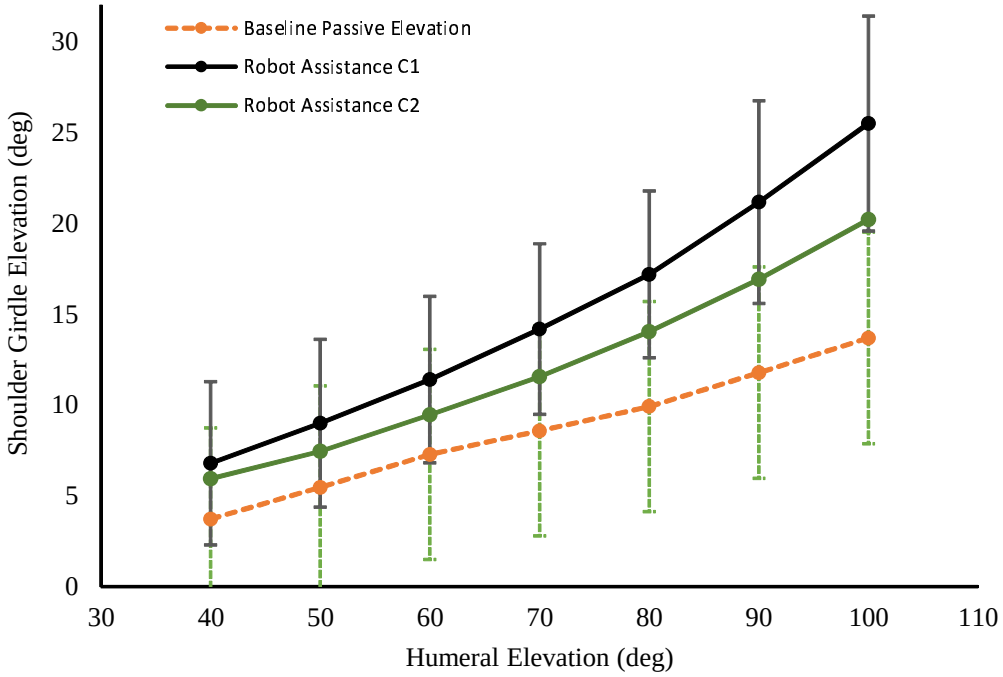

Figure 7.6: Averages and standard deviations of the shoulder kinematics in the three groups of passive elevation for all subjects

The one-way repeated measure analysis of variance (ANOVA) was used for the comparison of each pair when all the data groups of the three conditions fall in normality. The one-way repeated measure ANOVA and Wilcoxon signed-rank test were complementarily applied when at least one of the data groups of the three conditions does not follow normality. Outliers are maintained as long as they are not from measurement error. The significance level was 0.05 for all the cases.

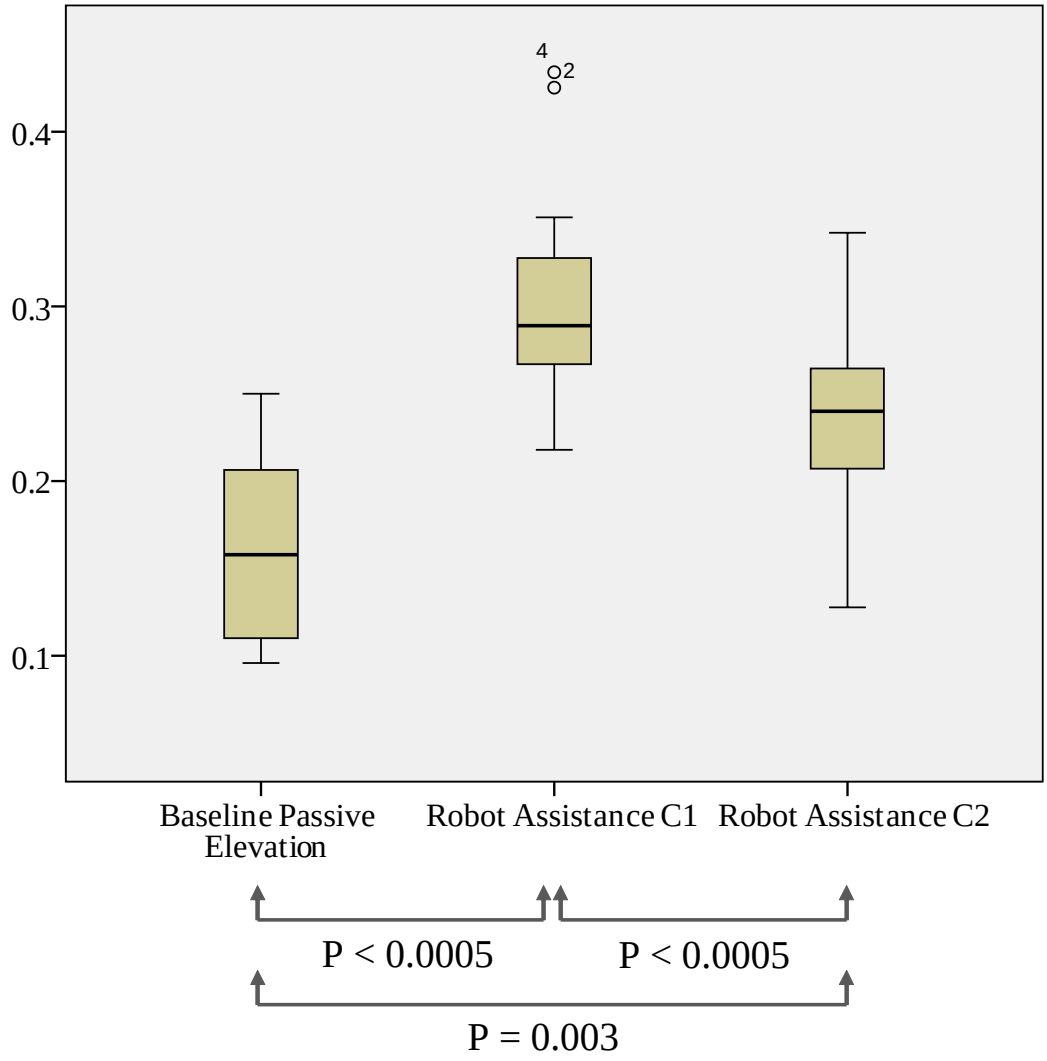

Figure 7.7: Box plots and statistical analysis results of the shoulder kinematics in the three groups of passive elevation by an overhead pulley

7.3 Result

In the passive elevation experiment, the shoulder kinematics was meaningfully changed by the robot assistance compared to the baseline passive elevation.

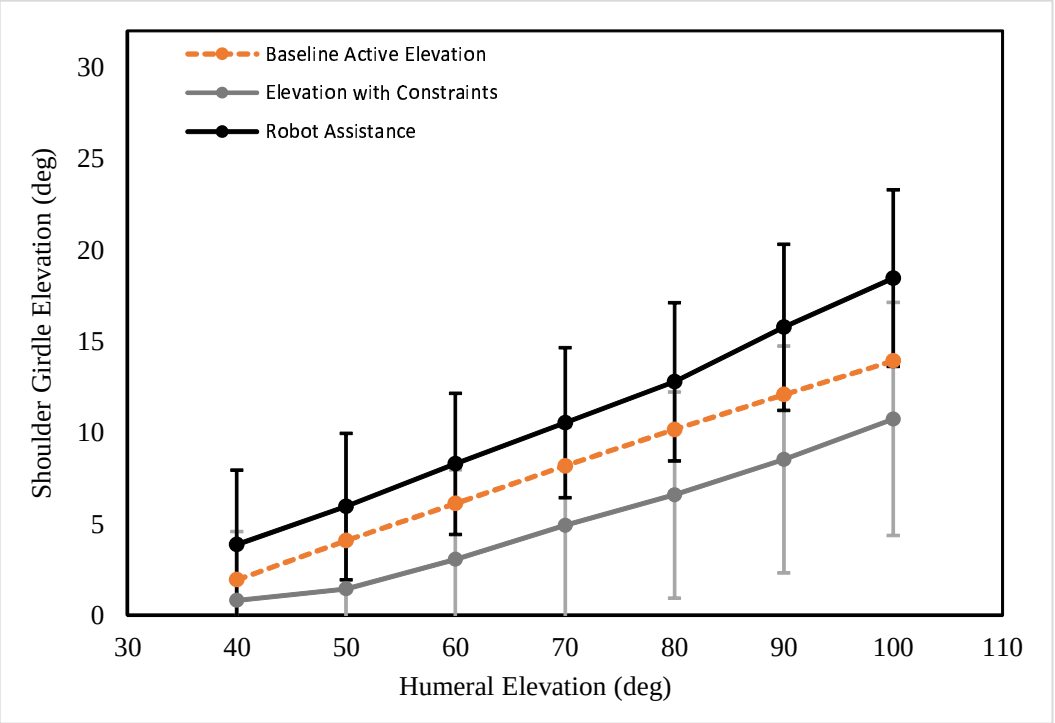

Figure 7.8: Averages and standard deviations of the shoulder kinematics in the three groups of active elevation

The averaged slope of the shoulder coordination at each condition showed an increasing trend (Figure 7.6), where the shoulder girdle positions of the participants were firstly averaged at each humeral position and then, the dots were connected. C1 indicates a higher rhythmic ratio than C2 in the SHR assistance. For statistical comparison, the mean slope of each participant at each condition was calculated first and the variances of all the slopes were analyzed. The result showed significant differences in the shoulder kinematics of the three conditions ($F(1.250, 12.497)=48.084$, $P<0.0005$, pairwise P values in Figure 7.7). Two outliers in the group of the robot assistance with C1 were included in the anlaysis since they were

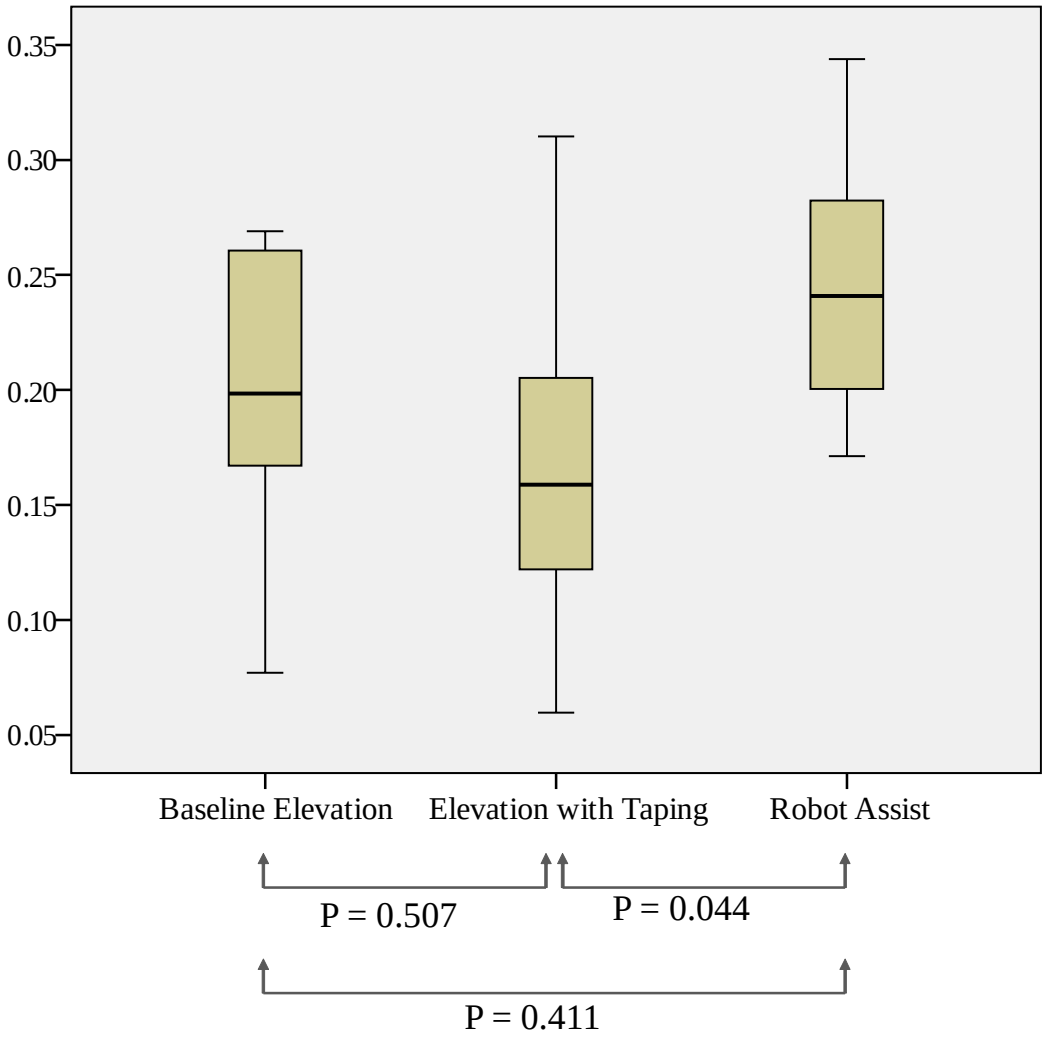

Figure 7.9: Box plots and statistical analysis results of the shoulder kinematics in the three groups of active elevation

not extreme and all the three data groups including the outliers followed a normal distribution. The sphericity assumption was violated, and the one-way repeated measures ANOVA was adjusted according to Greenhouse-Geisser.

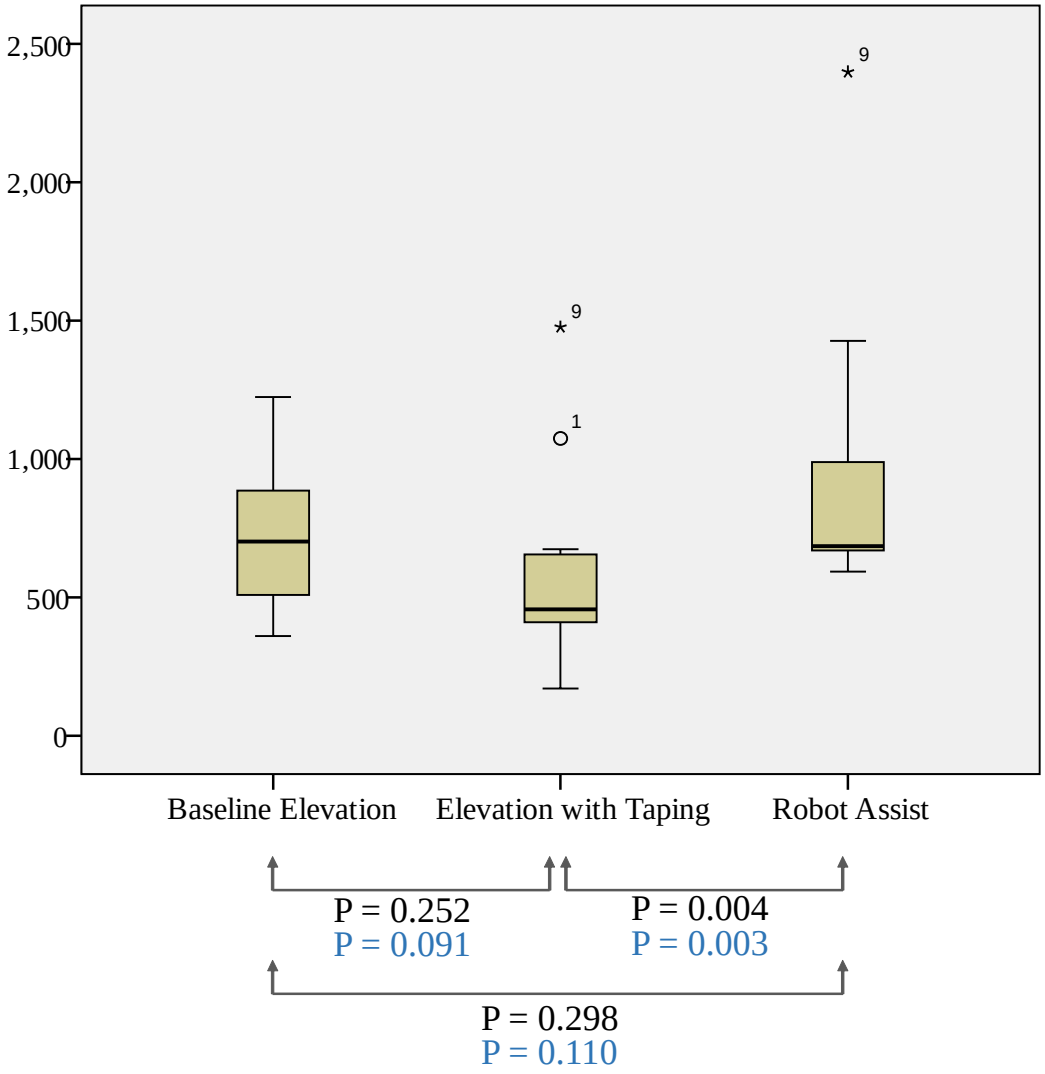

Figure 7.10: Box plots and statistical analysis results of the muscle efforts of the upper trapezius in the three groups of active elevation. The upper pairwise P values from the one-way repeated measures ANOVA and the lower from the Wilcoxon signed-rank test.

In the shoulder coordination of the active elevation case, the result showed that there was a significance difference between the constraint and the robot assis-

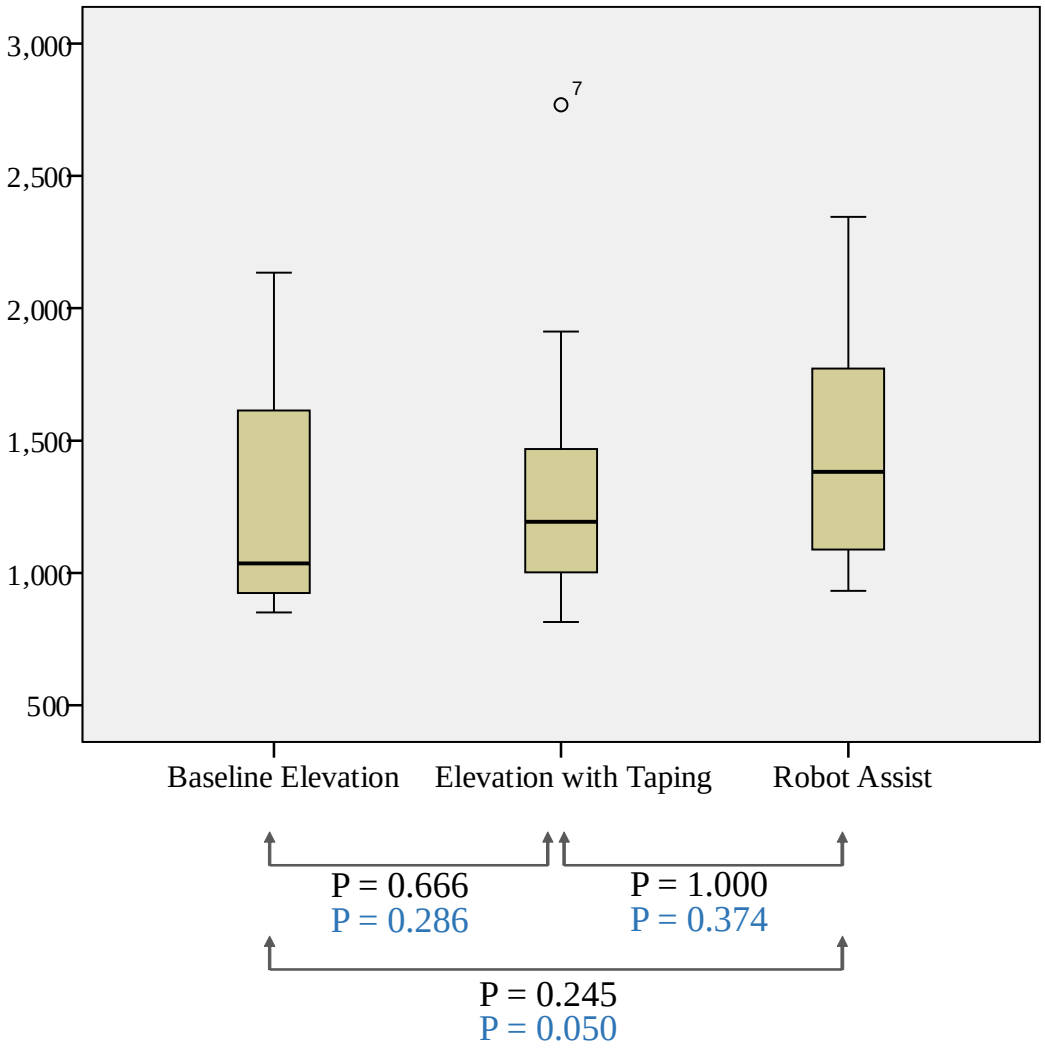

Figure 7.11: Box plots and statistical analysis results of the muscle efforts of the anterior deltoid in the three groups of active elevation. The upper pairwise P values from the one-way repeated measures ANOVA and the lower from the Wilcoxon signed-rank test.

tance case while the constraint did not induce a statistical significance in the slope of the shoulder kinematics (the one-way repeated measures ANOVA, F(2, 20)=4.668,

P=0.022, pairwise P values appears in Figure 7.9). Despite the insignificance, still, there was a tendency of reduction in the slope by the constraint. The averaged shoulder kinematics at each condition are shown in Figure 7.8. Regardless of the results of the slope, the constraint induced an offset in the shoulder coordination downward and the robot assistance recovered the offset as appeared in Figure 7.8.

In the muscle activation of the upper trapezius, there were two extreme outliers. The two outliers were due to the higher muscle activation than their MVC. The first outlier that showed around 120% of activation level was included in the analysis without modification. On the other hand, in the second outlier, the MVC exhibited a significantly lower value than other subjects' MVC in the upper trapezius leading around 300% of muscle activation level. Considering the MVC practice where the subject pushed against rigidly constraint environment while carrying the subject's own arm weight compared to the active elevation that carried only the subject's own arm weight, we suspected that there was a measurement error in the MVC. We conducted statistical analysis with and without modification on the second outlier. In the modification, the MVC of the second outlier was replaced by the average of the same gender's MVCs in the upper trapezius.

With the modified outlier, there was a significant difference in the muscle activation of the upper trapezius between the constraint and robot assistance case both in the ANOVA and non-parametric methods (pairwise P values in Figure 7.10). Without any modification, the non-parametric method delivered the same result while the ANOVA exhibited insignificance. The constraint did not induce a significant abnormality in the muscle activation compared to the baseline active

elevation. The one-way repeated measures ANOVA (with the modified outlier, $F(1.332, 13.319)=7.308$, $P=0.013$, pairwise P values appears in Figure 7.10) and non-parametric analysis (Wilcoxon signed-rank test) were complementarily used because the data violated the assumption of normality and had the extreme outliers. The sphericity assumption was violated, and the ANOVA was adjusted according to Greenhouse-Geisser. An extreme outlier was defined as one more than three box-lengths from the edge of the box in the boxplot.

The muscle activation of the anterior deltoid was not significantly changed by the constraint or the robot assistance. The one-way repeated measures ANOVA ($F(2, 20)=2.076$, $P=0.152$, pairwise P values appears in Figure 7.11) and non-parametric analysis (Wilcoxon signed-rank test) were complementarily used because the data violated the assumption of normality, and the statistical results were the same.

7.4 Discussion

The statistical result of the passive elevation experiment showed that the robot could significantly change the shoulder coordination during passive humeral elevation. The result suggests that the robot may be able to assist a paralyzed shoulder to achieve a proper coordination during robot-driven passive exercises. The robot may provide passive ROM exercises in wide ranges with a proper coordination around the shoulder, which would reduce a risk of injuries or pain caused by mal-coordination in the shoulder including impingement.

The limitation of the experiment is that the shoulder coordination that we

define can be different from scapulohumeral rhythm. Scapulohumeral rhythm is defined as the ratio between the humeral elevation versus the upward rotation of the scapula, while the shoulder coordination in this study is defined as the ratio between the humeral elevation versus the upward rotation of the line that runs from the SC to GH joint. This is partly due to the limited access to the surface above the scapula where the visibility of the markers on the surface to the cameras is limited by the blockage of the robot worn around the body. Also, the motion data from the markers on the surface above the scapula are usually unreliable because of artifacts from large skin movements with respect to the scapula [62]. We may still presume the angle of the line represents the scapulohumeral rhythm. This is because the elevation of the lateral angle of the scapula (elevation of the shoulder around the acromion and AC joint) more than the elevation in the superior angle of the scapula indicates the upward rotation of the scapula and no major elevation of the superior angle was observed during the shoulder elevation. Therefore, the changes in the angle of the line by the external engagements can be reasonable representation of the changes in scapulohumeral rhythm in a certain degree.

In the active elevation experiment, the robot assistance increased the muscle activation in the upper trapezius and scapulohumeral rhythm compared to the constraint case. There was a tendency of reduction both in the kinematics and upper trapezius activation by the constraint from the kinesiology taping compared to the baseline active elevation; however, the constraint induced limited abnormality in both the kinematics and muscle activation in statistically meaningful ways. Although an abnormality was not sufficiently introduced, the results imply that in

patient-active elevation the robot might be able to positively affect the shoulder with an abnormality by neuromuscular disorders.

The reason the kinematics did not exhibit significant differences by the constraint might be that the highly activated muscle around the shoulder to overcome gravity restricted the influence of the constraining forces by the tapes. As we were concerned for the comfort of the subjects during the experiment, the forces from the constraint may not have been strong enough to change the kinematics of the activated shoulder. However, the robot assistance was enough to change the scapulohumeral rhythm and muscle activation of the upper trapezius while counteracting the effect of the activated muscles and constraints. Despite of the statistical insignificance, there was a tendency of reduction both in the kinematics and muscle activation by the constraint. Also, there were no significant differences between the baseline active elevation and robot assistance case. From these facts, the robot might be considered to be capable of restoring the kinematics and muscle activation induced by the constraint to match those in the baseline elevation. On the other hand, the shoulder elevator, the anterior deltoid, was not significantly changed by any condition. This might be because the constraining forces applied only to the shoulder girdle proximally after the glenohumeral joint.

7.5 Conclusion

In this chapter, we evaluated the effects of HARMONY and its control algorithm on the shoulder coordination. Inspired by the flaccidity and spasticity of the hemiplegic shoulder after stroke, we simulated abnormalities in healthy subjects

during passive and active humeral elevation. In the passive elevation experiment that simulated the situation of an overhead pulley exercise with a flaccid shoulder, the robot effectively changed the shoulder coordination, implying an advantage of the robot in passive ROM exercises accompanying an assisted coordination. In the active elevation experiment, the robot assistance increased scapulohumeral rhythm and muscle activation of the shoulder girdle elevator (upper trapezius) implying an effectiveness of the robot on correcting an abnormal muscle activation pattern and shoulder coordination. In conclusion, we confirmed the capability of the robot in affecting the shoulder coordination during arm movements. Further investigation is necessary for examining the efficacy of the robot in positively affecting dyskinesia of the shoulder including the hemiplegic shoulder of a stroke subject.

Chapter 8

Discussion and Future Work

The work here was to develop an upper-body exoskeleton, called HARMONY, with the goal of promoting the efficacy of robotic rehabilitation. HARMONY supports the natural mobility of the upper body with kinematic compatibility and a wide range of motion. The robot also provides a minimal impedance behavior that promotes participant's voluntary movements while serving as a substrate for developing various robotic rehabilitation exercises based on force and impedance behaviors. The shoulder mechanism, one of the key challenges in designing an upper-body exoskeleton, was designed to offer an anatomical mobility with five DOFs. The experimental results showed that HARMONY supported a wide range of motion with a good kinematic compatibility, implying that almost all types of movements for therapeutic exercises could be implemented in the robot. The dynamic performance tests verified that the robot exhibits a very low impedance with well-commanded spatial force and impedance behaviors. With a gravity support to patient's arm weight, the minimum impedance will promote the chance of voluntary movements from the patient that is a key value in maximizing relearning. Also, a variety of force and impedance-based exercises can be superimposed to the baseline status without a major distortion from the robot dynamics. The stability analysis proved that the robot would remain stable in interacting with

the human body, serving as a critical criterion for safety of the exoskeleton. In the human subject experiments, the control for assisting the coordination of the shoulder induced desirable changes in the shoulder coordination in the presence of abnormalities. The experimental results suggest that the robot could shape the shoulder coordination and guide arm movements with a proper coordination in the hemiplegic shoulder with a flaccidity or spasticity. The SHR assistance is expected to reduce the risk of injuries that would be from a mal-coordinated arm traction, so that a large dose of passive exercises can be safely performed. The control scheme of the SHR assistance control can be easily extended to an assistance for other interjoint coordination.

Nevertheless, there are several mechanical and control aspects of the robot system that can be improved. For example, the robot body segments can be designed to be lighter. The torque and power of the electrical motor are limited due to the restricted space at the multi-DOF linkage structure with a wide ROM requirement. A higher power-to-weight ratio that can be achieved by reducing the weight will increase the ability to deal with variable demands including carrying a large load. From the control perspective, the joint-level torque response could be refined, for example, by taking into account the overall dynamics of the SEA unit and using a full-state feedback, which leads to better spatial force and impedance performances.

The robot is also missing the hand and wrist mobility. Most functional tasks of the upper limb recruit the functionality in the hand and wrist. Limited functional recovery after robotic rehabilitation, despite of improved motor control in the arm

and shoulder, may be partly due to the absence of the rehabilitation in the hand and wrist, as pointed out in the previous review studies [117, 92]. Inversely, without recovery at the arm and shoulder, functional recovery may also be limited because most functional tasks require the hand as an end-effector to be correctly placed or moved in task space by the arm and shoulder. The right question would be whether a concurrent functional training coordinated from the shoulder to fingers is necessary or not. If so, the robot would need to incorporate a module for the hand and wrist mobility. The correlation between the proximal and distal movements in functional recovery of upper limb remains uncertain and needs to be further investigated [79].

So far, this research is limited in showing any evidence that the advanced features equipped in the system will enhance motor recovery. Rather, the results here show that the exoskeleton may serve as a research platform for long-term clinical studies that are designed to prove or confirm contemporary neurological findings in motor learning and their effectiveness for rehabilitation. The advances of HARMONY in kinematic and dynamic features will allow us to design a variety of experimental environments to investigate the issues on voluntary effort, type of assistant forces, massed repetition versus variable task practice, context interference, explicit versus implicit learning, augmented feedback, or coordination that have been extensively discussed in neurological studies and rehabilitation research [75, 10, 133, 92, 68, 50, 157, 115, 83, 26, 11]. To date, many robotic rehabilitation protocols have followed a massed repetition paradigm, but its effectiveness has been doubted, especially in retention and in exhibiting functional recovery [117, 92]. By incorporating implications from the findings in motor learning

and neural plasticity, we will be able to develop rehabilitation protocols in HARMONY that maximize motor recovery after neurological injuries.

While the development of an effective protocol for motor recovery requires further investigation, HARMONY with the current control framework can be directly applied to passive range of motion (ROM) exercises. For example, we have conducted a preclinical test of HARMONY with a stroke patient for passive mobility exercises. The study focused on evaluating the eligibility of impedance-based robot-guided passive exercises and therapist-guided passive exercises with the help of HARMONY for gravity support to the patient's weight. The participant was a middle-aged male with a right hemispheric stroke (two years since the occurrence). The subject had severely impaired mobility at the left arm and shoulder with spasticity and muscle tone. The exercises consisted of several movements of the arm and shoulder with the coordination at the shoulder. The control algorithm was based on the baseline control with an additional gravity support for the patient's arm weight and impedance-based trajectory control. The session was held for one hour, four days a week, lasting three weeks in total. The study was not investigating any long-term effect of the exercises to draw any data-based conclusions. However, we observed an increased voluntary mobility under the gravity support mode, and the inferior subluxation was significantly reduced due to the gravity support while in the robot. The patient also reported comfort during robot-assisted movements without any pain around the joints. The participating physician and therapist also confirmed that muscle tone and spasticity were reduced after the passive exercises, and the scapula exhibited right coordination during humeral motions with HARMONY

through palpation. Toward the end of the 3-weeks session, it was confirmed that the patient started to use unused muscle group (the triceps) and exhibited much less compensatory torso movements during the resistive exercises. With these positive results, this preclinical test has convinced us that HARMONY was able to provide a safe and effective passive exercises, and the gravity support with the baseline control that exhibited a minimal impedance could enhance voluntary movements in the impaired arm during the assistance. Although the results were confirmed based on short-term observation, we believe that some of these positive effects of HARMONY may transfer to long-term efficacy leading better recovery, which will be investigated in the future.

HARMONY has the potential to serve as an assessment platform that evaluates motor impairments of patients. Many of commonly used assessment protocols such as Fugl-Meyer test (FM) and Chedoke-McMaster Stroke Assessment Scale consist of discrete index scales and rely on the subjective judgment of clinical practitioners. HARMONY can precisely and consistently measure and record movement qualities, ranges of motion, and forces applied by users both in joint and work space. Using the measurement capability of HARMONY, we may be able to develop an assessment protocol that can thoroughly diagnose motor abilities. The new protocol may provide a better insight to motor impairments allowing for clinical practitioners to prescribe user-specific exercises and training goals.

Chapter 9

Conclusion

This dissertation presented upper-body exoskeleton HARMONY with its kinematic design, modeling and control, kinematic and dynamic performances, and human subject study.

In this document, several critical issues on designing and controlling an upper-body exoskeleton have been discussed, which may help rehabilitation robotics community in developing next generation exoskeletons. The results of the kinematic and dynamic performance tests confirmed that HARMONY was designed to meet the design goals in mobility and physical interaction characteristics. The human subject experiments showed the capability of the robot in assisting shoulder coordination which was stressed as the main feature.

By utilizing the advanced features including natural mobility and dynamic behavior, HARMONY would serve as a research platform for developing control strategies for upper-body robotic rehabilitation based on neurological principles and investigating their clinical significances. Eventually, HARMONY is expected to provide advanced rehabilitation practices that further motor recovery after neuromuscular injuries.

Appendices

Bibliography

[1] Centers for disease control and prevention. available: http://www.cdc.gov.

[2] L Ada, CG Canning, JH Carr, SL Kilbreath, and RB Shepherd. Task-specific training of reaching and manipulation. *Advances in psychology*, 105:239–265, 1994.

[3] DS Andreasen, AA Aviles, SK Allen, RB Guthrie, BR Jennings, and SH Sprigle. Exoskeleton for forearm pronation and supination rehabilitation. In *International Conference of the IEEE Engineering in Medicine and Biology Society*, volume 1, pages 2714–2717, 2004.

[4] Robert Stawell Ball. The theory of screws: A study in the dynamics of a rigid body. *Mathematische Annalen*, 9(4):541–553, 1876.

[5] Stephen J Ball, Ian E Brown, and Stephen H Scott. MEDARM: a rehabilitation robot with 5DOF at the shoulder complex. In *IEEE/ASME International Conference on Advanced Intelligent Mechatronics*, pages 1–6, 2007.

[6] Sai K Banala, Suni K Agrawal, and John P Scholz. Active Leg Exoskeleton (ALEX) for gait rehabilitation of motor-impaired patients. In *IEEE 10th International Conference on Rehabilitation Robotics*, pages 401–407, 2007.

[7] ND Barnett, RDD Duncan, and GR Johnson. The measurement of three dimensional scapulohumeral kinematics–a study of reliability. *Clinical Biomechanics*, 14(4):287–290, 1999.

[8] Berta Bobath. *Adult hemiplegia: evaluation and treatment*. Elsevier Health Sciences, 1990.

[9] Bernadette Brady, Julie Redfern, Graeme Macdougal, and Jan Williams. The addition of aquatic therapy to rehabilitation following surgical rotator cuff repair: a feasibility study. *Physiotherapy Research International*, 13(3):153–161, 2008.

[10] Bambi R Brewer, Sharon K McDowell, and Lise C Worthen-Chaudhari. Poststroke upper extremity rehabilitation: a review of robotic systems and clinical results. *Topics in stroke rehabilitation*, 14(6):22–44, 2007.

[11] Nancy Byl, Jennifer Roderick, Olfat Mohamed, Monica Hanny, Josh Kotler, Amy Smith, Molly Tang, and Gary Abrams. Effectiveness of sensory and motor rehabilitation of the upper limb following the principles of neuroplasticity: patients stable poststroke. *Neurorehabilitation and Neural Repair*, 17(3):176–191, 2003.

[12] Nancy N Byl, Gary M Abrams, Erica Pitsch, Irina Fedulow, Hyunchul Kim, Matt Simkins, Srikantan Nagarajan, and Jacob Rosen. Chronic stroke survivors achieve comparable outcomes following virtual task specific repetitive training guided by a wearable robotic orthosis (UL-EXO7) and actual task

specific repetitive training guided by a physical therapist. *Journal of Hand Therapy*, 26(4):343–352, 2013.

[13] Lance L Cai, Andy J Fong, Chad K Otoshi, Yongqiang Liang, Joel W Burdick, Roland R Roy, and V Reggie Edgerton. Implications of assist-as-needed robotic step training after a complete spinal cord injury on intrinsic strategies of motor learning. *The Journal of neuroscience*, 26(41):10564–10568, 2006.

[14] Darwin G Caldwell, C Favede, and N Tsagarakis. Dextrous exploration of a virtual world for improved prototyping. In *IEEE International Conference on Robotics and Automation*, volume 1, pages 298–303, 1998.

[15] Darwin G Caldwell, Nikolaos G Tsagarakis, Sophia Kousidou, Nelson Costa, and Ioannis Sarakoglou. "Soft" exoskeletons for upper and lower body rehabilitationdesign, control and testing. *International Journal of Humanoid Robotics*, 4(03):549–573, 2007.

[16] Craig Carignan, Michael Liszka, and Stephen Roderick. Design of an arm exoskeleton with scapula motion for shoulder rehabilitation. In *IEEE International Conference on Advanced Robotics*, pages 524–531, 2005.

[17] Craig Carignan, Jonathan Tang, S Roderick, and M Naylor. A configuration-space approach to controlling a rehabilitation arm exoskeleton. In *IEEE International Conference on Rehabilitation Robotics*, pages 179–187, 2007.

[18] Janet H Carr. *Movement science: foundations for physical therapy in rehabilitation*. Aspen Publishers, 1987.

[19] James H Cauraugh, Neha Lodha, Sagar K Naik, and Jeffery J Summers. Bilateral movement training and stroke motor recovery progress: a structured review and meta-analysis. *Human Movement Science*, 29(5):853–870, 2010.

[20] Centers for Disease Control and Prevention. Prevalence and most common causes of disability among adults–united states, 2005. *MMWR: Morbidity and Mortality Weekly Report*, 58(16):421–426, 2009.

[21] J Chaco and E Wolf. Subluxation of the glenohumeral joint in hemiplegia. *American journal of physical medicine & rehabilitation*, 50(3):139–143, 1971.

[22] Jim D Chapel and Renjeng Su. Coupled stability characteristics of nearly passive robots. In *Robotics and Automation, 1992. Proceedings., 1992 IEEE International Conference on*, pages 1342–1347. IEEE, 1992.

[23] Haiwen Chen, Jane Epstein, and Emily Stern. Neural plasticity after acquired brain injury: evidence from functional neuroimaging. *PM&R*, 2(12):S306–S312, 2010.

[24] James Edward Colgate and Neville Hogan. Robust control of dynamically interacting systems. *International journal of Control*, 48(1):65–88, 1988.

[25] Stephanie A Combs, Stephanie P Kelly, Rebecca Barton, Megan Ivaska, and Kara Nowak. Effects of an intensive, task-specific rehabilitation program for

individuals with chronic stroke: A case series. *Disability & Rehabilitation*, 32(8):669–678, 2010.

[26] Michael A Conditt, Francesca Gandolfo, and Ferdinando A Mussa-Ivaldi. The motor system does not learn the dynamics of the arm by rote memorization of past experience. *Journal of Neurophysiology*, 78(1):554–560, 1997.

[27] Laura Cushman and Bruce Caplan. Multiple memory systems: Evidence from stroke. *Perceptual and motor skills*, 64(2):571–577, 1987.

[28] Filiep Debaere, Nicole Wenderoth, Stefan Sunaert, Paul Van Hecke, and SP Swinnen. Changes in brain activation during the acquisition of a new bimanual coordination task. *Neuropsychologia*, 42(7):855–867, 2004.

[29] Michael J DePalma and Ernest W Johnson. Detecting and treating shoulder impingement syndrome: the role of scapulothoracic dyskinesis. *The Physician and Sportsmedicine*, 31(7):25–32, 2003.

[30] Natalia Dounskaia. The internal model and the leading joint hypothesis: implications for control of multi-joint movements. *Experimental Brain Research*, 166(1):1–16, 2005.

[31] Julien Doyon and Habib Benali. Reorganization and plasticity in the adult brain during learning of motor skills. *Current opinion in neurobiology*, 15(2):161–167, 2005.

[32] Alexander W Dromerick, Dorothy F Edwards, and Ashok Kumar. Hemiplegic shoulder pain syndrome: frequency and characteristics during inpa-

tient stroke rehabilitation. *Archives of physical medicine and rehabilitation*, 89(8):1589–1593, 2008.

[33] Aaron Edsinger-Gonzales and Jeff Weber. Domo: a force sensing humanoid robot for manipulation research. In *IEEE/RAS International Conference on Humanoid Robots*, volume 1, pages 273–291, 2004.

[34] Steven D Eppinger and Warren P Seering. Understanding bandwidth limitations in robot force control. In *Robotics and Automation. Proceedings. 1987 IEEE International Conference on*, volume 4, pages 904–909. IEEE, 1987.

[35] Mehmet Alper Ergin and Volkan Patoglu. ASSISTON-SE: A self-aligning shoulder-elbow exoskeleton. In *IEEE International Conference on Robotics and Automation*, pages 2479–2485, 2012.

[36] Rafael F Escamilla, Kyle Yamashiro, Lonnie Paulos, and James R Andrews. Shoulder muscle activity and function in common shoulder rehabilitation exercises. *Sports Medicine*, 39(8):663–685, 2009.

[37] Roy Featherstone. The calculation of robot dynamics using articulated-body inertias. *The International Journal of Robotics Research*, 2(1):13–30, 1983.

[38] Roy Featherstone. *Robot Dynamics Algorithms*. Kluwer Academic Publishers, 1987.

[39] Roy Featherstone and David Orin. Robot dynamics: equations and algorithms. In *ICRA*, pages 826–834, 2000.

[40] Tamar Flash and Neville Hogan. The coordination of arm movements: an experimentally confirmed mathematical model. *The journal of Neuroscience*, 5(7):1688–1703, 1985.

[41] Robert T Floyd and Clem W Thompson. *Manual of structural kinesiology*. McGraw-Hill, 2004.

[42] Felipe Camargo Forte, Marcelo Peduzzi de Castro, Joelly Mahnic de Toledo, Daniel Cury Ribeiro, and Jefferson Fagundes Loss. Scapular kinematics and scapulohumeral rhythm during resisted shoulder abduction–Implications for clinical practice. *Physical Therapy in Sport*, 10(3):105–111, 2009.

[43] Antonio Frisoli, Fabio Salsedo, Massimo Bergamasco, Bruno Rossi, and Maria C Carboncini. A force-feedback exoskeleton for upper-limb rehabilitation in virtual reality. *Applied Bionics and Biomechanics*, 6(2):115–126, 2009.

[44] P Garrec, JP Friconneau, Yvan Measson, and Yann Perrot. ABLE, an innovative transparent exoskeleton for the upper-limb. In *IEEE/RSJ International Conference on Intelligent Robots and Systems*, pages 1483–1488, 2008.

[45] Lynne V Gauthier, Edward Taub, Christi Perkins, Magdalene Ortmann, Victor W Mark, and Gitendra Uswatte. Remodeling the brain plastic structural brain changes produced by different motor therapies after stroke. *Stroke*, 39(5):1520–1525, 2008.

[46] Alan S Go, Dariush Mozaffarian, Véronique L Roger, Emelia J Benjamin, Jarett D Berry, Michael J Blaha, Shifan Dai, Earl S Ford, Caroline S Fox, Sheila Franco, et al. Heart disease and stroke statistics–2014 update: a report from the american heart association. *Circulation*, 129(3):e28, 2014.

[47] Scott T Grafton, Eliot Hazeltine, and Richard Ivry. Functional mapping of sequence learning in normal humans. *Journal of Cognitive Neuroscience*, 7(4):497–510, 1995.

[48] Judy W Griffin. Hemiplegic shoulder pain. *Physical therapy*, 66(12):1884–1893, 1986.

[49] Abhishek Gupta, Marcia K O'Malley, Volkan Patoglu, and Charles Burgar. Design, control and performance of ricewrist: A force feedback wrist exoskeleton for rehabilitation and training. *The International Journal of Robotics Research*, 27(2):233–251, 2008.

[50] Robert E Hanlon. Motor learning following unilateral stroke. *Archives of physical medicine and rehabilitation*, 77(8):811–815, 1996.

[51] Dustin D Hardwick and Catherine E Lang. Scapular and humeral movement patterns of people with stroke during range of motion exercises. *Journal of Neurologic Physical Therapy*, 35(1):18, 2011.

[52] Andrew Heller, DT Wade, Victorine A Wood, A Sunderland, R Langton Hewer, and E Ward. Arm function after stroke: measurement and recovery

over the first three months. *Journal of Neurology, Neurosurgery & Psychiatry*, 50(6):714–719, 1987.

[53] Neville Hogan. Impedance control: An approach to manipulation: Part IIIApplication. *Journal of Dynamic Systems, Measurement, and Control*, 107(1):17–24, 1985.

[54] Neville Hogan. Controlling impedance at the man/machine interface. In *Robotics and Automation, 1989. Proceedings., 1989 IEEE International Conference on*, pages 1626–1631. IEEE, 1989.

[55] Neville Hogan, Hermano Igo Krebs, J Charnnarong, P Srikrishna, and Andre Sharon. MIT-MANUS: a workstation for manual therapy and training. I. In *IEEE International Workshop on Robot and Human Communication*, pages 161–165. IEEE, 1992.

[56] John M Hollerbach and Tamar Flash. Dynamic interactions between limb segments during planar arm movement. *Biological cybernetics*, 44(1):67–77, 1982.

[57] Ewa Jaraczewska and Carol Long. Kinesio® taping in stroke: improving functional use of the upper extremity in hemiplegia. *Topics in Stroke Rehabilitation*, 13(3):31–42, 2006.

[58] Barbro B Johansson. Brain plasticity and stroke rehabilitation the willis lecture. *Stroke*, 31(1):223–230, 2000.

[59] Margaret Johnstone. *Restoration of motor function in the stroke patient: a physiotherapist's approach*. Churchill Livingstone, 1987.

[60] Leonard E Kahn, Peter S Lum, W Zev Rymer, and David J Reinkensmeyer. Robot-assisted movement training for the stroke-impaired arm: Does it matter what the robot does? *Journal of Rehabilitation Research and Development*, 43(5):619, 2006.

[61] PE Kaplan, J Meridith, G Taft, and HB Betts. Stroke and brachial plexus injury: a difficult problem. *Archives of physical medicine and rehabilitation*, 58(9):415–418, 1977.

[62] Andrew R Karduna, Phil W McClure, Lori A Michener, and Brian Sennett. Dynamic measurements of three-dimensional scapular kinematics: a validation study. *Journal of biomechanical engineering*, 123(2):184–190, 2001.

[63] Avi Karni, Gundela Meyer, Christine Rey-Hipolito, Peter Jezzard, Michelle M Adams, Robert Turner, and Leslie G Ungerleider. The acquisition of skilled motor performance: fast and slow experience-driven changes in primary motor cortex. *Proceedings of the National Academy of Sciences*, 95(3):861–868, 1998.

[64] H Kazerooni. Robust, non-linear impedance control for robot manipulators. In *Robotics and Automation. Proceedings. 1987 IEEE International Conference on*, volume 4, pages 741–750. IEEE, 1987.

[65] Kazuo Kiguchi, Koya Iwami, Makoto Yasuda, Keigo Watanabe, and Toshio Fukuda. An exoskeletal robot for human shoulder joint motion assist. *IEEE/ASME Transactions on Mechatronics*,, 8(1):125–135, 2003.

[66] Bongsu Kim and Ashish D Deshpande. Controls for the shoulder mechanism of an upper-body exoskeleton for promoting scapulohumeral rhythm. In *2015 IEEE International Conference on Rehabilitation Robotics (ICORR)*, pages 538–542. IEEE, 2015.

[67] Bongsu Kim, Aurelien Rodot, and Ashish D Deshpande. Impedance control based on a position sensor in a rehabilitation robot. In *ASME 2014 Dynamic Systems and Control Conference*, page V003T43A005. American Society of Mechanical Engineers, 2014.

[68] Tomoko Kitago and John W Krakauer. Motor learning principles for neurorehabilitation. *Handb Clin Neurol*, 110:93–103, 2013.

[69] Verena Klamroth-Marganska, Javier Blanco, Katrin Campen, Armin Curt, Volker Dietz, Thierry Ettlin, Morena Felder, Bernd Fellinghauer, Marco Guidali, Anja Kollmar, Andreas Luft, Tobias Nef, Corina Schuster-Amft, Werner Stahel, and Robert Riener. Three-dimensional, task-specific robot therapy of the arm after stroke: a multicentre, parallel-group randomised trial. *The Lancet Neurology*, 13(2):159–166, 2014.

[70] J Klein, SJ Spencer, J Allington, K Minakata, ET Wolbrecht, R Smith, JE Bobrow, and DJ Reinkensmeyer. Biomimetic orthosis for the neurorehabilita-

tion of the elbow and shoulder (BONES). In *IEEE RAS & EMBS International Conference on Biomedical Robotics and Biomechatronics*, pages 535–541, 2008.

[71] Mary D Klein Breteler, Cornelis W Spoor, and Frans CT Van der Helm. Measuring muscle and joint geometry parameters of a shoulder for modeling purposes. *Journal of Biomechanics*, 32(11):1191–1197, 1999.

[72] Yoshiaki Kon, Naoya Nishinaka, Kazuyoshi Gamada, Hiroaki Tsutsui, and Scott A Banks. The influence of handheld weight on the scapulohumeral rhythm. *Journal of Shoulder and Elbow Surgery*, 17(6):943–946, 2008.

[73] Kyoungchul Kong, Joonbum Bae, and Masayoshi Tomizuka. A compact rotary series elastic actuator for human assistive systems. *Mechatronics, IEEE/ASME Transactions on*, 17(2):288–297, 2012.

[74] Kyoungchul Kong, Hyosang Moon, Doyoung Jeon, and Masayoshi Tomizuka. Control of an exoskeleton for realization of aquatic therapy effects. *Mechatronics, IEEE/ASME Transactions on*, 15(2):191–200, 2010.

[75] John W Krakauer. Motor learning: its relevance to stroke recovery and neurorehabilitation. *Current opinion in neurology*, 19(1):84–90, 2006.

[76] H Igo Krebs, Neville Hogan, Mindy L Aisen, and Bruce T Volpe. Robot-aided neurorehabilitation. *IEEE Transactions on Rehabilitation Engineering,*, 6(1):75–87, 1998.

[77] Hermano Krebs, Laura Dipietro, Shelly Levy-Tzedek, Susan E Fasoli, Avrielle Rykman-Berland, Johanna Zipse, Jennifer Fawcett, Joel Stein, Howard Poizner, Albert C Lo, et al. A paradigm shift for rehabilitation robotics. *Engineering in Medicine and Biology Magazine, IEEE*, 27(4):61–70, 2008.

[78] Hermano Igo Krebs and Neville Hogan. Therapeutic robotics: A technology push. *Proceedings of the IEEE*, 94(9):1727–1738, 2006.

[79] Gert Kwakkel, Boudewijn J Kollen, and Hermano I Krebs. Effects of robot-assisted therapy on upper limb recovery after stroke: a systematic review. *Neurorehabilitation and Neural Repair*, 22:111–121, 2008.

[80] Francesco Lacquaniti and John F Soechting. Coordination of arm and wrist motion during a reaching task. *The Journal of Neuroscience*, 2(4):399–408, 1982.

[81] Claude Lagoda, Alfred C Schou, Arno HA Stienen, Edsko EG Hekman, and Herman van der Kooij. Design of an electric series elastic actuated joint for robotic gait rehabilitation training. In *Biomedical Robotics and Biomechatronics (BioRob), 2010 3rd IEEE RAS and EMBS International Conference on*, pages 21–26. IEEE, 2010.

[82] HVK Van Langenberghe, CJ Partridge, MS Edwards, and R Mee. Shoulder pain in hemiplegia-a literature review. *Physiotherapy Theory and Practice*, 4(3):155–162, 1988.

[83] Timothy D Lee, Stephan P Swinnen, and Deborah J Serrien. Cognitive effort and motor learning. *Quest*, 46(3):328–344, 1994.

[84] Pamela K Levangie and Cynthia C Norkin. *Joint structure and function: a comprehensive analysis*. FA Davis, 2011.

[85] TE LeVere. Recovery of function after brain damage: A theory of the behavioral deficit. *Physiological Psychology*, 8(3):297–308, 1980.

[86] Mindy F Levin, Jeffrey A Kleim, and Steven L Wolf. What do motor recovery and compensation mean in patients following stroke? *Neurorehabilitation and neural repair*, 2008.

[87] Joachim Liepert, Heike Bauder, Wolfgang HR Miltner, Edward Taub, and Cornelius Weiller. Treatment-induced cortical reorganization after stroke in humans. *Stroke*, 31(6):1210–1216, 2000.

[88] Albert C Lo, Peter D Guarino, Lorie G Richards, Jodie K Haselkorn, George F Wittenberg, Daniel G Federman, Robert J Ringer, Todd H Wagner, Hermano I Krebs, Bruce T Volpe, Christopher T Jr Bever, Dawn M Bravata, Pamela W Duncan, Barbara H Corn, Alysia D Maffucci, Stephen E Nadeau, Susan S Conroy, Janet M Powell, Grant D Huang, and Peter Peduzzi. Robot-assisted therapy for long-term upper-limb impairment after stroke. *New England Journal of Medicine*, 362(19):1772–1783, 2010.

[89] Ho Shing Lo and Sheng Quan Xie. Exoskeleton robots for upper-limb re-

habilitation: state of the art and future prospects. *Medical engineering & physics*, 34(3):261–268, 2012.

[90] Rui CV Loureiro, William S Harwin, Kiyoshi Nagai, and Michelle Johnson. Advances in upper limb stroke rehabilitation: a technology push. *Medical & Biological Engineering & Computing*, 49(10):1103–1118, 2011.

[91] Paula M Ludewig, Vandana Phadke, Jonathan P Braman, Daniel R Hassett, Cort J Cieminski, and Robert F LaPrade. Motion of the shoulder complex during multiplanar humeral elevation. *The Journal of Bone and Joint Surgery*, 91(2):378–389, 2009.

[92] Peter S Lum, Charles G Burgar, Peggy C Shor, Matra Majmundar, and Machiel Van der Loos. Robot-assisted movement training compared with conventional therapy techniques for the rehabilitation of upper-limb motor function after stroke. *Archives of physical medicine and rehabilitation*, 83(7):952–959, 2002.

[93] Peter S Lum, Charles G Burgar, Machiel Van der Loos, Peggy C Shor, Matra Majmundar, and Ruth Yap. Mime robotic device for upper-limb neurorehabilitation in subacute stroke subjects: A follow-up study. *Journal of rehabilitation research and development*, 43(5):631, 2006.

[94] DJ Magermans, EKJ Chadwick, HEJ Veeger, and FCT Van Der Helm. Requirements for upper extremity motions during activities of daily living. *Clinical Biomechanics*, 20(6):591–599, 2005.

[95] Ying Mao and Sunil Kumar Agrawal. Design of a cable-driven arm exoskeleton (CAREX) for neural rehabilitation. *IEEE Transactions on Robotics*, 28(4):922–931, 2012.

[96] Kevin J McQuade and Gary L Smidt. Dynamic scapulohumeral rhythm: the effects of external resistance during elevation of the arm in the scapular plane. *Journal of Orthopaedic & Sports Physical Therapy*, 27(2):125–133, 1998.

[97] KJ McQuade, Shun Hwa Wei, and GL Smidt. Effects of local muscle fatigue on three-dimensional scapulohumeral rhythm. *Clinical Biomechanics*, 10(3):144–148, 1995.

[98] Matjaz Mihelj, Tobias Nef, and Robert Riener. ARMin II-7 DoF rehabilitation robot: mechanics and kinematics. In *IEEE International Conference on Robotics and Automation*, pages 4120–4125, 2007.

[99] Matjaž Mihelj, Tobias Nef, and Robert Riener. A novel paradigm for patient-cooperative control of upper-limb rehabilitation robots. *Advanced Robotics*, 21(8):843–867, 2007.

[100] Marie-Hélène Milot, Steven J Spencer, Vicky Chan, James P Allington, Julius Klein, Cathy Chou, James E Bobrow, Steven C Cramer, David J Reinkensmeyer, et al. A crossover pilot study evaluating the functional outcomes of two different types of robotic movement training in chronic stroke survivors using the arm exoskeleton BONES. *Journal NeuroEngineering Rehabilitation*, 10:112, 2013.

[101] H Moskowitz, CR Goodman, E Smith, E Balthazar, and HZ Mellins. Hemiplegic shoulder. *New York state journal of medicine*, 69(4):548–550, 1969.

[102] Timothy H Murphy and Dale Corbett. Plasticity during stroke recovery: from synapse to behaviour. *Nature Reviews Neuroscience*, 10(12):861–872, 2009.

[103] T Najenson, E Yacubovich, and SS Pikielni. Rotator cuff injury in shoulder joints of hemiplegic patients. *Scandinavian journal of rehabilitation medicine*, 3(3):131–137, 1970.

[104] Tobias Nef, Marco Guidali, and Robert Riener. ARMin III–arm therapy exoskeleton with an ergonomic shoulder actuation. *Applied Bionics and Biomechanics*, 6(2):127–142, 2009.

[105] Tobias Nef, Matjaz Mihelj, Gabriela Kiefer, Christina Perndl, Roland Muller, and Robert Riener. ARMin-exoskeleton for arm therapy in stroke patients. In *IEEE International Conference on Rehabilitation Robotics*, pages 68–74, 2007.

[106] Tobias Nef, Matjaz Mihelj, and Robert Riener. ARMin: a robot for patient-cooperative arm therapy. *Medical & Biological Engineering & Computing*, 45(9):887–900, 2007.

[107] Randolph J Nudo, Erik J Plautz, and Garrett W Milliken. Adaptive plasticity in primate motor cortex as a consequence of behavioral experience and neuronal injury. In *Seminars in Neuroscience*, volume 9, pages 13–23. Elsevier, 1997.

[108] NJ O'Dwyer, L Ada, and PD Neilson. Spasticity and muscle contracture following stroke. *Brain*, 119(5):1737–1750, 1996.

[109] Romeo Ortega, Julio Antonio Loría Perez, Per Johan Nicklasson, and Hebertt Sira-Ramirez. *Passivity-based control of Euler-Lagrange systems: mechanical, electrical and electromechanical applications*. Springer Science & Business Media, 2013.

[110] Nicholas Paine, Sehoon Oh, and Luis Sentis. Design and control considerations for high-performance series elastic actuators. *IEEE/ASME Transactions on Mechatronics*, 19(3):1080–1091, 2014.

[111] James L Patton, Mary Ellen Stoykov, Mark Kovic, and Ferdinando A Mussa-Ivaldi. Evaluation of robotic training forces that either enhance or reduce error in chronic hemiparetic stroke survivors. *Experimental Brain Research*, 168(3):368–383, 2006.

[112] Y Paulignan, M Dufosse, M Hugon, and J Massion. Acquisition of co-ordination between posture and movement in a bimanual task. *Experimental Brain Research*, 77(2):337–348, 1989.

[113] Joel C Perry and Jacob Rosen. Design of a 7 degree-of-freedom upper-limb powered exoskeleton. In *Biomedical Robotics and Biomechatronics, 2006. BioRob 2006. The First IEEE/RAS-EMBS International Conference on*, pages 805–810. IEEE, 2006.

[114] Joel C Perry, Jacob Rosen, and Stephen Burns. Upper-limb powered exoskeleton design. *IEEE/ASME Transactions on Mechatronics*, 12(4):408–417, 2007.

[115] T Platz, P Denzler, B Kaden, and K-H Mauritz. Motor learning after recovery from hemiparesis. *Neuropsychologia*, 32(10):1209–1223, 1994.

[116] NK Poppen and PS Walker. Normal and abnormal motion of the shoulder. *Journal of Bone and Joint Surgery*, 58(2):195–201, 1976.

[117] Gerdienke B Prange, Michiel JA Jannink, Catharina GM Groothuis-Oudshoorn, Hermie J Hermens, and Maarten J IJzerman. Systematic review of the effect of robot-aided therapy on recovery of the hemiparetic arm after stroke. *Journal of Rehabilitation Research and Development*, 43(2):171, 2006.

[118] Gill Pratt, Matthew M Williamson, et al. Series elastic actuators. In *Intelligent Robots and Systems 95.'Human Robot Interaction and Cooperative Robots', Proceedings. 1995 IEEE/RSJ International Conference on*, volume 1, pages 399–406. IEEE, 1995.

[119] Jerry E Pratt, Benjamin T Krupp, Christopher J Morse, and Steven H Collins. The roboknee: an exoskeleton for enhancing strength and endurance during walking. In *Robotics and Automation, 2004. Proceedings. ICRA'04. 2004 IEEE International Conference on*, volume 3, pages 2430–2435. IEEE, 2004.

[120] Christopher IM Price, Paul Franklin, Helen Rodgers, Richard H Curless, and Garth R Johnson. Active and passive scapulohumeral movement in healthy persons: a comparison. *Archives of physical medicine and rehabilitation*, 81(1):28–31, 2000.

[121] Veerle Puttemans, Nicole Wenderoth, and Stephan P Swinnen. Changes in brain activation during the acquisition of a multifrequency bimanual coordination task: from the cognitive stage to advanced levels of automaticity. *The Journal of Neuroscience*, 25(17):4270–4278, 2005.

[122] Daniel Ragonesi, Sunil Agrawal, Whitney Sample, and Tariq Rahman. Series elastic actuator control of a powered exoskeleton. In *Engineering in Medicine and Biology Society, EMBC, 2011 Annual International Conference of the IEEE*, pages 3515–3518. IEEE, 2011.

[123] Yupeng Ren, Hyung-Soon Park, and Li-Qun Zhang. Developing a whole-arm exoskeleton robot with hand opening and closing mechanism for upper limb stroke rehabilitation. In *IEEE International Conference on Rehabilitation Robotics*, pages 761–765, 2009.

[124] Michel Rijntjes, Kerstin Haevernick, Anne Barzel, Hendrik van den Bussche, Gesche Ketels, and Cornelius Weiller. Repeat therapy for chronic motor stroke: a pilot study for feasibility and efficacy. *Neurorehabilitation and Neural Repair*, 23:275–280, 2009.

[125] Randall K Roberts, RP Paul, and Benjamin M Hillberry. The effect of wrist force sensor stiffness on the control of robot manipulators. In *Robotics*

and Automation. Proceedings. 1985 IEEE International Conference on, volume 2, pages 269–274. IEEE, 1985.

[126] Ian H Robertson and Jaap MJ Murre. Rehabilitation of brain damage: brain plasticity and principles of guided recovery. *Psychological bulletin*, 125(5):544, 1999.

[127] David William Robinson. *Design and analysis of series elasticity in closed-loop actuator force control*. PhD thesis, Massachusetts Institute of Technology, 2000.

[128] A Roby-Brami, A Feydy, M Combeaud, EV Biryukova, B Bussel, and MF Levin. Motor compensation and recovery for reaching in stroke patients. *Acta Neurologica Scandinavica*, 107(5):369–381, 2003.

[129] Charles A Rockwood Jr, Frederick A Matsen III, Michael A Wirth, and Steven B Lippitt. *The shoulder*. Elsevier Health Sciences, 2009.

[130] RJ Sanchez Jr, E Wolbrecht, R Smith, J Liu, S Rao, S Cramer, T Rahman, JE Bobrow, and DJ Reinkensmeyer. A pneumatic robot for re-training arm movement after stroke: Rationale and mechanical design. In *IEEE International Conference on Rehabilitation Robotics*, pages 500–504, 2005.

[131] Robert A Scheidt and Tina Stoeckmann. Reach adaptation and final position control amid environmental uncertainty after stroke. *Journal of neurophysiology*, 97(4):2824–2836, 2007.

[132] Andre Schiele and Frans CT van der Helm. Kinematic design to improve ergonomics in human machine interaction. *Neural Systems and Rehabilitation Engineering, IEEE Transactions on*, 14(4):456–469, 2006.

[133] Richard A Schmidt and Tim Lee. *Motor control and learning*. Human kinetics, 1988.

[134] Jean-Jacques E Slotine, Weiping Li, et al. *Applied nonlinear control*, volume 199. Prentice-hall Englewood Cliffs, NJ, 1991.

[135] Kim C Stewart, James H Cauraugh, and Jeffery J Summers. Bilateral movement training and stroke rehabilitation: a systematic review and meta-analysis. *Journal of the Neurological Sciences*, 244(1):89–95, 2006.

[136] Arno HA Stienen, Edsko EG Hekman, Gerdienke B Prange, Michiel JA Jannink, Arthur MM Aalsma, Frans CT van der Helm, and Herman van der Kooij. Dampace: Design of an exoskeleton for force-coordination training in upper-extremity rehabilitation. *Journal of Medical Devices*, 3(3):031003, 2009.

[137] Arno HA Stienen, Edsko EG Hekman, Frans CT Van Der Helm, and Herman Van Der Kooij. Self-aligning exoskeleton axes through decoupling of joint rotations and translations. *IEEE Transactions on Robotics*, 25(3):628–633, 2009.

[138] Aurore Thibaut, Camille Chatelle, Erik Ziegler, Marie-Aurélie Bruno, Steven

Laureys, and Olivia Gosseries. Spasticity after stroke: physiology, assessment and treatment. *Brain Injury*, 27(10):1093–1105, 2013.

[139] Catherine A Trombly and Ching-Yi Wu. Effect of rehabilitation tasks on organization of movement after stroke. *American Journal of Occupational Therapy*, 53(4):333–344, 1999.

[140] Nikolaos G. Tsagarakis and Darwin G Caldwell. Development and control of a soft-actuated exoskeleton for use in physiotherapy and training. *Autonomous Robots*, 15(1):21–33, 2003.

[141] Lynne Turner-Stokes and Diana Jackson. Shoulder pain after stroke: a review of the evidence base to inform the development of an integrated care pathway. *Clinical Rehabilitation*, 16(3):276–298, 2002.

[142] Leslie G Ungerleider. Functional mri evidence for adult motor cortex plasticity during motor skill learning. *Nature*, 377(155):58, 1995.

[143] Leslie G Ungerleider, Julien Doyon, and Avi Karni. Imaging brain plasticity during motor skill learning. *Neurobiology of learning and memory*, 78(3):553–564, 2002.

[144] Heike Vallery, Jan Veneman, Edwin Van Asseldonk, Ralf Ekkelenkamp, Martin Buss, and Herman Van Der Kooij. Compliant actuation of rehabilitation robots. *Robotics & Automation Magazine, IEEE*, 15(3):60–69, 2008.

[145] Frans CT Van der Helm. Analysis of the kinematic and dynamic behavior of the shoulder mechanism. *Journal of Biomechanics*, 27(5):527–550, 1994.

[146] Frans CT Van der Helm, HEJ Veeger, GM Pronk, LHV Van der Woude, and RH Rozendal. Geometry parameters for musculoskeletal modelling of the shoulder system. *Journal of Biomechanics*, 25(2):129–144, 1992.

[147] Richard Q Van der Linde, Piet Lammertse, Erwin Frederiksen, and B Ruiter. The hapticmaster, a new high-performance haptic interface. In *Proc. Eurohaptics*, pages 1–5, 2002.

[148] HEJ Veeger. The position of the rotation center of the glenohumeral joint. *Journal of Biomechanics*, 33(12):1711–1715, 2000.

[149] HEJ Veeger and FCT Van Der Helm. Shoulder function: the perfect compromise between mobility and stability. *Journal of biomechanics*, 40(10):2119–2129, 2007.

[150] Jan F Veneman, Ralf Ekkelenkamp, Rik Kruidhof, Frans CT van der Helm, and Herman van der Kooij. A series elastic-and bowden-cable-based actuation system for use as torque actuator in exoskeleton-type robots. *The International Journal of Robotics Research*, 25(3):261–281, 2006.

[151] Rocco Vertechy, Antonio Frisoli, Andrea Dettori, Massimiliano Solazzi, and Massimo Bergamasco. Development of a new exoskeleton for upper limb rehabilitation. In *IEEE International Conference on Rehabilitation Robotics*, pages 188–193, 2009.

[152] Bruce T Volpe, Hermano I Krebs, and Neville Hogan. Is robot-aided senso-

rimotor training in stroke rehabilitation a realistic option? *Current opinion in neurology*, 14(6):745–752, 2001.

[153] Sandy McCombe Waller and Jill Whitall. Bilateral arm training: why and who benefits? *NeuroRehabilitation*, 23(1):29–41, 2008.

[154] Jill Whitall, Sandy McCombe Waller, Kenneth HC Silver, and Richard F Macko. Repetitive bilateral arm training with rhythmic auditory cueing improves motor function in chronic hemiparetic stroke. *Stroke*, 31(10):2390–2395, 2000.

[155] Kay Wing, James V Lynskey, and Pamela R Bosch. Whole-body intensive rehabilitation is feasible and effective in chronic stroke survivors: a retrospective data analysis. *Topics in Stroke Rehabilitation*, 15(3):247–255, 2008.

[156] Carolee J Winstein. Knowledge of results and motor learningimplications for physical therapy. *Physical therapy*, 71(2):140–149, 1991.

[157] Carolee J Winstein, Alma S Merians, and Katherine J Sullivan. Motor learning after unilateral brain damage. *Neuropsychologia*, 37(8):975–987, 1999.

[158] Eric T Wolbrecht, Vicky Chan, David J Reinkensmeyer, and James E Bobrow. Optimizing compliant, model-based robotic assistance to promote neurorehabilitation. *IEEE Transactions on Neural Systems and Rehabilitation Engineering*, 16(3):286–297, 2008.

[159] Ge Wu, Frans CT Van der Helm, HEJ DirkJan Veeger, Mohsen Makhsous, Peter Van Roy, Carolyn Anglin, Jochem Nagels, Andrew R Karduna, Kevin

McQuade, Xuguang Wang, et al. Isb recommendation on definitions of joint coordinate systems of various joints for the reporting of human joint motion-part ii: shoulder, elbow, wrist and hand. *Journal of biomechanics*, 38(5):981–992, 2005.

[160] Maria Wyke. The effects of brain lesions on the learning performance of a bimanual co-ordination task. *Cortex*, 7(1):59–72, 1971.

[161] Michael Zinn, Bernard Roth, Oussama Khatib, and J Kenneth Salisbury. A new actuation approach for human friendly robot design. *The International Journal of Robotics Research*, 23(4-5):379–398, 2004.

Vita

Bongsu Kim was born in Miryang, South Korea. He received the B.S. degree in mechanical engineering from Hanyang University in Seoul, Korea, in 2004, and M.S. degree in mechanical engineering from Korea Advanced Institute of Science and Technology (KAIST), Daejeon, Korea, in 2006. He had fulfilled a military service at the Korean Army from 1998 to 2000. Bongsu Kim had been working at the research institute of Korea Electric Power Corporation (KEPCO) as a research engineer from 2006 to 2011. He joined the Ph.D. program in the department of mechanical engineering at The University of Texas at Austin in 2011.

Permanent address: bskim@utexas.edu

This dissertation was typeset with LaTeX[†] by the author.

[†]LaTeX is a document preparation system developed by Leslie Lamport as a special version of Donald Knuth's TeX Program.